بسم الله الرحمن الرحيم

قُلِ الرُّوحُ مِنْ أَمْرِ رَبِّي وَمَا أُوتِيتُمْ مِنَ الْعِلْمِ إِلَّا قَلِيلا

الاسراء (85)

DUAL-BAND RF ENERGY HARVESTING RECTENNA DESIGN WITH OMNI-DIRECTIONAL RADIATION PROPERTIES

THESIS

SUBMITTED TO THE COMMUNICATION TECHNIQUES ENGINEERING DEPARTMENT IN PARTIAL FULFILLMENT OF THE REQUIREMENTS FOR THE DEGREE OF MASTER

By

MARWA JASIM MOHAMMED

Supervised by

Dr. Salim Muhsin Wadi

11 / 2021

Dedication

For the best women, my great mother. You are the torch that lights my path, with prayer, love, and support.

To my father for his care, patience and encouragement throughout the study period.

To my dear husband Mohammed AL-Hasmmoty, you encourage me, support me. Thank you for the great love and for helping me in my study, this thesis would not have been complete without you.

To my brother and sister. Thank you for all the love, affection, and help.

To my husband family, thank you for helping me and support me and for everything.

Finally, to my inspirations, my lovely daughter Shahad, and my smart son Mostafa.

Supervisor Certification

We certify that we have read this thesis titled **"Dual-band RF Energy Harvesting Rectenna design with Omni-directional Radiation Properties"** which is being submitted by **Marwa Jasim Mohammed** was prepped under our supervisor at Communications Techniques Engineering Department, Engineering Technical Collage-Najaf, Al-Furat Al-Awsat Technical University, as a partial fulfillment of requirement for the degree of Master.

Signature:

Name: **Dr. Salim Muhsin Wadi**

(Supervisor)

Date: / / 2021

In view of th available recommendation, I forward this thesis for debate by the examining committee.

Signature:

Name: **Prof. Dr. Ahmad T. Abdulsadda**

(Head of Communication Technology Engineering. Dept.)

Date: / / 2021

Committee Report

We certify that we have read this thesis titled **"Dual-band RF Energy Harvesting Rectenna design with Omni-directional Radiation Properties"** which is being submitted by **Marwa Jasim Mohammed** and as Examining Committee, examined the student in its contents. I our opinion, the thesis is adequate for award of degree of Master.

Signature:
Name:**Dr. Salim Muhsin Wadi**
(Supervisor)
Date: / / 2021

Signature:
Name: **Asst. Prof. Dr. Saad Mutashar**
(Member)
Date: / / 2021

Signature:
Name:**Dr. Mohanad A. Al-Ibadi**
(Member)
Date: / / 2021

Signature:
Name:**Prof. Dr. Faris Mohammed Ali**
(Chairman)
Date: / / 2021

Approval of the Technical Engineering Collage

Signature:
Name:**Asst. Prof. Dr. Hassanain Ghani Hameed**
Dean of Technical Engineering Collage
Date: / / 2021

Linguistic Certification

This is to certify this thesis entitled **"Dual-band RF Energy Harvesting Rectenna design with Omni-directional Radiation Properties"** was reviewed linguistically. Its language was amended to meet the style of the English language.

Signature:

Name:

Date: / / 2021

Abstract

Energy harvesting is a promising technology since the IoT network depends highly on sensors, which in turn, they need continuously power sources. This is by itself is a big challenge because batteries should be replaced from time to another. However, looking for a solution becomes imperative. The solution is to recycle the wasted energy in Radio Frequency (RF) signals in order to provide the necessary power.

Most rectenna designs reported in the literature operate at high input power. In most cases, this amount of high power cannot be obtained since the RF power density is low. A design of any rectenna array needs a large size because the antennas should separate with a specific distance to avoid the mutual coupling. Generally, arrays capture RF signals from a certain range of angles. By itself, this would be a problem.

Because RF Schottky diode HSMS 2850 has a low threshold voltage-junction, it is a good candidate used for low input power. The proposed rectifiers operate at frequencies 1.8GHz and 2.4GHz which are GSM and WiFi frequency bands, respectively, with a low range of input power from -30 to -5 dBm. The Composite Right-Left-Handed CRLH transmission lines are adopted using lumped elements only to implement an RF rectifier with a small size of 5×5.5 mm^2. The closed-equations formulas based on dual-band matching network design are derived as well with full detail.

Next, to adopt an antenna operating at two bands exploiting the same antenna aperture without extra parts, the U-slot patch antenna is used to resonate at 1.8GHz and 2.4GHz with gains of 6.7dBi and 6.8dBi, respectively. The RF rectifier is placed on the backside of the antenna to miniaturize the overall size. The output voltage from single rectenna is 0.5V and the output power is 167μW. The single rectenna mentioned

above is employed to build a cube rectenna. The cube of multi Rectenna consisting of five patch antennas with a size of 65×65×65 mm^3 can capture power from five directions with a high gain.

Multi Rectenna is implemented where each antenna connects to its rectifier directly. Then, outputs of rectifiers are combined in somehow to produce the final output DC power. Two type of DC combine are used, at the parallel DC connection, the voltage produces is 0.5V, while the current is 1mA, thereby producing is 500μW DC power at -5dBm input power and conversion efficiency of 48.9%. At series DC connection the voltage is 2.1 V and the current is 333μA, while DC power is 460μW at the same input power.

Acknowledgment

First and foremost, I thank almighty ALLAH for giving me the determination and the will to complete this research study.

I would like to express my sincere gratitude and acknowledgment for my supervisor, Dr. Salim Wadi for his guidance, advice, and support throughout my research.

I would like to acknowledge the help of Dr. Nasr Al-Khafaji for his continuous support throughout this work. Thank you for the invaluable comments and advice, I learned so much from you.

Great thanks to the Dean of the College of Technical Engineering, Heads, and Staff of Communication Technical Engineering Department in AL-Furat AL-Awsat Technical University for their facilities and assistance throughout this thesis

Special thanks are to my many friends who have given me their support and help.

Finally, I must express my very profound gratitude to my family for providing me with unfailing support. This accomplishment would not have been possible without them. Thank you.

DECLARATION

I hereby declare that the work in this thesis is my own except for quotations and summaries which have been duly acknowledged.

1/November/2021 MARWA JASIM MOHAMMED

Table of Content

List of Tables

List of Figure

List of Symbols

ε_r	Relative Permittivity
λ_o	Free Space Wavelength
λ_g	Guided Wavelength
Γ	Reflection Coefficient
η	Efficiency
η_{eff}	Effective Efficiency
α	Attenuation
Ae	Effective Capture Area
G	Gain
I_d	Diode Current
P_t	Power Transmission
P_r	Power Receiver
P_{di}	Isotropic Power Density
P_d	Power Density
S_{11}	Reflection Coefficient
S_{21}	Transmission Coefficients
V_d	Diode Voltage
Z_o	Reference Impedance
Z_{in}	Input Impedance

List of Abbreviations

AC	Alternating Current
ADS	Advanced Design System
$CRLH$	Composite Right Left Handed
CPW	Co Planar Waveguide
DAC	data Access Component
DC	Direct Current
DLP	Dual Linear Polarization
GSM	Global System Mobile
$HFSS$	High Frequency
HB	Harmonic Balanced
$HPBW$	Half Power Beam Width
IoT	Internet of Think
LED	Light Emitting Diode
LPF	Low Pass Filter
$LSSP$	large-signal S-parameter
LoS	Line of Site
MPT	Maximum Power Transfer
RF	Radio Frequency
SMA	Sub Miniature version A
SWR	Standing Wave Ratio
PEC	Perfect Electric Conductor
WPT	Wireless Power Transfer

CHAPTER ONE

Introduction and Literature Review

1.1 Introduction

The history of Wireless Power Transfer (WPT) belongs to 1864 when Maxwell's equations that explain the concept of how to generate the electric and magnetic field have been reported. In 1888, Heinrich Hertz implemented the first experiment of transmitting electricity in a small gap that confirms the existence of an electromagnetic field [1].

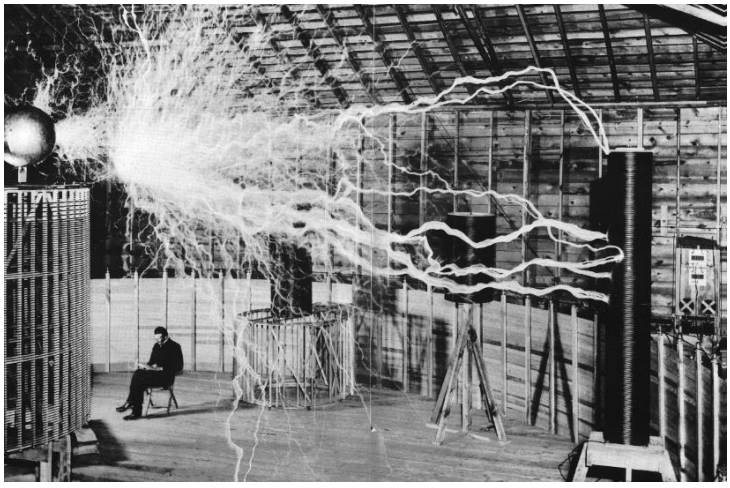

Figure 1.1: Tesla's experiment of power transmission via radio wave, 1899 [2]

The first attempt to transmit power wirelessly in space with a low-frequency band in the range of 150KHz and high power of about 300KW was implemented by Nikola Tesla. Figure 1.1. shows Tesla's picture implementing his first experiment that depicts the movement of electricity in space in 1899. Due to the technology limitations at that time, this invention did not see the light of day. Also, large-scale electricity makes the efficiency very low [2] . H.V. Noble in 1933 successfully transmitted a kilowatt of power for a long distance due to the use of power in the range of hundred MHz frequencies [3]. As time went on, the first antenna used to receive and rectify microwave

power called rectennas was investigated by William C. Brown in 1960. In 1968, Peter Glaser developed the concepts of energy harvesting for satellites where solar energy was converted to microwave power on the same satellite platforms [4].

A wireless device and IoT sensors need continuous power sources to operate without interruptions. Usually, batteries are used as a source of power, but they have a limited life-time and should be replaced periodically. This by itself is a big challenge and it represents a heavy burden for the IoT designers due to the increment of sensor nodes every year. Thus, looking for another type of energy source to provide the required power becomes in high demand. The energy sources that can be converted into DC power, enabling sensors to operate without batteries or to increase their time life. In the subsequent sections, the energy sources will be explained in detail [5].

1.1.1 Thermal Power

Thermal energy is either heat available in the environment or waste power in machines [6]. Many applications use thermal as a power source such as electronic devices or mechanical machines that dissipated heat when they run. The first application was implemented in 1999 when designing Wrist watches that depend on the heat of the human body [7]. The advantage of thermal energy is not moving, long life span has high reliability, and can be used for human warm applications [8]. The drawback of thermal power is that it has a low density of 20 µW to 10 mW per cm^2 and is large size.

1.1.2 Photovoltaic Cell

There are two types of photovoltaic sources, outdoor (solar cell) and indoor (light cell). Solar cell considers the best technology for producing electricity due to high output power but it has a large size [9]. Light cells use Light Emitting Diode(LED) lamps, fluorescent tubes, and incandescent lamps whereas a source of light has a very low

density of 10 mW/cm^2 compared to outdoor source intensity of 100-1000 W/m^2 [10]. There are many applications of photovoltaic such as temporary traffic signs, remote guard posts, lighting for roadways, and wireless sensors in a house or office.

1.1.3 Mechanical Energy

A mechanical energy harvesting system is used to convert mechanical power like (vibration, mechanical stress, winding, and rain-drop) into electrical energy. Mechanical vibration can have a natural source of power like wind and water flow that can rely upon using turbine or windmill. This type of power is used at a large scale due to its high efficiency, but it is expensive and not efficient in someplace [11]. Another type of mechanical vibration uses piezoelectric materials that can be utilized to produce electrical energy by applying straining or deformity material causing separation of charge in material, thereby producing electrical power [12].The advantage of this type of energy, it does not need a voltage source and its utilization for wasted mechanical power, but it is required to check and monitoring periodically [13].

1.1.4 Radio Frequency Power

RF energy harvesting system is used to convert the power stored in electromagnetic waves to Direct Current (DC) power. RF energy sources exist in an urban environment like broadcasting, Wireless Fidelity (WiFi), digital TV, and Global System of Mobile (GSM) cellular signals [14]. The principle of its work depends on capturing wasted power from the ambient environment and converting it to useful power which can be used to charge IoT sensors. The structure of this system is composed of three main parts: an antenna that should be designed to scavenge maximum amount of electromagnetic energy wirelessly; a rectifier is used to convert AC power to DC at high efficiency; and in the end, an impedance matching network should be placed between the antenna and the rectifier to ensure having the maximum power transfer [15]. The

efficiency of the system depends on the topology of the rectifier and the diode type used in the system. One of its advantages is that the system can operate for 24 hours indoors and outdoors, although it has a low power density (i.e., <0.1 μW/cm^2). Owing to its small size, it is suitable for embedded devices and sensors [16]. These advantages attract a lot of researchers to come up with new designs or to enhance the performance of the RF energy harvesting systems. Also, this thesis aims to convert the RF energy into DC power being useful in powering low power sensors. In the following section, some works reported in the literature will be reviewed because of their relevance to this work investigated here.

1.2 The Literature Review

Radio frequency energy harvesting is a technique used to scavenge energy especially to energize low power devices. It is used for harvesting electromagnetic and converting it into electrical energy from surrounding RF sources which have various densities in an ambient environment which is about 1 mW for GSM, 16 μW-54 μW for the TV station, and 10 nW-0.1μW for Wi-Fi band [17]. The energy harvesting system consists of three main parts which are an antenna, an impedance matching network, and a rectifier.

1.2.1 Rectifier and Matching Network

The rectifier is the main part of the energy harvesting system used to convert the AC power to DC which is in a usable form in the low power electronic devices. The rectifier can take different topologies such as a single series diode, single shunt diode [18], voltage dabbler [19], Dickson charge pump [20], and Cockcroft–Walton voltage multiplier [21]. The rectifier behavior depends on the diode response due to its nonlinearity where the input impedance of a diode becomes so sensitive to the input power, the resistive load value, and the frequency. The other part which is no less vital than

the ones mentioned above in the energy harvesting is a matching network placed between the antenna and rectifier to help the system transferring the maximum amount of power, resulting in capturing power from space as much as possible. Accordingly, a lot of research was carried out to design systems capable of having high efficiencies which are the main criteria to evaluate the performance of the system. For example, in [22], one stage voltage multiplier with a size of 45×7.8 mm^2 is designed to make the output voltage. The matching network made of an L-shaped microstrip transmission line operating at 800 MHz is reported. The author uses high input power of 12dBm to achieve 3.1 V at the output. The conversion efficiency is 49% being low proportional to the high input power utilized in the conversion. In [23] another structure is used at the same input power but with enhancing performance. A differential voltage rectifier is designed at 875 MHz where it has two different topologies: one of them a two brunches rectifier with a Common-Matching network (CM) as in Figure 1.2a, and the other is Two-Brunches with Two-Matching networks (TBM) as shown in Figure 1.2b. Both topologies consist of two stages voltage multiplier and two DC filters to produce high output voltage due to the use of eight diodes, four in each brunch. The diodes in the two branches are connected in opposite directions as a step to obtain high output voltages as 5.8 V. The efficiencies obtained from the CM and TBM topologies are 66% and 70%, respectively, at 12 dBm input power. The design has a size of 66×60 mm^2 which consider as a large footprint. Also, the design has a large number of diodes, being a complicated structure and causing more losses. These designs are not fit for our proposed works since high input power is required to power on all diodes.

In [24] , two single-stage voltage multipliers with 180 hybrid junctions in a ring form are reported. The 180-hybrid is a passive device having four ports. Ports 2 and 3 are used as inputs, port 1 is used as a combiner for the input power coming from ports 2 and 3, and port-4 is used as a differential port. A voltage multiplier with one

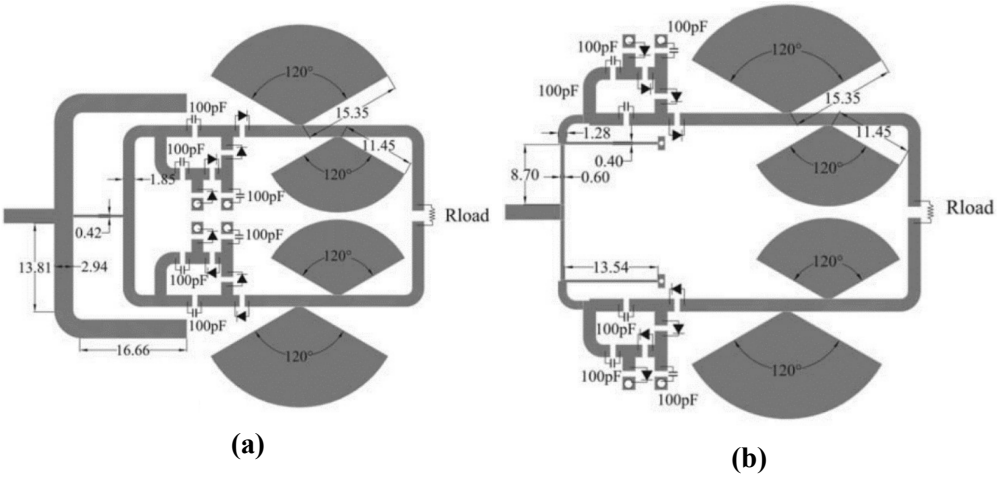

Figure 1.2: Differential rectifier (a) Two brunches with a Common-Matching network (CM). (b) Two-Brunches with Two-Matching network (TBM) [23].

diode is connected at each brunch to eliminate the losses of diodes and to enhance the system efficiency. The obtained conversion efficiency is about 70%, leading to having 20% enhancement more than conventional designs. The design has large size, while in [25], a compact size of 16×18 mm2 single shunt diode is associated with bandstop filter as shown in Figure 1.3 using a tapered transition line to match rectifier at 50 ohm. C1 is used to prevent DC voltage, a $\lambda_g/4$ transition line, a C2 operates as a DC filter, and $\lambda_g/8$ short-end microstrip line is connected in series to operate as a bandstop filter that prevents the second harmonic from passing through the diode. The bandstop filter is not complicated so its losses are low. The rectifier has a high conversion efficiency of 80% at 20 dBm input power and a frequency of 2.4 GHz. The proposed design has high conversion efficiency owing to the use of high input power. However, available power in the ambient has a lower density of RF power about 0.1 µW/cm^2. In this situation, a rectifier with a single diode is preferred to overcome the problem of the low power densities in space. Furthermore, multi rectifiers can harvest more power. Also, researchers were seeking to increase the amount of the harvested power with a single design. Thus, they have developed several designs able to harvest power from different signals. The main key to do so is to make the matching circuit operating at different frequency bands. Here, some multiband impedance matching networks will be

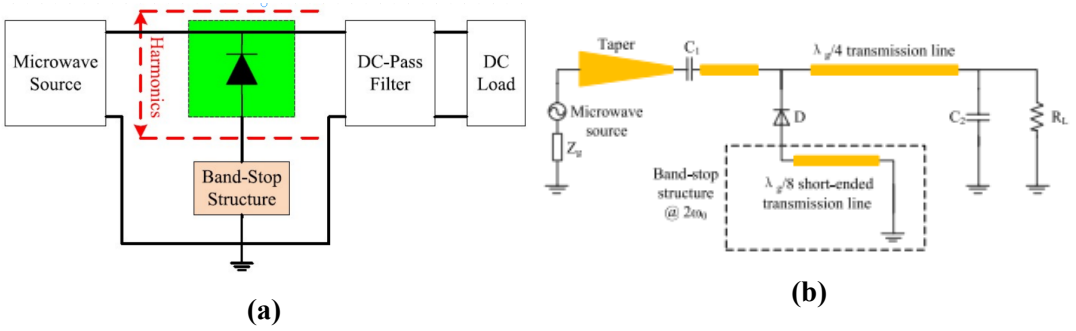

Figure 1.3: A single shunt diode topology with (a) Proposed structure bandstop filter (b) Schematic of the proposed microwave rectifier [25].

discussed below. The achievement in this energy harvesting part includes works simplifying the impedance matching networks with low complexity, single layer, and low cost, development of RF rectifiers with compact form factors yet robust performance. A dual-band matching network has attracted a lot of attention owing to increasing the scavenged power but several challenges that represent the main obstacle in the design are the performance sensitivities of the input impedance to varying the input power, the operating frequency, and the load impedance. Authors, in [26], implement a dual-band rectifier with a harmonic control circuit, see Figure 1.4. The matching network consists of two open stubs and two transmission lines. Other open-end stub is 0 c.onnected in series with the diodes to reject harmonics. Notch filter is added after diode operate as a band stop filter, prohibiting AC signals to move into the DC storage capacitor. The key point of using the bandstop filter is to enhance the performance. The rectifier operates at 2.4 GHz and 5.8 GHz with an efficiency of 64% and 62%, respectively, at an input power of 10 dBm. However, the efficiency becomes lower than by 40% at a power less than 0 dBm because of a large number of components. The larger the number of components used in a design, the more losses will be incurred. In [27], a dual-band impedance matching network with a voltage multiplier with a compact size of 18×10 mm2 is addressed. The two diodes for the voltage multiplier are used to get double the output voltage. A microstrip transmission line matching network is used to achieve high efficiency of 63 % and 69% for 1.95 GHz and 2.5 GHz, respectively, with a high

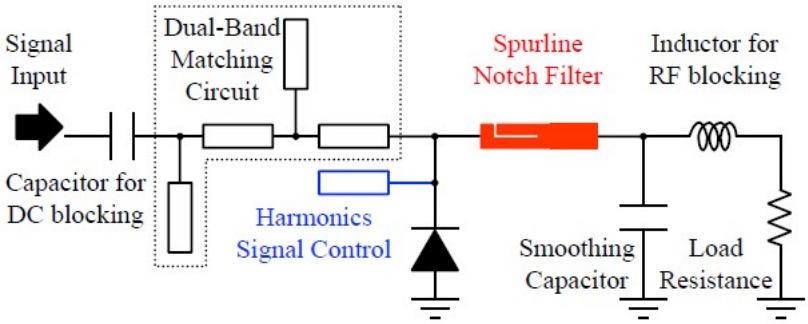

Figure 1.4: A dual-band rectifier with a bandstop filter to reflect power. [26].

input power of 15 dBm. The good results owing to the use of high input power that is not always available in space are not the case. While in [28], a lower input power of -10 dBm is assigned as a power level to the proposed design. The presented design aims to operate at very low power levels to simulate the real power levels in space. A design with a T-section transmission line matching network is introduced. A Voltage multiplier rectifier topology is utilized without using the DC filter. The design has good efficiency of 50% at 2.45 GHz while only 20% at 5.8 GHz due to the losses at high frequencies. It has a large size of 33×24 mm^2.

In [29], authors have used a differential rectifier circuit with one Villard voltage multiplier to obtain relatively equal efficiency at the two bands 1.8 GHz and 2.45 GHz. As shown in Figure 1.5, a phase shifter is applied to obtain 180 phase shifts between the two input sources with two brunches and each one with a matching network composed of the open and redial stubs with different dimensions. This structure has a size of 80×60 mm^2 and has low efficiency at low power due to the use of two diodes that increase losses. In [30], authors have used a voltage multiplier incorporating with the Composite Right Left-Handed matching network (CRLH). The CRLH, adopted in this paper, consists of conventional transmission lines representing the right-hand RH part and lumped elements denoting the left-hand LH part as illustrated in Figure 1.6. The input power is 2 dBm producing a high efficiency of about 59% at 2.45 GHz and 41%

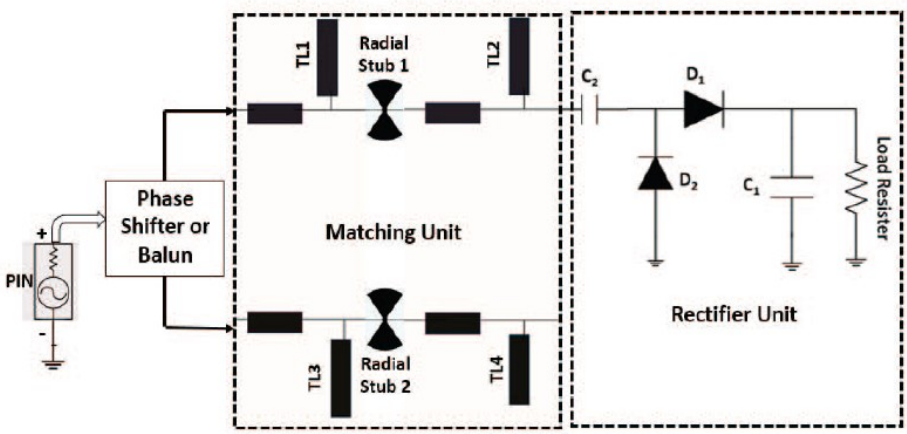

Figure 1.5: A dual-band differential rectifier topology with a phase shifter [29].

at 3.6 GHz. Th1e low efficiency at the high band is due to the high losses of lumped elements at the high frequencies. Although we have used lumped elements in the rectifier design, it has a large size of 40×24 mm^2.

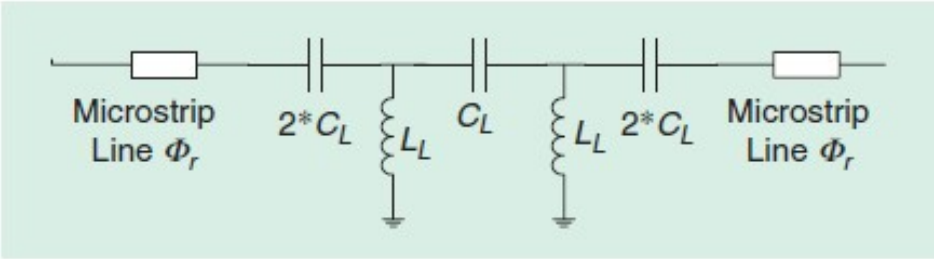

Figure 1.6: Two cells with transmission line dual-band composite right left-handed matching network [30].

1.2.2 Single element energy harvesting

The first part in the energy harvesting is an antenna which is used to capture the RF power. The most influential parameters which govern the antenna operation are the antenna gain and radiation pattern. If the attention is paid carefully during the design, the energy harvesting performance with one way or another will be quite improved. Therefore, here different structures of energy harvesting with various types of antennas will be discussed. In the beginning, in [31] a rectangular patch antenna with microstrip feeding is reported, and this type of feeding is easy to matching and integrating with the patch but makes the antenna dimensions larger. The antenna gain is 3.38

dB. A voltage multiplier rectifier topology is used with an impedance matching network composed entirely of five elements to reduce harmonics generated by the diode. The conversion efficiency of 43% is relatively low concerning the high input power of 20 dBm. In[32] , the good conversion efficiency of 55% at 3 dBm input power is obtained and an E-shaped meandered line patch antenna is used to reduce the size of the antenna at the low-frequency band of 2.4 GHz. The two layers of the substrate with an air gap between them and the partial ground technique are adopted to enhance the reflection coefficient and the gain which is about 3.9 dB. The size is 60×60×4.6 mm^3. A T-shaped matching network incorporated with a horizontal H-shaped slot operates as a bandpass filter to eliminate harmonics. The structure is so complex and the gain is low.

A different way to enhance the gain of the antenna, authors, in [33], have used a rectangular patch antenna with two microstrip lines as a parasitic element to widen the bandwidth. Also, two perfect electric conductors, Perfect Electric Conductor (PEC) walls are placed at two edges of the substrate to enhance the antenna gain. Figure 1.7 illustrates the structure. The design has a large size of 150×150 mm^2. The rectifier is printed on the backside of the substrate to make the structure more compact. The rectifier consists of tapered impedance matching, a DC stop filter (open stub and capacitance), a band-stop filter (i.e., three stubs forming a fan shape), and a bandstop filter connected with a load. All these components are used to help a rectifier getting better efficiency which is about 70% at 23 dBm input power The system is complicated and large. To get more gain, in [34], another way is conducted by placing a metal structure underneath the radiating element acting as a reflector at a distance of 25 mm as shown in Figure 1.8. A configuration used to implement the four arms of the antenna is trapezoidal. The dipole four arms are separated by 60° angle in order to have different polarizations. Each arm has a rectangular slot to eliminate the inductive effect of the arm. The system has good performance with a medium power level of 5 dBm where the

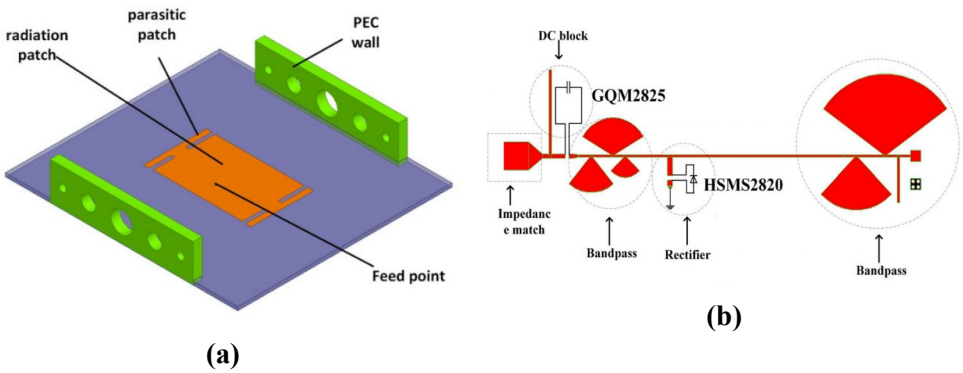

Figure 1.7: Two part of rectenna (a)Rectangular patch antenna. (b) Rectifier with matching network and bandpass filter [33]

conversion efficiency is about 69% at 2.4 GHz band and gain of 6 dB. The drawback of this structure, it operates at a single frequency meaning capturing a low amount of power that is not enough to produce high voltage.

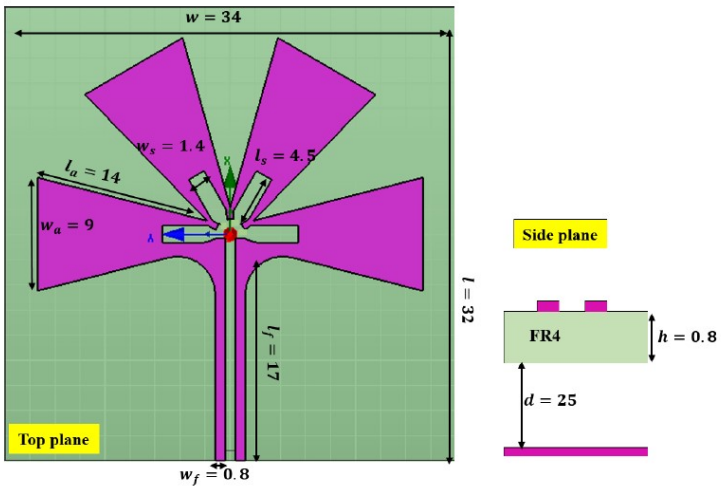

Figure 1.8: A trapezoidal dipole antenna with 4 arms in angle difference of 60 degrees [34].

To increase the captured power, a dual-band antenna is proposed, in [35], a spiral planar antenna with two slot rings to operate at 0.9 GHz and 1.8 GHz is depicted in Figure 1.9. A balun is added to the antenna for converting its impedance to 50 ohm. The antenna gain is low at the two bands 3 GHz and 3.8 GHz. A Delon voltage doubler topology is used to produce high conversion efficiencies which are 28% and 20% at a low input power of -20 dBm. Rectenna has a large size and low gain. On the contrary,

(a) **(b)**

Figure 1.9: Spiral rectenna (a) A spiral planar antenna with a balun. (b) Spiral antenna with rectifier (rectenna) [35].

in [36] , a folded dipole antenna is proposed to reduce the size of the antenna designed at 0.915 GHz with a dimension of 60×60×60 mm3. A half wavelength slot is loaded in the middle of the antenna to generate the second band at 2.45 GHz. At the backside of the antenna, a rectifier of the single series diode and a matching circuit are implemented to work at a low input power of -9 dBm. The rectenna efficiency is about 37% at the lower band and 30% at the high band with gains of 1.87 dB and 4.48 dB at the two bands. In [37], a dual-band rectenna is designed by using a dumbbell-shaped slot antenna. The antenna operates at two frequency bands and its radiation pattern is omnidirectional to capture more power. One of its disadvantages is that it has a low gain of about 1.7 dB at 2.4 GHz and 4.4 dB at 5.2 GHz. A voltage multiplier rectifier topology is used with the microstrip impedance matching network. The proposed system has bad performance despite the use of high input power of about 10 dBm, resulting in system efficiency of about 19.4%. In [35] [36] [37], rectennas operate with dual-frequency bands. However, the gain is very low due to using a combination of slot and dipole antennas. An antenna with an effective radiation pattern will produce a high gain. A patch antenna operating at 2.4 GHz and loaded with a slot on it to generate the second band at 5 GHz is proposed in [38]. The antenna has high gain of 7.7 dB and 8 dB at the two frequencies. A single series diode and a microstrip transmission line matching

network are proposed to design a rectenna achieving efficiencies of 56% and 37% at the input power of 12 dBm. The rectenna also has a large size of 85×64×9 mm3. As can be observed from all designs discussed above, a rectenna, which operates at either single or dual bands, has only one antenna aperture, so it will not be able to harvest a large amount of power. This problem becomes dominant when the antenna utilized in the design has a small aperture size. To collect more power, more rectenna elements are required. In other words, we can say the antenna array will be a good candidate to do so.

1.2.3 Multi Antenna Energy Harvesting

Many single-element antennas are placed together in a planner or cubic, well-known as an antenna array, to increase the harvested power. A large number of the antennas lead to high harvested power. There are several ways for connecting multi antenna elements (i.e., array topology). The RF signals entering the single elements may first be rectified or combined. In the former way, the DC signals are combined, so it is called DC combining technique. However, RF signals that first are combined and then rectified as in the latter way, this mechanism is called RF combining technique. RF combining method used in [39] where 2×2 antenna array operates at a single frequency of 2.45 GHz with a new feeding technique which has a simpler structure compared to the use of Wilkinson power divider as shown in Figure 1.10 is reported. The RF signals coming from four antennas are combined and then fed into one rectifier. The rectifier circuit is a single series diode with three T-shaped matching networks and then the DC pass filter is applied. This type of connection has high performance when the incident power is in line of sight with the array beam. Power decreases as the line of sight become poorer. To harvest more power, making the antenna array operating at dual-band is a good solution. In [40], two elements of monopole circular modified-slot patch antennas are combined using the power combining technique. Then, the RF

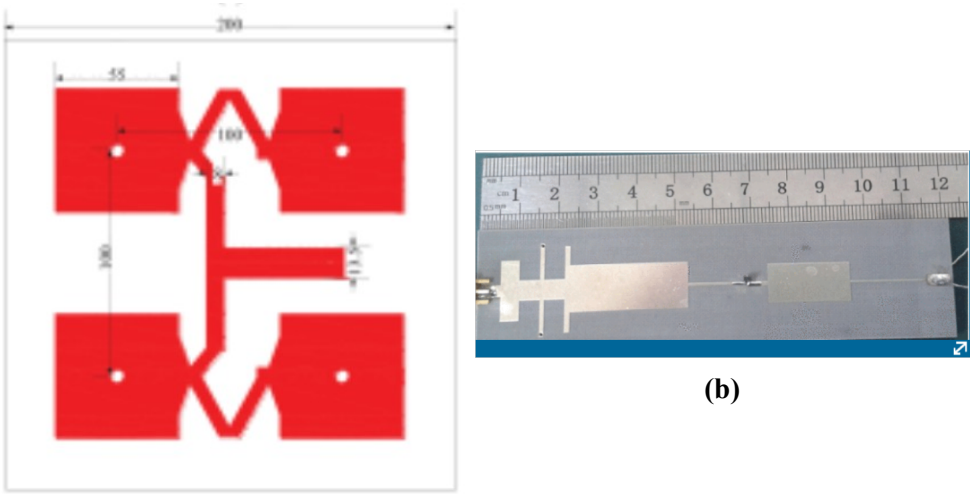

(a) **(b)**

Figure 1.10: Rectenna array consist of (a) 2 X 2 patch antenna array with serial feeding. (b) a rectifier with T-shape impedance matching [39]

signal is rectified. The proposed antenna array has gains of 3.5 dB and 5 dB at 1.8 GHz and 2.4 GHz, respectively. Two symmetrical rectification branches are connected in a differential form. The adopted method is advantageous to cancel the odd harmonics and to enhance efficiency. A voltage multiplier rectifier topology for each branch with the three-stage matching network is shown in Figure 1.11, to enhance the matching and bandwidth. The size of an array is about 100×45 mm^2 that is connected by the SubMinature version A (SMA) with a rectifier of size 40×40 mm^2, making an entire rectenna with a large size.

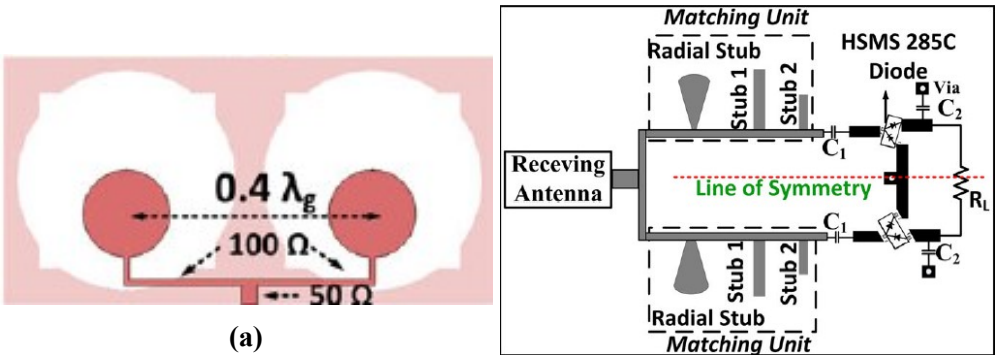

(a) **(b)**

Figure 1.11: Rectenna consist of (a) Two modified circular slot antenna. (b) Symmetrical differential rectifier circuit [40]

When operating with a dual-band and dual-polarization antenna array, the polarization mismatch will not have a big effect on the amount of the harvested power. The captured signal should then be fed into a dual-band rectifier. As in [41], a 4-element stacked array of dual-band dual-polarization is proposed, operating at 1.85 GHz and 2.45 GHz. Every single element has two coaxial feeding ports to produce the circular polarization then while parasitic elements are in array fed by stacked technique as shown in Figure 1.12. The element is placed on one side of the substrate with a sufficient distance between elements to overcome the mutual coupling. Diplexer of three-port is placed after antenna to combine the RF power of each frequency band. A T-shaped matching network is presented at the input port of the diplexer, and then output ports are connected with a single series diode rectifier with a DC pass filter. An open stub is placed before the diode allowing the rectifier to work at dual-band. The system operates at a lower power level, whereas the use of a diplexer will increase the circuit losses, so the efficiency is reduced.

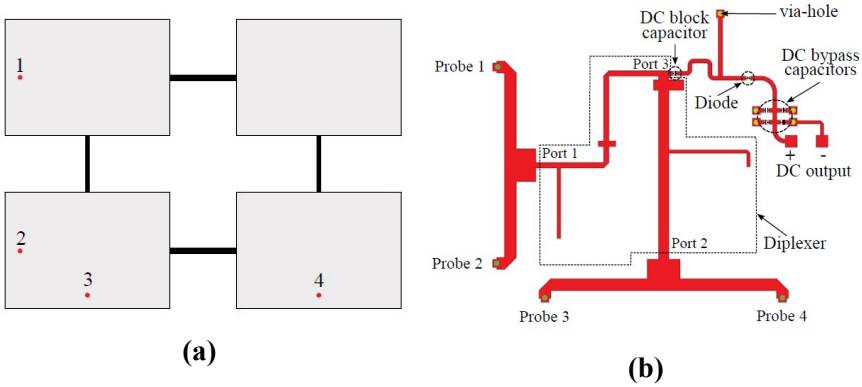

Figure 1.12: Rectenna array of (a) 4-element stacked array of dual-band dual polarization. (b) Rectifier with diplexer [41] .

A DC combiner is another type of rectenna array connection as in [42]. Two patch antennas are used. Each antenna is directly connected with a voltage doubler rectifier to eliminate the usage of the splitter, resulting in a reduction in losses and improving efficiency. The output DC voltage of two rectifiers is combined in series to produce a

high output voltage that becomes four-fold of the input voltage. The rectifier works at 2.45 GHz with an efficiency of 70% at the input power of 10 dBm. The benefit of this connection makes the antenna operating with a broader beam pattern. The design will be less sensitive to the incident angle of the RF signals. Rectenna has dimensions of 117×40 mm^2 using only two elements. In the former structure, the power is harvested from one direction only. This requires that the RF power source location should be known. To combat this deficit, an array with omnidirectional properties is needed. In [43], two elements of a square ring split resonator antennas printed on the microstrip substrate shown in Figure 1.13 are depicted. The antenna operates at 885MHz with an omnidirectional radiation pattern and a gain of 1.75 dB. The single series diode rectifier topology is fabricated using Coplanar Waveguide CPW without an underneath ground for simple integration and without using the impedance matching network. The fabricated circuit has few electronic elements. Rectenna is designed to operate with low input power of -20 dBm and compact size due to adopting the 3D architecture. Rectenna has a low gain for the adopted array and low efficiency of 40% at 0 dBm.

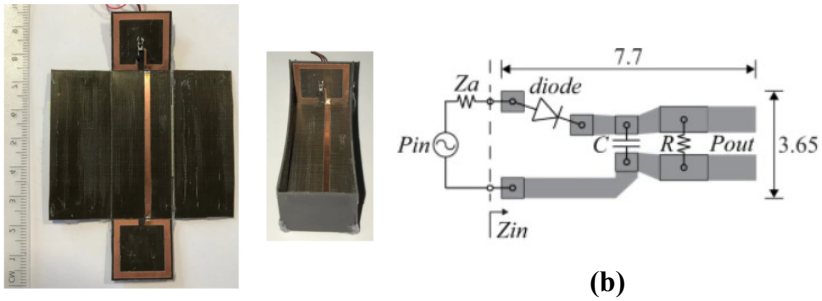

Figure 1.13: Omni-directional Rectenna array consist of (a) 3D arrangement of square ring spilt antenna. (b) compact size rectifier [43]

Typically, antenna arrays in the literature are in the planar form where they receive the incident signals from one direction. A 3D arrangement is utilized to harvest power from multiple directions with high gain. Moreover, a 3D arrangement has a compact size in comparison with the planer. In[44] six unit cells are packaged in a 3D hex-

ahedron antenna array with an overall size of 150×150×75 mm3 as can be shown in Figure 1.14. Each cell has a single patch antenna utilizing the aperture coupling feeding to produce Dual Linear Polarization (DLP). 90 hybrids are used to combine the power coming from vertical and horizontal polarization ports. Modified rectifiers that consist of two branches for each cell are proposed. One diode incorporated with $\lambda_g/4$ transmission line work as DC filter and $\lambda_g/8$ open stub work as a capacitor to enhance efficiency. When operating at a low power level of -5 dBm, the efficiency is about 40%. Each cell represents an individual rectenna operating at 2.45 GHz and gain of 7.8 dB. Despite using a 3D arrangement, the size of the whole rectenna array is still large.

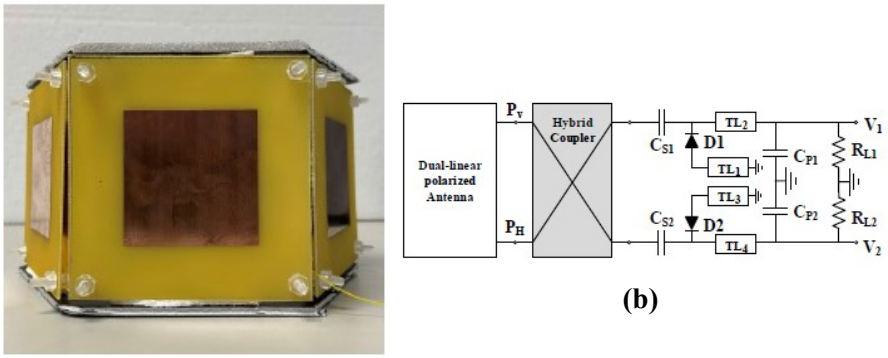

(a) **(b)**

Figure 1.14: 3D rectenna array (a) Six-cell hexahedron rectenna array. (b) Schematic of 90 hybrids and two brunches modified rectifier[44].

Another form of multidirectional rectenna is designed in [45] where six rectennas are placed on a circular shape with a radius of 90 mm^2. Furthermore, the rectifier is designed to operate at moderate levels of input power of -20 dBm with a single series diode. The output DC voltages of all cells are combined in a series form to increase the output voltage. The occupied volume of the structure is large and not suitable for IoT applications. In [46], a 3D origami structure is utilized to design a rectenna with two orthogonal-polarized patch antennas as shown in Figure 1.15. One patch antenna is located on the top side of the cube with vertical polarization and the other one is put on the bottom side of the cube with horizontal polarization to overcome mutual coupling between the antennas. The antenna resonates at 2.3 GHz with a gain of 4 dB. A DC

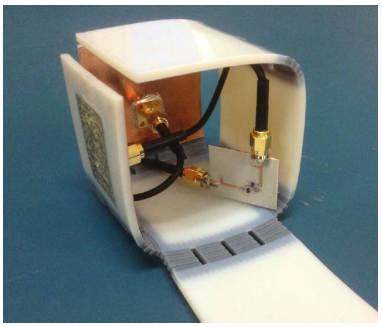

Figure 1.15: 3D origami rectenna with two antenna and two rectifier circuits[46]

combining is used where each antenna connects with an individual rectifier. The two rectifiers are placed in the same substrate to eliminate the need for a connecter, leading to low losses. The size of the rectenna is 57×57×57 mm^3.

Table 1.1 illustrates the comparison between the state of artwork discussed above.

1.3 The Most Relative Work

In [47] four patch antennas operating at 2.45 GHz are arranged in a cube arrangement with a gain of 5.23 dB as shown in Figure 1.16. The size of the cube is 60×60×60 mm^3 with a simi-omnidirectional radiation pattern. The rectifier board is placed in a cube form to use space effectively. Hence, the rectifier of each antenna is connected in parallel form to increase output power. If the difference between the highest power brunch and another brunch is over 5dB, the performance of rectenna will be good.

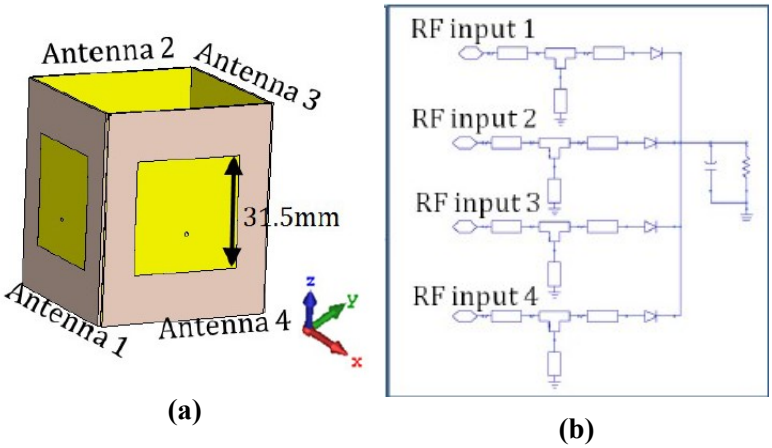

Figure 1.16: 3D multi rectenna consist of (a) 4-patch antenna in a cube package. (b) 4-rectifier circuit connect in parallel [47]

Table 1.1: Literature Review Summery Of Different Types Rectenna Design

Source	Frequency (GHz)	Antenna type	gain	input power (dBm)	efficiency (%)	Size (mm^3)
[34]	2.45	single-patch	3.38	20	43	91 X 37 X 1.6
[36]	2.4	E-shape mender line	3.9	3	55	60 X 60 X 4.6
[36]	2.45	patch	7.8	23	70	150 X 150 X 21
[37]	2.4	trapezoi-dal dipole	6	5	69	47 X 34
[38]	0.9 & 1.8	spiral planer	3 & 3.8	-20	28 & 20	not men-tioned
[39]	0.915 & 2.45	folded dipole	1.87 & 4.48	-9	37 & 30	60 X 60 X 60
[40]	2.4 & 5.2	slot	1.7 & 4.4	9	64 & 9	
[41]	2.4 & 5	patch	7.7 & 8.8	12	56 & 37	85 X 64 X 9
[42]	2.45	2X2patch array	13.4	21	77.2	200 X 200 X 5
[43]	1.8 & 2.4	1X2 circular slot array	3.5 & 5	9	70 % 68	140 X 84 X 1.6
[44]	1.85 & 2.85	2 X 2 stacked array	2.19 & 4.9	-8	not men-tioned	100 X 130
[45]	2.45	two patch	5.9	5.5	69	117 X 40 X 1.6
[46]	0.885	2square ring	1.75	0	40	50 X 24 x 24
[47]	2.45	hexahed-ron array	7.8	-5	40	150 X 150 X 75
[48]	2.45	6patch with 60degree	4	-20	not men-tioned	90 X 40
[49]	2.3	cube with two patch	4	-15	not men-tioned	57 X 57 X 57

The cube rectennas operate at a single frequency, so in this thesis, a dual-band cube antenna array is proposed to increase the scavenged RF power.

1.4 Problem Statements

Although RF energy sources are always available everywhere and at any time regardless of environmental conditions, significant challenges have been found for existing energy harvesters (i.e., rectennas). Here, in this thesis, two substantial challenges will be addressed, investigated, and solved.

1. In the most reported works, most rectifiers operate at a single frequency band, so no sufficient power can be gathered and stored for later processing. Another thing that makes the situation difficult is the low power densities of ambient electromagnetic waves in the surrounding space (i.e., <0.1 μW/cm2).

2. In state-of-the-art, RF energy harvesters usually obtain their energies from one direction. Thus, the transmitting source location should be specified. On most occasions, this is not the case. In other words, the transmitting source locations are not known. These two challenges let designers think somehow to mitigate their influences. Also, the size and complexity are other problems that we should consider in our designs although they are not our main problems.

1.5 Thesis Objectives

1. Design and simulate multiband energy harvesters (i.e., rectenna), single and rectenna array. This objective will be a good solution for the first problem mentioned above.

2. To fight and reduces the effects of the second problem, an array will design and simulate to be able to receive signals from most directions (i.e., omnidirectional-like radiation pattern). As known, the omnidirectional antenna has low gain, but

building an array with omnidirectional properties is a useful way to have a high gain omnidirectional radiation.

3. Design and simulate antenna are able to capture energy at different orientations in space with DC power combining capabilities.

1.6 Contributions

Design an energy harvesting array with capabilities is not reported in previous such as

1. Dual band structure that is able to harvest power from two frequencies 1.8 and 2.4 GHz to increase harvesting power.
2. The multi Rectennas that are used in the design have a different orientation and directions to overcome the unknown direction of power sources.
3. The Whole structure has simple and small size due to the arrangement of the cube.
4. Using the DC filter that reuse the harmonic power by adding it to the source power making high RF-to-DC conversion efficiency.

1.7 Applications

The proposed Energy harvesting system can be used to charge the sensors that operate at low power, like building automation, smart grid, industrial monitoring, and more. A sensor used to measure a temperature as in [75] can operate with power in Nano Watt. Anther application [76] is used to gather information also operate with very lower power.

1.8 Outline of thesis

This thesis consists of five chapters that mainly focuses on the design, simulation of multi-band rectennas in an array form with a Simi-omnidirectional radiation pattern, and compact size at low RF power for IoT sensor application. The thesis structure is organized as follows:

i. Chapter 2 introduces the theory of energy harvesting including antennas, matching networks, and rectifiers with focusing on a study of the diode equivalent circuit and its diode mathematical model.

ii. Chapter 3 discusses the implementation and results of a single rectifier circuit, a matching network with its mathematical model, and a single element antenna.

iii. Chapter 4 introduces the proposed design methodology and the results of the rectenna array designed in a cube form with two types of DC power connections (i.e., DC series and parallel connections).

iv. Chapter 5 provides a summary of the major contributions of this thesis. In addition, some future work recommendations for this research topic are suggested as well.

CHAPTER TWO

Energy harvesting system

2.1 Introduction

In this chapter, an overview of the energy harvesting system is clarified. The mechanism of the transmit and receive power by the antenna is cleared, with the benefit of the patch antenna. The type of matching network is depicted briefly. Then the rectification theory with the diode properties is studied. After that, a comparison between diode types and rectifier topologies is implemented to choose the suitable type for the low power system.

2.2 Energy harvesting system

The block diagram of the conventional rectenna (i.e., a rectifier integrated with an antenna) is shown in Figure 2.1, where the receiving antenna captures RF energy from the ambient environment and converts it to AC electrical signal. Typically, antennas have 50ohm input impedances. Thus, matching circuits become necessary, inserted between the antenna and the rectifier because most rectifiers have complex impedances, varying with the input power, the load resistance, and the operating frequency. Matching circuits ensure the Maximum Power Transfer (MPT). Moreover, the matching circuits act to reject any high harmonic, propagating back into the antenna resulting from the AC to DC conversion process that occurs inside diodes. The third part which is the rectifier topology (i.e., either a single diode or a combination of diodes) is a core of the rectification process that converts AC to DC power. A complex impedance of the rectifier due to the non-linear behavior of the diode becomes so sensitive to change in frequency, input power, and load. DC, RF, and all higher harmonics are injected into the Low Pass Filter (LPF), which in turn, attenuates all components except the DC

one. The load placed at the last-stage represents the equivalent impedance for any real application that will be supplied by power from the rectifier. All these parts operate as one system, but they should be optimized separately to reach the optimal design [51].

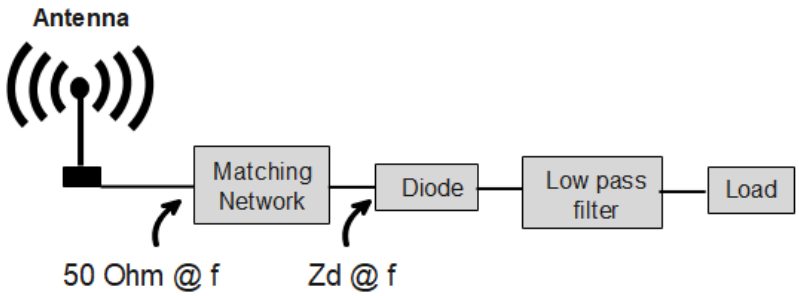

Figure 2.1: Block diagram of conventional rectenna with single-band matching network.

2.2.1 Antenna

The antenna is a vital element in RF energy harvesters, which is used to capture the electromagnetic waves from the ambient space and then send them into the rectifier. Therefore, the energy harvesting antenna should be designed carefully to meet the system requirements. Antenna configurations were and still are a very hot topic in research for both electrical and physical communities. For designers, there are a lot of techniques developed to design antennas as illustrated in the state of art, so the principle and characteristics of an antenna will be discussed. However, the discussion focused on the antenna design that is suitable for IoT devices. This type of antennas has a challenge due to capturing a low range of power available in space [52]. Studying the requirement of the antenna design, a transmitted equation will be discussed first, and then the parameters of sending and receiving antenna preferred for energy harvesting systems will be discussed as well.

2.2.1.1 Transmission Equation for the Microwave Signals

Figure 2.2 shows the experimental setup of the rectenna under test. A source of

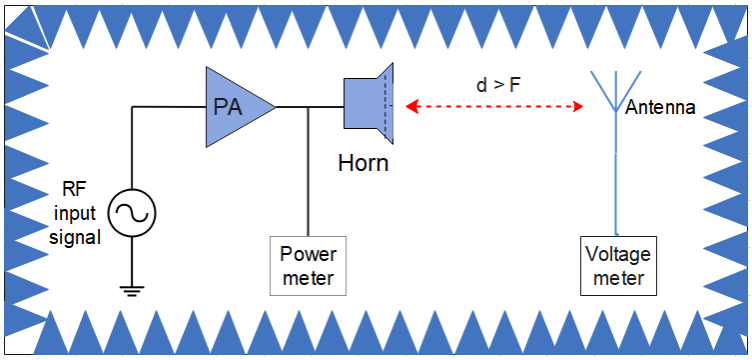

Figure 2.2: Connection arrangement

power which is a transmitting antenna, a rectenna (i.e., receiving the power), a Vector Network Analyzer (VNA), and cables, represent parts of the experimental setup. To describe mathematically power transmission of the microwave signals from an emitter to a receiver, the Friis equation is given as[53].

$$\frac{P_r}{P_t} = G_r G_t (\frac{\lambda}{4\pi d})^2 \tag{2.1}$$

It represents a ratio between receiving power P_r to transmitting power P_t, where G_t is the gain of the transmitting antenna, G_r is the gain of the receiving antenna, d is the distance between the two antennas, and λ is the wavelength of the microwave signals.

The antenna pattern is a response of the antenna to the incident wave in the desired direction. For observing a radiation pattern at the far-field region, a Fraunhofer distance should be calculated from Equation (2.2) , representing the limit between regions of the far and near fields. Consequently, the distance between transmitting and receiving antenna for a far-field region must be larger than the Fraunhofer distance.

$$d_f = \frac{2D^2}{\lambda} \tag{2.2}$$

where D is the largest physical dimension of the emitting antenna. For example, if the emitting antenna area is 18 cm and the frequency is 2.4 GHz, then the distance between

the two antennas should be at least equal to 0.518 m.

2.2.1.2 Patch Antenna

The printed antenna is the optimal choice due to its easy manufacturing. Various types of antennas can be met the design demands such as a patch antenna, a monopole antenna, dipole antenna, and so on. For narrowband microwave wireless applications, a microstrip patch antenna is the most commonly used as resonant antenna, because it has a low profile, low cost, lightweight, and has easy fabrication. The microstrip patch antenna can be easily printed on the circuit board [66].

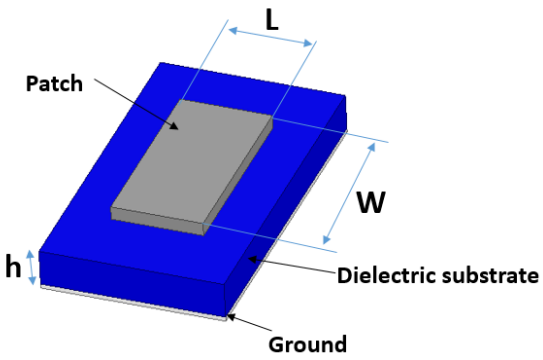

Figure 2.3: Component of patch antenna

The patch antenna consists of four-part: a radiating element (patch), a dielectric substrate, a ground plane, and a feeding source as illustrated in Figure 2.3. Dielectric substrate material should be chosen carefully because a material with a high dielectric constant produces a compact antenna, but the gain will be degraded due to increasing losses, and decreasing efficiency. On the other hand, the substrate with a low dielectric constant has high efficiency and large bandwidth, but the size is large. A ground plane made of metal is placed at the bottom of the substrate with the same dimensions. The radiating element can take any geometrical shape, while the popular forms are rectangular and circular. In the end, four types of feeding techniques can be used with the patch antenna. The impedance matching of the patch antennas will be discussed later in this chapter to know a perfect position, making the element more effective in the

radiation mechanism.

A rectangular patch antenna with a length of half wavelength at the resonant frequency radiate as two slot aperture as shown in Figure 2.4. In practice, the effective length of the patch should be less than a half wavelength due to the fringing fields which make the patch seeming larger. The current is zero at the patch edges and maximum at the center while the voltage is maximum at the edges. The current is out-of-phase with voltage while the current at the edges is in phase. Thus the current is added in-phase in space to produce the patch antenna radiation [58].

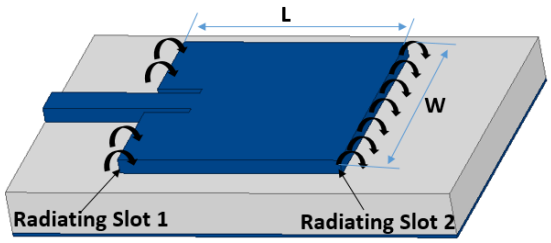

Figure 2.4: Top view of patch antenna

Meanwhile, the impedance at the patch edges is maximum because the current is zero (Z=V/ I), so the edge feeding is not always a good choice, and to overcome this problem the microstrip feed line will be inserted inside the patch matched at (50 ohm). However, this impedance can be inverted to zero, if the penetration depth of the feeding insertion is equal to a quarter wavelength, typically located at the patch center. As known, the impedance is inverted if move on a transmission line with a distance equal to a quarter wavelength. Hence, the feeding probe is not positioned at the center of the patch to avoid the grounding phenomena.

2.2.2 Impedance Matching Network

The impedance matching is an important part of the energy harvesting systems. This part is a two-port network, and each port has an impedance that is equal to a

conjugate impedance of the adjacent port of the closest circuit in the whole system. This ensures to get on phenomena of the maximum power transfer. In energy harvesting, the impedance of the rectifier is complex due to the non-linearity of the diode. The rectifier impedance is sensitive to change in frequency, load, and input power. As mentioned before, all these variables are considered as constant values at single band matching network, but in this thesis, we have made a noticeable modification on the matching part in the conventional rectifier, see Figure 2.5. A Dual-band matching network is utilized. Making a circuit operating at any two arbitrary frequencies is not a simple task. The reason behind that, the rectifier has two different complex input impedances, so the rectifier input impedance is a function with frequency. Moreover, powers and loads can influence the rectifier input impedance [59]. Impedance matching can be

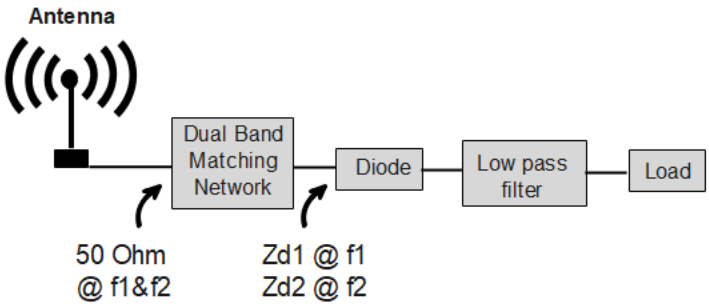

Figure 2.5: Schematic of dual band energy harvesting system

implemented using the smith chart which is used to convert the complex impedance of the load (Z_L) to a real value that is equal to 50 ohm or 75 ohm. The load will be matched well when it lies in the center of the chart. The matching performance depends on the reflection coefficient value that can be determined according to the incident and reflected voltage as in the following equation

$$\Gamma = \frac{V_{ref}}{V_{inc}} = \mid \Gamma \mid \angle\theta_r \tag{2.3}$$

where Γ is the reflection coefficient, V_{ref} is the reflected voltage, and V_{inc} is the incident voltage. If the Γ is equal to one that means all voltage has been reflected to the source

and no voltage reaches to the load, while all voltage will transfer to the load if the reflection coefficient is zero. The reflection coefficient is given in below utilizing the normalized value of the load and source impedance as:

$$\Gamma = \frac{Z_L - Z_o}{Z_L + Z_o} = \frac{Z_L/Z_o - 1}{Z_L/Z_o + 1} = \frac{z_L - 1}{z_L + 1} \tag{2.4}$$

where Z_L is the load impedance, Z_o is the characteristic impedance, and z_L is the normalized value of load expressed as $z_L = r_L + x_L$. An r_L is the resistance and x_L is the reactance of the load impedance. The matching network can be implemented using lumped elements, transmission lines, or both.

2.2.2.1 Lumped Elements

The matching circuit can be designed using only reactive components such as capacitors and inductors. The resistors are not preferred because they are not able to diminish the imaginary part in the complex load impedance. In addition, they add losses to the circuit, thereby reducing the system efficiency. When the capacitor and inductor were selected for matching, some parameters should be taken into account. The quality factor Q should be high, and its value depends on the frequency. In capacitors, the Q value is inversely proportional to the frequency. The Q is low at high frequencies, whereas, in inductors, the Q value is high at high frequencies. But at high frequency, there is another issue that will appear in the inductor which is the DC resistor. This parasitic effect should be low as much as possible. Also, there is another issue causing a big challenge when we want to deal with lumped elements. This issue is the Self-Resonant Frequency (SRF). Parasitic effects, for example, make the inductor having capacitive behaviors or vice versa. Consequently, the reactive element will be like a resonant tank. Therefore, to avoid this problem, the element must operate under the SRF. The component characteristic depends on the manufacturer; for example, the

Murata Company is one of the leading manufactures in the electronic markets [60].

2.2.2.2 Transmission Lines

A transmission line can be used to move the complex impedance of the load in a form of circles on the Smith chart. There are different ways of matching using transmission lines like single stub tuning, shunt stub, series stub transmission lines [61]. The use of lumped elements reduces the size of the circuit but it has high losses compared to using the transmission lines. A matching circuit with the transmission lines occupies a large space, so the choice relies on the allowed circuit size.

2.2.3 Rectification Theory

The rectifier is a key of the rectenna system because it is responsible for converting AC voltage to DC, utilizing the diode. A nonlinear RF Schottky diode is used due to its low forward voltage. The nonlinearity of the Schottky diode is due to the equivalent junction capacitance (C_j) and junction resistance (R_j), see Figure 2.6. The series resistance (R_S) is considered a linear element because it varies slowly compared with frequency and power [51]. Furthermore, the C_P is parasitic capacitance and L_P is the parasitic inductance due to the IC-packaging. C_j value is proportional with (V_D)

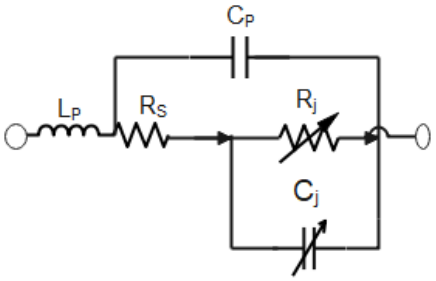

Figure 2.6: The equivalent circuit of the Schottky diode with its package

that represents the voltage on the terminal of R_j.

$$C_j \propto V_d^{-1/2} \tag{2.5}$$

Consider V_o is the maximum input sinusoidal signal voltage which has zero phase shift then

$$V_d = V_o cos(wt + \phi) at(\phi = 0) \implies V_d = V_o cos(wt) \tag{2.6}$$

The current follow through $R_j$is

$$I_d = I_S(exp^{\frac{qV_d}{NKT}} - 1) \tag{2.7}$$

where Is is the saturation current (typically $1x10^{-}12A$).

q is the charge of electron ($1.6x10^{-}19Coulom$).

k is Boltzmann's constant ($1.38x10 - 23JK^{-}1$).

T is the junction temperature in Kelvins (290 K).

N is the emission coefficient (typically between 1 and 2)

assume $\frac{q}{NKT}$ is one value α and it about (1/25 mW).

To simplify equation 2.7 it will written in the form of

$$I_d = I_S(\text{exp}^{\alpha V_d} - 1) \tag{2.8}$$

Equation (2.8) shows that the relationship between current and voltage is nonlinear, so the output current consists of DC and harmonic components. The nonlinearity due to exponential expansion in Equation 2.8 is evident, which can be expanded using the Taylor series as following [63]

$$e^x = \sum_{n=1}^{\infty} \frac{x^n}{n} = 1 + x + \frac{x^2}{2} + \frac{x^3}{3} + ... \tag{2.9}$$

Then Equation (2.8) becomes

$$I_d = I_s(1 + (\alpha V_d) + \frac{(\alpha V_d)^2}{2} + \frac{(\alpha V_d)^3)}{3} + ...) \tag{2.10}$$

From the equations above, it is concluded that there is one DC component in addition to the original signal and harmonic components. This behavior can be understood from the results of the circuit illustrated in Figure 2.7a. Also, Figure 2.7 shows phenomena of the nonlinearity in time and frequency domains. To improve the RF to DC conversion efficiency, the fundamental and harmonic frequency components should be prohibited to pass into the load. If they are returned back to the rectification process, this results in enhancing the system performance [62] . In this thesis, low pass filter and DC filter will utilize to reject harmonics from passing to the load as will be discussed later in Chapter 3.

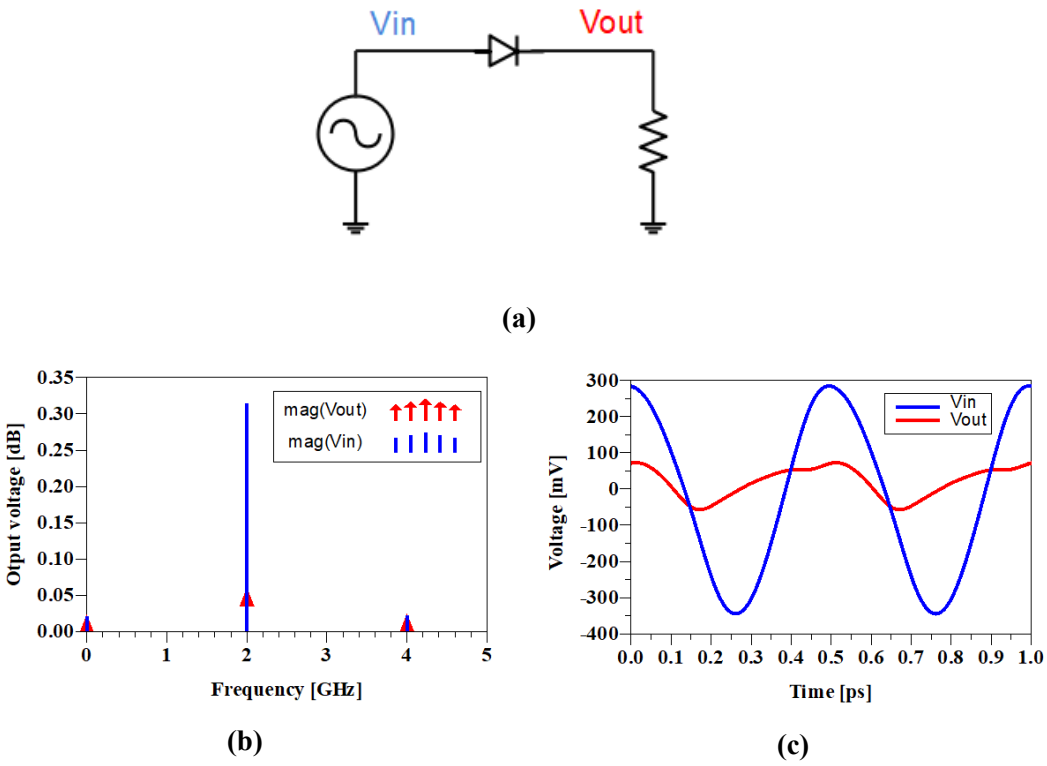

Figure 2.7: A rectifier schematic with its responses (a) circuit schematic (b) response in the frequency domain (c) response in time domain

For figuring out the (I-V) characteristic of the diode, a DC simulation in ADS (advanced design system) software is implemented using vendor model of the diode in program library and SPICE (Simulation Program with Integrated Circuit Emphasis)

model that can be designed using datasheet information of the diode. The two model circuits are illustrated in Figure 2.8.

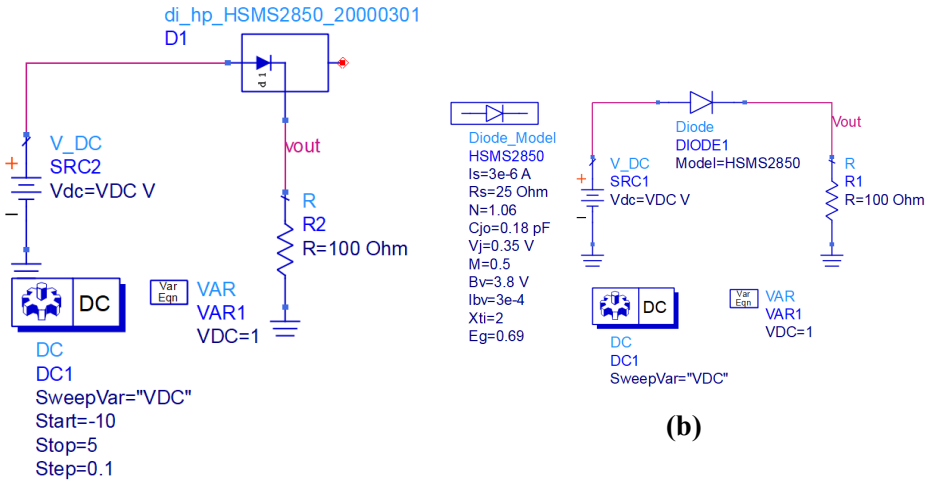

Figure 2.8: DC simulation for (a) vendor model (b) SPICE model

When the DC voltage applied is larger than the threshold voltage of the diode, the diode will turn "ON" and then the current and voltage will pass through the diode. Otherwise, the diode is turned "OFF" and no current can follow through it. When the negative part of the input signal is applied to the positive terminal of a diode with a value larger than the breakdown voltage, the diode behavior will be exotic. The (I-V) characteristic curves of the vendor and SPICE models are shown in Figure 2.9. It can be observed that both curves exactly fit because their DC characteristics are the same. The (I-V) characteristic relationship of the diode is nonlinear owing to the nonlinear behavior of the Schottky diode [63].

The input impedance of the diode is complex and it can calculate as [65]

$$Z_{in} = \frac{\pi R_S}{cos\theta_{off}(\frac{\theta_{off}}{cos\theta_{off}} - sin\theta_{off}) + jwC_jR_S(\frac{\pi-\theta_{off}}{cos\theta_{off}} + \theta_{off})} \tag{2.11}$$

where R_S is the wasted power in the diode, W is the angular frequency $= (2\pi f)$, and

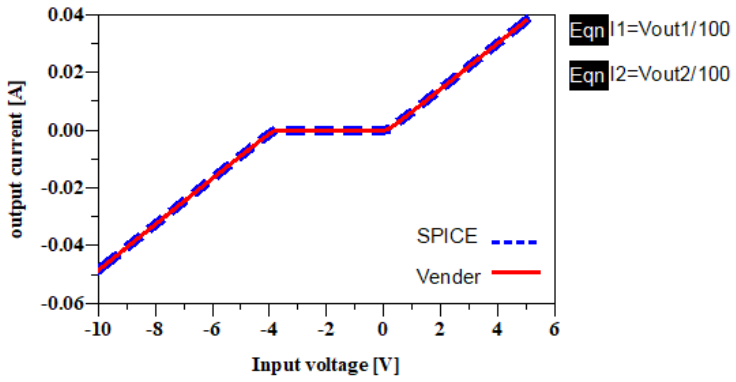

Figure 2.9: (I-V) characteristic of (HSMS2850) diode for vendor and SPICE model

θ_{off} can calculate as [64]

$$cos\theta_{off} = \frac{V_f + V_o}{V_{in}} \tag{2.12}$$

where V_f is the forward voltage, V_o is the output voltage, and V_{in} is the input voltage. To be clear see Figure 2.10. The nonlinear capacitance C_j can be calculated by [64]

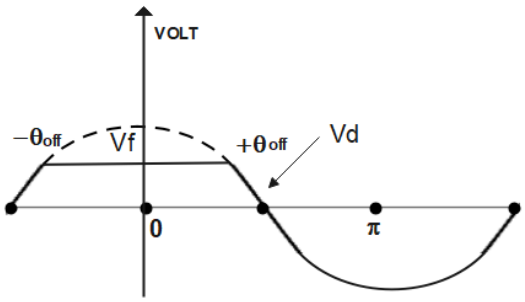

Figure 2.10: Input signal

$$C_j = C_{jo}(1 + \frac{V_o}{V_f})^{-M} \tag{2.13}$$

where C_{jo} is zero bias capacitance junction and M is grading coefficient. As can be observed from the input impedance equations, the results are affected by a change in frequency (w), input power (V_{in}), and load (R_L) where $V_o = R_L * I$. To illustrate these dependencies, input diode impedance is calculated concerning a change in input power and frequency as shown in Figures 2.11 a and b. The real part of the input impedance varies from 50ohm to 300 ohm when the input power is high (i.e., >-15

dBm) and frequency is less than 2 GHz. Furthermore, the imaginary part is changed from -500 ohm to 0 ohm. The one thing that has been noticed here is that the imaginary part is not sensitive to the change in the input power as a real part of the diode input impedance does. Thus, much attention should be paid to the imaginary part to mitigate its impacts on the circuit matching. In Figure 2.12 a,b, the real and imaginary parts of the rectifier input impedance are plotted versus the load resistance ranged from 100 ohm to 1500ohm, knowing that all the results, introduced in Figures 2.11 and 2.12,

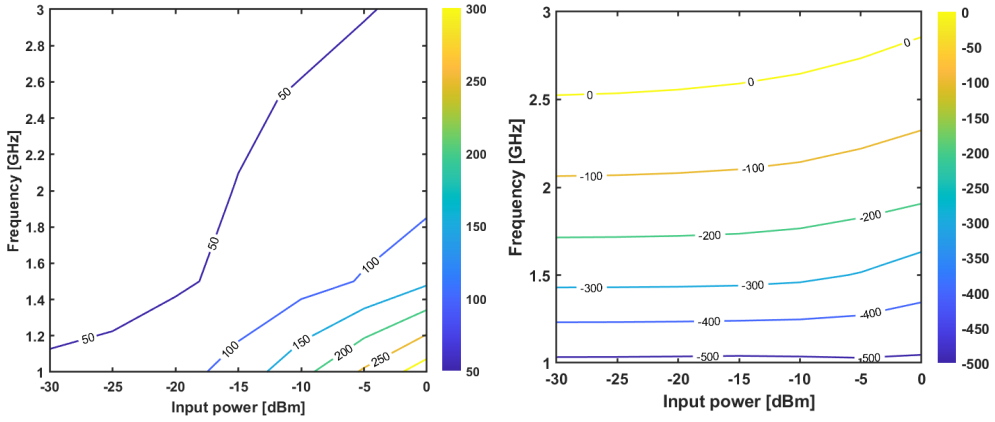

(a) **(b)**

Figure 2.11: Input impedance of a rectifier without matching versus frequency and input power with a load of 1500 ohm (a) real part (b) imaginary part

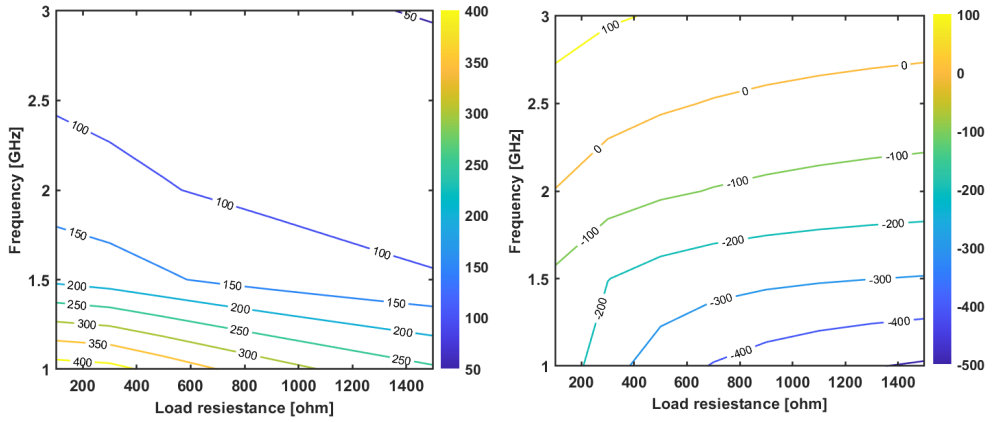

(a) **(b)**

Figure 2.12: The input impedance of rectifier without a matching network versus frequency and load resistive for an input power of -5 dBm (a) real part (b) imaginary part

belong to a single series diode rectifier without a matching circuit. This investigation aids to know the values of the circuit impedance to ease the matching process.

CHAPTER THREE

Single rectenna

3.1 Introduction

This chapter present methodology that following to design single rectenna. At first the rectifier circuit is design then a comparison between diode type is utilized to select the best one for low power range. the rectifier topology also depend on the range of input power so a comparison between two type is present. after that a matching network oparte with dual band is design and its results is compote. At the end, the single rectenna results is illustrated.

3.2 Rectifier circuit

The rectifier is a main part of the rectenna due to its capability to convert RF signals into DC signals then power saved at the power storage (i.e., capacitors). The amount of power storages depends on the performance of the rectifier, it will add much amount of power at the same input power range, if the rectifier acts well. As a consequence, the rectifier design should be high sensitivity to low input power due to the low range of power available in the ambient. A Large-Signal S-Parameter (LSSP) and Harmonic Balanced (HB) tools in ADS software are utilized to design a rectifier operate at dual-bands 1.8 GHz (GSM band) and 2.4 GHz (WiFi band).

3.2.1 Diode Selection

The important part of the rectifier is the diode because of its function of converting the power. A Schottky diode will be utilized due to its low threshold voltage.
All the products in the HSMS-28xx Schottky diode family handle the same chip but they vary only in package forms. Therefore, a vendor model of the diode is used in the

rectifier circuit to compute the conversion efficiency of each diode type as a function of the input power. The circuit used in the analysis consists of a resistance load R= 820 ohm and capacitance C=82 pF. A result of the comparison is shown in Figure 3.1. As deduced, the HSMS-2820 diode is suitable for high input power, while the HSMS-2860 is a good choice for the medium power level. Furthermore, the HSMS-2850 is the best selection for the low power due to its low forward voltage (0.15 mV) as shown in Figure 3.1. This comparison aims to give the interested readers an impression of how to select a diode to operate well with that application. Table 3.1 illustrates the SPICE

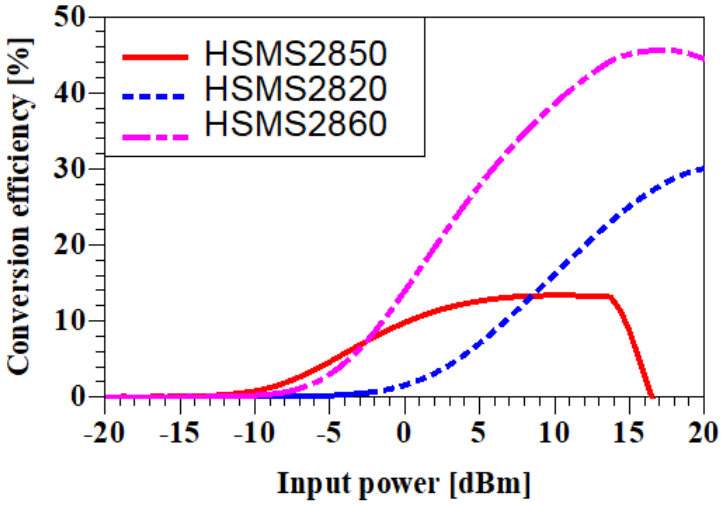

Figure 3.1: Comparison of three types of Schottky diode HSMS-2850, HSMS-2860, HSMS2820

parameters of the Schottky diode HSMS-28xx. B_V is the reverse breakdown voltage. I_{BV} is the current at the breakdown voltage. EG is the bandgap energy. XTI is the saturation-current temperature exponent (3 for P-N junction; 2 for Schottky). XTI and E_G take part in defining the dependence of Is. V_f is the forward voltage drop, which depends on the forward current. In this work, an HSMS 2850 Schottky diode is used because it the optimum choice for a low power range that will depend in this thesis.

3.2.2 Rectifier Topology Selection

Having chosen the suitable diode, the other important thing that should be figured

Table 3.1: A SPICE model of the Schottky diode HSMS 28XX group.

Diode type	HSMS 2820	HSMS 2850	HSMS 2860
B_V(V)	15	3.8	7
I_{BV}(A)	10E-4	10E-4	10E-5
C_{jo}(pF)	0.7	0.18	0.18
E_G(eV)	0.69	0.69	0.69
I_S(A)	2.2E-8	3E-6	5E-8
N	1.08	1.06	1.08
$R_S(\omega)$	6	25	5
V_j(V)	0.65	0.35	0.65
X_{TI}	2	2	2
M	0.5	0.5	0.5
V_f	340 mV ($I_f = 1mA$)	250 mV ($I_f = 1mA$)	350mV($I_f = 1mA$)

out is the rectifier topology. There is a bunch of rectifier typologies and each topology has its benefits over others relying on the application and the power density available in space. The most common typologies are the single series diode for low power applications and the voltage doubler for moderate and high power applications as shown in Figure 3.2. To demonstrate their operations with the same range of power and a frequency of 2.4 GHz. The HSMS2850 Schottky diode is used with a series inductor L=14nH and a shunt capacitor C=47 pF to operate as a DC filter that will be discussed later in chapter 3.

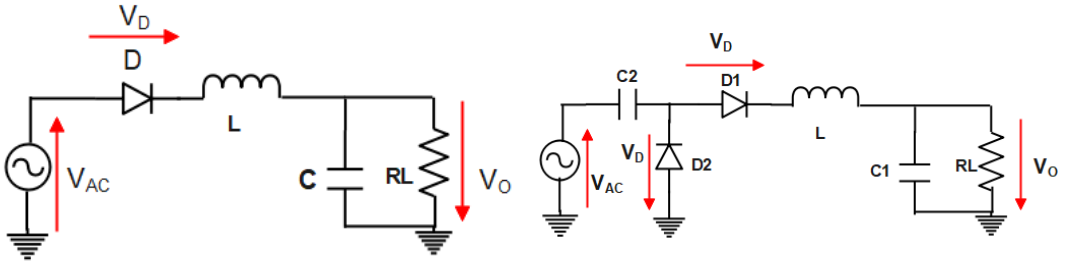

Figure 3.2: Configurations of the rectifier topology (a) single series (b) voltage doubler

Figure 3.3 displays the RF to DC conversion efficiencies for both circuits. As can be seen, the single series rectifier performs very well with low input power and the effi-

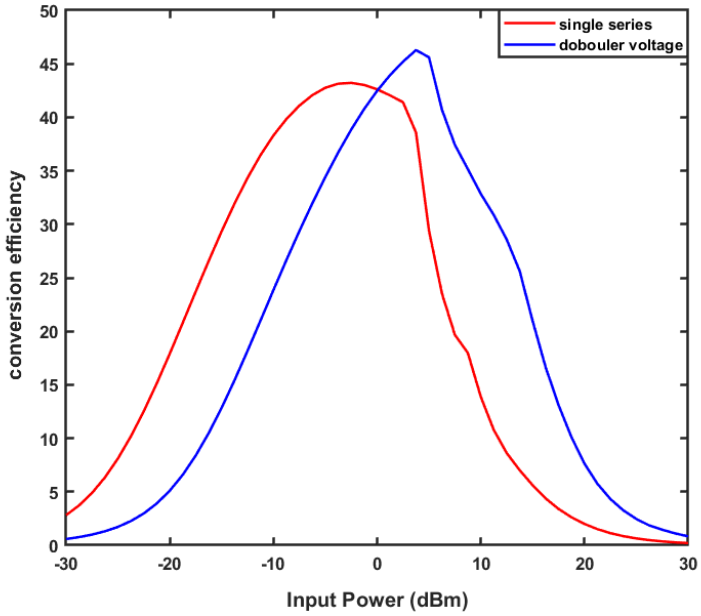

Figure 3.3: Simulated RF to DC conversion efficiencies for the series single rectifier and voltage doubler rectifier typologies

ciency reaches its maximum value of about 42% at the input power of -5 dBm, whereas the voltage doubler has a maximum efficiency of about 46% at nearly 5 dBm. Therefore, the designers will select the appropriate topology depending on how much power they should deal with. Because the voltage doubler has two diodes in its underlying design, it consumes high power. The single series rectifier is considered as the optimum option for low input power due to utilizing only one diode. Its conversion performance degrades when the input power is larger than 0 dBm since the input voltage exceeds the breakdown voltage of the diode. From the discussion given above, the single series rectifier will be chosen in the proposed design because the purpose is to scavenge the low power.

3.2.3 Rectifier Circuit Competent Selection

It's important to select the perfect value of rectifier component capacitance (C) and resistive load (R_L) to be suitable for both operating frequencies. A calibration between conversion efficiency and output voltage results should be taken into account because the output voltage has a directional relationship to the load value where $V_o =$

R_L/I_L, thus it increases when the load increase. The high value of resistive load will reduce the efficiency of the circuit because the losses will increase. An optimization in the ADS software is implemented as shown in Figure 3.4 to have the optimum value for the rectifier component where the resistive load (R_L) is 1500 ohm and capacitance (C) is 47 pF.

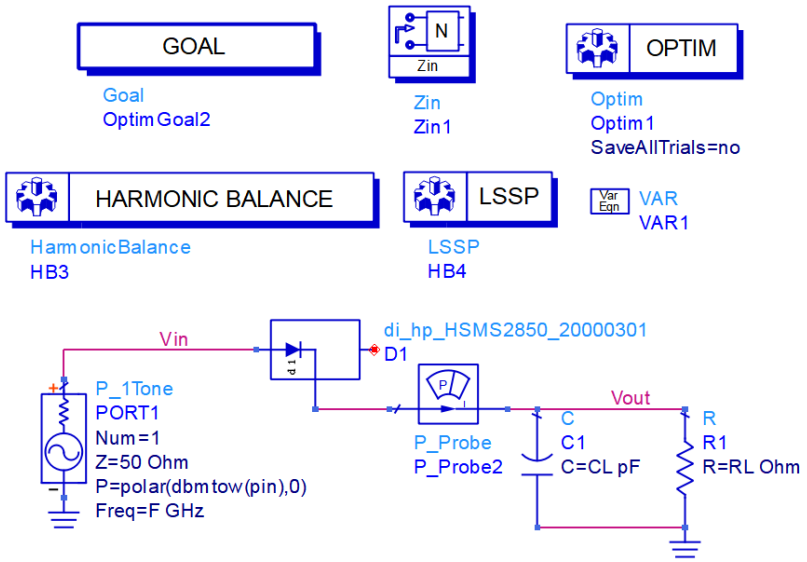

(a)

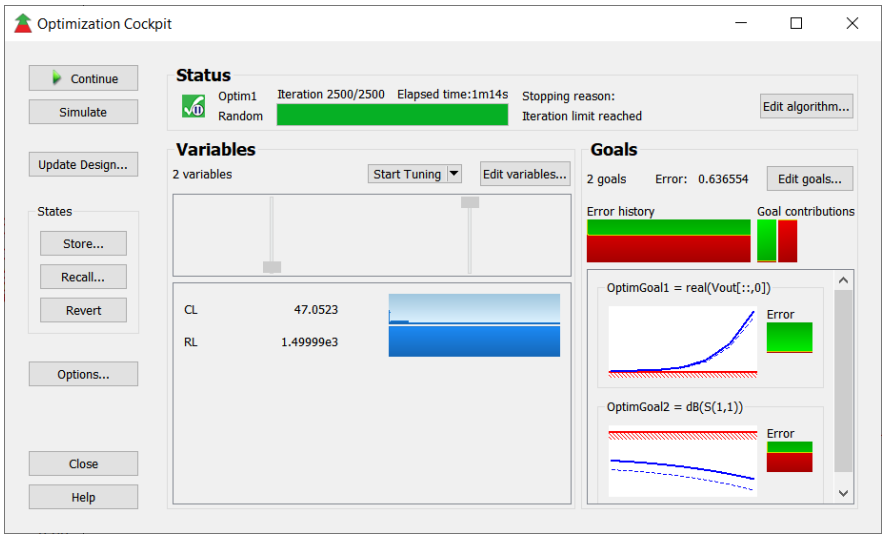

(b)

Figure 3.4: An optimization process to select the rectifier circuit component (a) schematic circuit (b) Optimization

3.2.4 DC Filter Non-Linearity

The non-linearity response of the Schottky diode will generate harmonics so, a part of the power will reflect to the source and the overall efficiency of the circuit will degrade. A DC filter is applied after the diode to prevent harmonics reach to the load. A series indicator (L_1= 14 nH) and shunt capacitance (C_1=47 pF) is added after the diode as shown in Figure 3.5 to operate as a low pass filter. Only the DC component reaches the load while fundamental and other harmonics are eliminated.

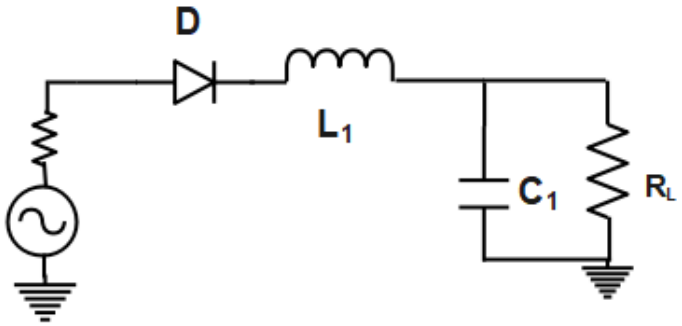

Figure 3.5: Schematic of rectifier circuit with a series inductor

Figure 3.6 illustrates the effect of the added inductor on the harmonics. It can observe the affect of the inductor on the third harmonic by reduced it from (-80 to -103) dB, while the second harmonic is eliminated by using a good matching circuit. Furthermore, Figure 3.7 illustrates the response of the rectifier circuit before and after the inductor was added. As shown the efficiency of the circuit rising from (5 to 42) % and the output voltage also rises from (0.16 to 0.5) V. This results can increase by implementing a good matching network.

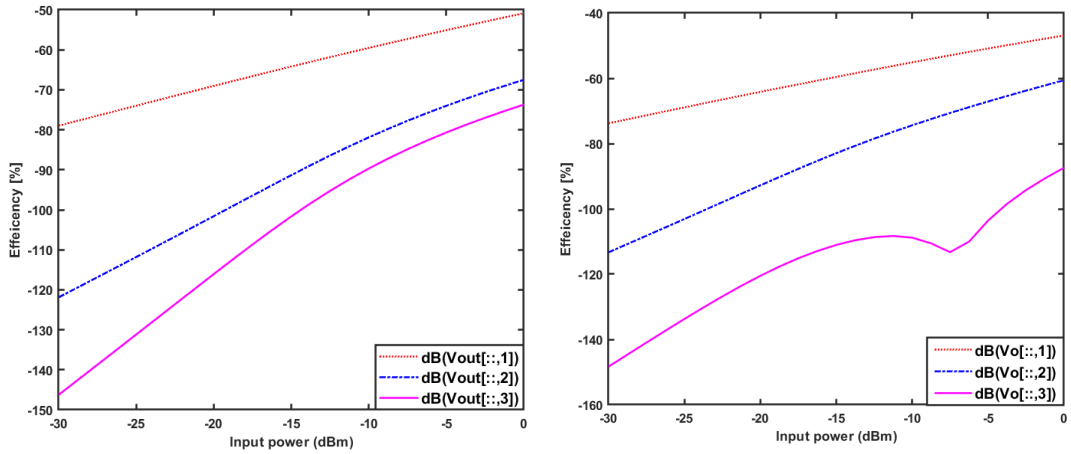

(a) **(b)**

Figure 3.6: Affect of DC filter (a) harmonics at the output without inductor (b) harmonics after series inductor added

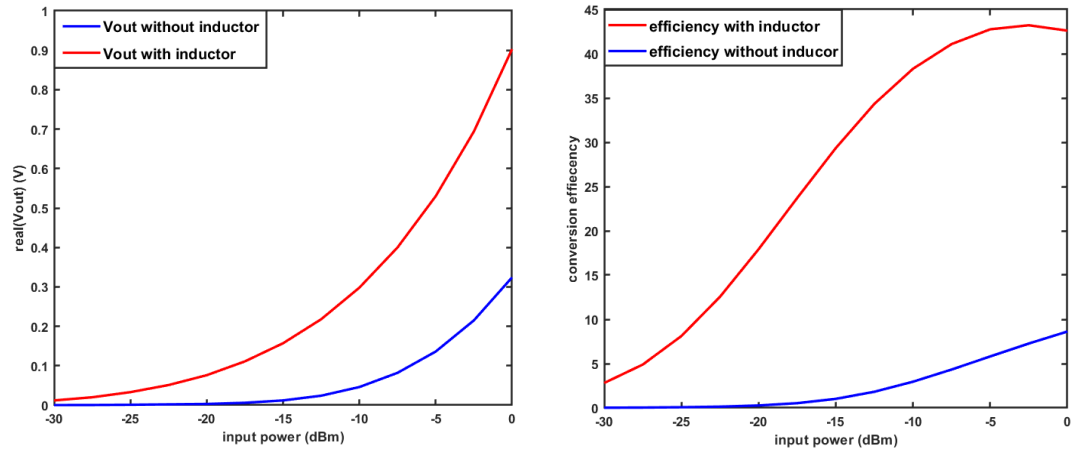

(a) **(b)**

Figure 3.7: Affect of DC filter(a) output DC voltage with and without inductor (b) the conversion efficiency of the rectifier with and without inductor

3.3 Matching Network

Impedance matching network is a key part of most microwave and RF circuits because it ensures the maximum power transfer among parts of the one circuit. Furthermore, it rejects the harmonics propagating backward from one part to another because it acts as a bandpass filter BPF, but with unequal port impedance, unlike the conventional filters. When the microwave circuit operates at a fixed frequency, input power, and fixed load this leads to the circuit operating under fixed circumstances. However,

as mentioned earlier, in rectifiers, impedance is variable. Unless the matching circuit is designed carefully, the overall performance will deteriorate with a slight change in the diode impedance. Typically, the matching circuits are designed to operate at only one frequency and this is normal in the RF circuits because they work at that frequency. On the contrary, it is desirable to harvest the ambient power from a wide range of frequencies to collect power as much as can. As the number of frequency bands is increased, the circuit complexity increases. Both circuit parts and sizes are matter. If lumped elements are used, sizes will be smaller than circuits consisting of transmission line, but extra losses introduced by lumped elements will be added. Mostly, the compromise has been made to achieve in between goals. Hence, the goal is to build very small footprint circuits with lumped elements.

The mathematical analysis of the adopted Composite Right Left handed (CRLH) technique to design the proposed dual-band matching circuit is introduced in the following discussion. The complex input impedance can calculate using the ABCD matrix then converted to S-parameter matrix.

The input impedance of any two port network perfect matching (ie.reflection coefficient of load equal zero) can be given by [67].

$$Z_{in} = Z_0 \frac{1 + S_{11}}{1 - S_{11}} \tag{3.1}$$

where Z_o is reference impedance and S_{11} is reflection coefficient. S_{11} can be calculate by using ABCD to S-matrix matrix conversion.

$$\begin{bmatrix} S_{11} & S_{12} \\ S_{21} & S_{22} \end{bmatrix} = \frac{1}{A + B/Z_r + CZ_r + D} \begin{bmatrix} A + B/Z_r - CZ_r - D & 2(AD - BC) \\ 2 & -A + B/Z_r - CZ_r + D \end{bmatrix} \tag{3.2}$$

where Z_r is the reference impudence of converting from ABCD matrix to S-matrix. For complex impedance transforming Equation (3.2) can not be used else $Z_r = Z_o$ thus, for a complex input impedance of using lumped element a modification for Equation (3.2) will performed. However, a new method for calculating complex Z_r will explained.

The using current and voltage equation for two complex port network can determined as [68].

$$I_i = \frac{2\sqrt{R_e Z_{ri}}(a_i - b_i)}{Z_{ri} + Z_{ri}^*} \tag{3.3}$$

$$V_i = \frac{2\sqrt{ReZ_{ri}(a_i Z_{ri}^* + b_i Z_{ri})}}{Z_{ri} + Z_{ri}^*} \tag{3.4}$$

where i is the port number in the two port network.a_i and b_i are incident and reflected wave respectively. Assume that Z_{r1} is real and Z_{r2} is complex for complex impedance transforming.

To obtain S_{11}, ABCD matrix parameter can be calculated by using Equations (3.3) and (3.4)

$$A = \frac{V_1}{V_2}_{I_2=0} = \sqrt{\frac{R_{r1}}{R_{r2}}}\frac{a_1 + b_1}{2a_2}, \qquad C = \frac{I_1}{V_2}_{I_2=0} = \frac{1}{\sqrt[R_{r1}]{R_{r2}}}\frac{a_1 - b_1}{2a_2} \tag{3.5}$$

When $I_2 = 0$ port two is open circuit so, the reflection wave is in the same phase with incident wave (ie. $a_2 = b_2$)

$$B = \frac{V_1}{I_2}_{V_2=0} = \sqrt{R_{r1}R_{r2}}\frac{Z_{r2}}{Z_{r2}^*}\frac{a_1 + b_1}{2a_2}, \quad D = \frac{I_1}{I_2}_{V_2=0} = \sqrt{\frac{R_{r2}}{R_{r1}}}\frac{Z_{r2}}{Z_{r2}^*}\frac{a_1 - b_1}{2a_2} \tag{3.6}$$

When $V_2 = 0$ port two is short circuit and the reflection wave is out of phase with incident wave (ie. $a_2 = -b_2$). From Equation (3.5) and (3.6), S_{11} can be

$$S_{11} = \frac{b_1}{a_1} = \frac{A\sqrt{\frac{R_{r2}}{R_{r1}}} + B/\sqrt{R_{r1}R_{r2}}Z_{r2}^{'} - C\sqrt{R_{r1}R_{r2}} - D\sqrt{\frac{R_{r1}}{R_{r2}}}/Z_{r2}^{'}}{A\sqrt{\frac{R_{r2}}{R_{r1}}} + B/\sqrt{R_{r1}R_{r2}}Z_{r2}^{'} + C\sqrt{R_{r1}R_{r2}} + D\sqrt{\frac{R_{r1}}{R_{r2}}}/Z_{r2}^{'}} \tag{3.7}$$

where $Z_{r2}^{'}$ is Z_{r2}/Z_{r2}^{*}. Substituting Equation (3.7) in (3.1) to optain the input complex impedance as given

$$Z_{in} = Z_o \frac{AR_{r2}Z_{r2}^{'} + BjZ_o tan\theta}{DR_{r1} + CjY_o R_{r1}R_{r2}Z_{r2}^{'} tan\theta} \tag{3.8}$$

This equation can used to calculate an input impedance of circuit used transmission line, thus it should be equal to the conventional equation of transmission line

$$Z_{in} = Z_o \frac{Z_L + jZ_o tan\theta}{Z_o + jZ_L tan\theta} = Z_o \frac{R_{r2}Z_{r2}^{'} + jZ_o tan\theta}{R_{r1} + jY_o R_{r1}R_{r2}Z_{r2} tan\theta} \tag{3.9}$$

From equation 3.9, reference impedance can defined as

$$Z_{r1} = Z_o, \qquad R_{r2}Z_{r2}^{'} = Z_L \tag{3.10}$$

The assumption of Z_{r1} is real and Z_{r2} is complex achieve. Substituting Equation (3.10) into (3.8), input impedance of two port network using ABCD matrix can calculate as

$$Z_{in} = \frac{AZ_L + B}{D + CZ_L} \tag{3.11}$$

where Z_L is the load impedance, it consists of real and imaginary parts as in $Z_L = R_L + jX_L$ Values of A, B, C, and D rely on the type of the circuit utilized in the matching network and values of lumped elements. This equation is employed to design a dual-band matching network. Besides, it is used to calculate the scattering S-

parameters. Various types can be found in [69] regarding dual-band matching networks using lumped elements, but only one type is adopted here to achieve research task. This circuit is the series-shunt type shown in Figure 3.8.

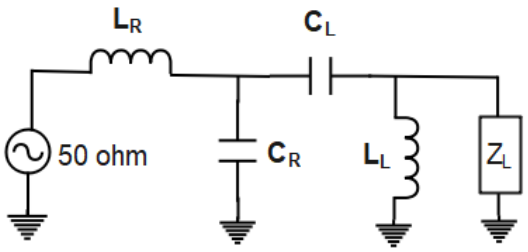

Figure 3.8: Series-Shunt connection of dual band impedance transforming

The proposed circuit operates at 1.8 GHz and 2.4 GHz. These two frequencies are chosen since they are always available in the indoor and outdoor space. A smith chart in ADS software is used to design the dual-band series shunt matching network. To demonstrate how it occurs, let us follow this procedure. First, the circuit is designed at the lower frequency of 1.8 GHz, where the shunt inductance L_L and series capacitance C_R lumped elements are responsible for doing. Then, the series inductance L_R and shunt capacitance C_R are optimized to match the circuit at the higher frequency of 2.4 GHz. The subscript L stands for the left or lower frequency band, while the subscript R stands for the right or high-frequency band. Due to a rule of thumb, that when selecting a matching component, the component should have more impact in the target band and less effect in the other band. For example, the series inductance L_R is one of the components used to match the circuit at the second frequency, and it should have a zero or close to zero impedance at the first frequency. In other words, this lumped element does not have any impact on the matching of the other frequency [60].

The ABCD matrix of series shunt type can calculate by multiplying ABCD matrix

of series impedance and ABCD matrix of shunt admittance then obtain

$$\begin{bmatrix} 1 - X_p X_q & jX_p \\ jX_q & 1 \end{bmatrix} \tag{3.12}$$

Where $jX_p = Z$ and $jX_q = Y$

By using Equation (3.11) and ABCD matrix of((3.12)) input impedance of series shunt can be obtained as

$$Z_{in} = \frac{R_L + j\{X_L - X_L^2 X_q - R_L^2 X_q + (1 - 2X_L X_q + R_L^2 X_q^2 + X_L^2 X_q^2) X_p\}}{(1 - X_L X_q)^2 + (R_L X_q)^2} \tag{3.13}$$

From the input impedance of the diode mentioned in Equation (2.11) is

$$Z_{in} = \frac{\pi R_S cos\theta_{off} \left(\frac{\theta_{off}}{cos\theta_{off}} - sin\theta_{off}\right) - j\pi w C_j R_S^2 \left(\frac{\pi - \theta_{off}}{cos\theta_{off}} + \theta_{off}\right)}{(\theta_{off} - cos\theta_{off} sin\theta_{off})^2 + \left(\frac{wC_j R_S}{cos\theta_{off}} \left(\pi - \theta_{off} + \frac{\theta_{off}}{cos\theta_{off}}\right)\right)^2} \tag{3.14}$$

It equal to the input impedance of series shunt connection so, after separated the input impedance for real and imaginary parts. The real part of input impedance become

$$\frac{\pi R_S cos\theta_{off} \left(\frac{\theta_{off}}{cos\theta_{off}} - sin\theta_{off}\right)}{(\theta_{off} - cos\theta_{off} sin\theta_{off})^2 + \left(\frac{wC_j R_S}{cos\theta_{off}} \left(\pi - \theta_{off} + \frac{\theta_{off}}{cos\theta_{off}}\right)\right)^2} = \frac{R_L}{(1 - X_L X_q)^2 + (R_L X_q)^2} \tag{3.15}$$

Then using equation of the constitution to calculate X_q from Equation ((3.15)) as

$$X_q = \frac{\pi R_S cos\theta_{off} \left(\frac{\theta_{off}}{cos\theta_{off}} - sin\theta_{off}\right) \left(X_L \stackrel{+}{-} R_L\right)}{R_L \left(X_L^2 + R_L^2\right) \left[(\theta_{off} - cos\theta_{off} sin\theta_{off})^2 + \left(\frac{wC_j R_S}{cos\theta_{off}} \left(\pi - \theta_{off} + \frac{\theta_{off}}{cos\theta\, off}\right)\right)^2\right]} \tag{3.16}$$

From imaginary part of input impedance X_p can be calculate as

$$X_p = \frac{X_q\left(X_L^2 + R_L^2\right)}{\left(1 - X_L X_q\right)^2 + \left(R_L X_L\right)^2} - \frac{\pi w C_j R_S^2 \left(\frac{\pi - \theta_{off}}{cos\theta_{off}} + \theta_{off}\right)}{\left(\theta_{off} - cos\theta_{off} sin\theta_{off}\right)^2 + \left(wC_j R_S \left(\frac{\pi - \theta_{off}}{cos\theta_{off}} + \theta_{off}\right)\right)^2} \tag{3.17}$$

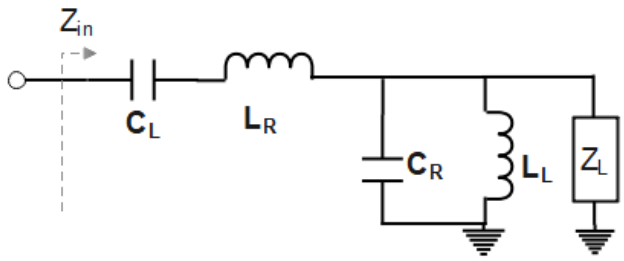

Figure 3.9: CRLH connection of dual band impedance transforming topology

The one deficit of this approach is that the radicals of X_q and X_p must be always a positive value. To overcome this problem, a combination of two series-shunt circuit types is used as in [69]. The adopted modification aids to increase the degree of design freedom and ensures that the radicals of X_q and X_p can be either positive or negative values. One of these combinations is the composite right left-handed (CRLH), is widely used in the last two decades to synthesize dual-band transmission lines. The synthesized transmission lines can be implemented using only lumped elements. Here in this thesis, a CRLH transmission line with only lumped elements will be used to have small footprints. Figure 3.9 shows a dual-band CRLH transmission line, acting as a dual-band matching network, connected to a load impedance Z_L varying with the frequency. As known, the CRLH has dual-band has band pass characteristics, where the resonance coming from the series resonant tank is called series resonance W_{ES} and the resonance coming from the shunt resonant tank is called the shunt resonance W_{SH}. The series and shunt resonant tanks have impedance Z and admittance Y, respectively, given as

$$Z = jX_p = j\left(w_s L_R - \frac{1}{w_s C_L}\right), \qquad Y = jX_q = j\left(w_s C_R - \frac{1}{w_s L_L}\right) \tag{3.18}$$

where w_s is the solution angular frequency. X_p and X_q can calculate from Equation (3.16),(3.17) of series shunt connection. Then for CRLH X_{p1} and X_{p2} can compute as

$$X_{p1} = w_s L_R - \frac{1}{w_s C_L} \qquad at f_{s1} \tag{3.19}$$

$$X_{p2} = K w_s L_R - \frac{1}{K w_s C_L} \qquad at f_{s2} \tag{3.20}$$

where K is frequency ratio, $K = f_{s2}/f_{s1} = w_{s2}/w_{s1}$ and $K > 1$. f_{s1} and f_{s2} are a first and second frequency respectively. Then to compote X_{q1} and X_{q2} the same procedure is flow.

Using solving disparate Equation of (3.19) and (3.20) to compote C_L

$$C_L = \frac{K^2 - 1}{w_s K \left(X_{p2} - K X_{p1}\right)} \tag{3.21}$$

then compote L_R from equation (3.19) as

$$L_R = \frac{1}{w_s}\left(X_{p1} + \frac{1}{w_s C_L}\right) \tag{3.22}$$

In the same way L_L and C_R are obtain

$$L_L = \frac{K^2 - 1}{w_s K \left(X_{q2} - K X_{q1}\right)} \tag{3.23}$$

$$C_R = \frac{1}{w_s}\left(X_{q1} + \frac{1}{w_s L_L}\right) \tag{3.24}$$

Having discussed and analyzed all the important information regarding the rectifier and the proposed dual-band impedance transformer, in this work, the proposed dual-band energy rectifier will be designed to operate at frequencies 1.8GHz and 2.4 GHz, but any two arbitrary frequencies can be considered. To evaluate its performance, the reflection coefficient, output voltage, and efficiency are optimized to obtain the best results as much as possible. The input power, load, and frequency are the most three

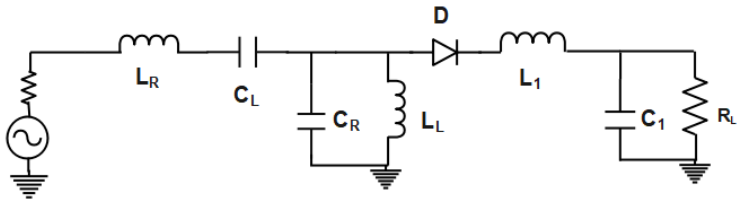

Figure 3.10: Schematic of rectifier with CRLH dual band matching network transforming

parameters that effectively impact rectifier performance. Thus, trading-off among them is imperative. In all simulations, real-world lumped components from Murata are utilized in order to make the results closer to the practical ones because each element in Murata has its associated parasitic effects. The circuit schematic is depicted in Figure

Table 3.2: Circuit component used in design

D	Schottky diode	HSMS2850 Skyworks
L_R	6.9 nH	LQW04AN6N9C00 Murata
C_L	0.4 pF	GRM0115C1CR40BE01 Murata
C_R	0.2 pF	GRM0115C1CR20BE01 Murata
L_L	4.6 nH	LQW04AN4N6C00 Murata
L_1	14 nH	LQW04AN14NJ00 Murata
C_1	47 pF	GRM0115C1C470GE01 Murata
R_L	1.5 Kohm	

3.10 R_L and C_1 represent the load and the low pass filter, respectively. The larger the R_L is, the larger the output voltage, but the efficiency is smaller. C_1 can be considered the main storage of the DC power, and it can also work to shorten out the AC signals. The latter function can be carried out with a help of the series inductor L_1. This inductor tends to have bigger impedance as the frequency increases, so fundamental and higher harmonics are attenuated to some acceptable extent. In the schematic, D_1 is the diode which is the main component, responsible for the rectification process, while all other remaining elements L_L, C_L, L_R, and C_R form the dual-band matching circuit.

Table 3.2 introduces a summary of the lumped element part number and its value. Furthermore, the traces connecting among all the circuit components are electromagnetically simulated and then are exported into the main schematic to take into account their losses. This procedure is called co-simulation and is achieved by the ADS software.

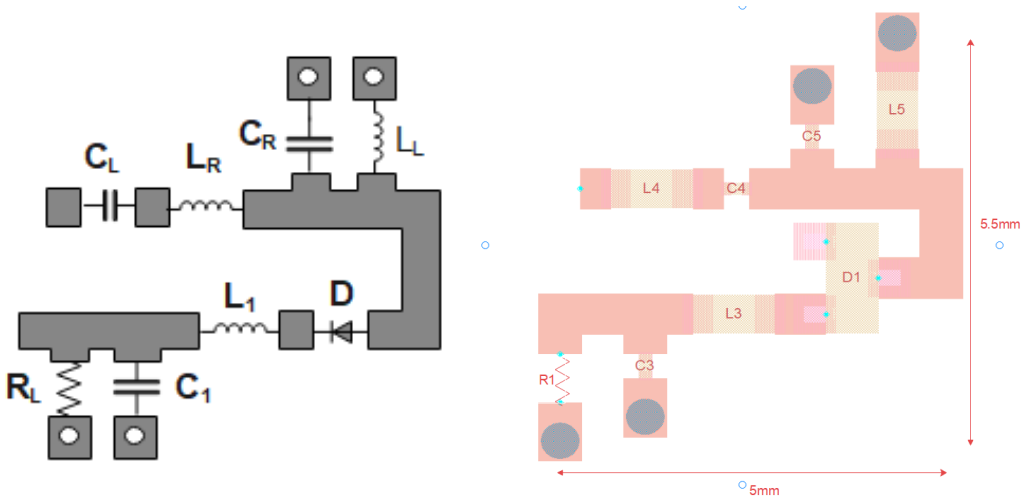

Figure 3.11: Final topology of the proposed dual-band rectifier where the fianl size on the PCB is 5.5X5mm2 (a) layout with lumped element symbols (b) layout with true layouts of lumped elements taken from the ADS software

The final real circuit with the true footprint layout for each lumped element is shown in Figure 3.11 The Roger Duroid 3010 laminate is used with a relative permittivity of 10.2 and a thickness of $0.5mm^2$.

3.3.1 Results and Discussion (Rectifier Performance)

The simulated reflection coefficient S_{11} of the rectifier circuit with different input power levels is depicted in Figure 3.12a. with a fixed load resistance of 1.5 kohm. As can be seen, the proposed rectifier is matched very well at frequencies of 1.8 GHz and 2.4 GHz even with varying input power. For both bands, the matching frequency tends to slightly shift to a lower frequency. This means that the matching operates well with the new resonant frequencies. However, matching of all bands is still satisfactory.

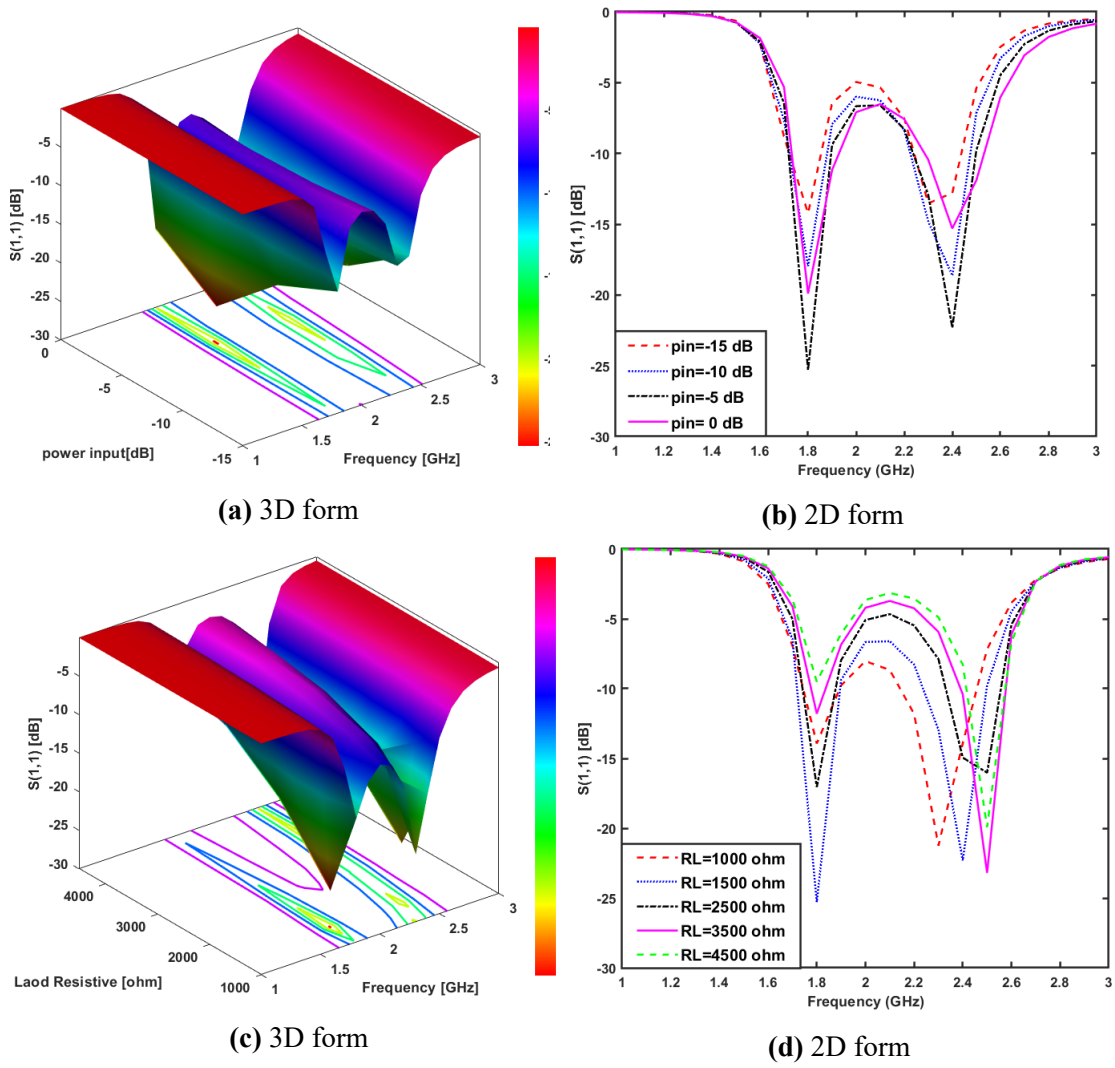

(a) 3D form

(b) 2D form

(c) 3D form

(d) 2D form

Figure 3.12: Reflection coefficient S11 of the rectifier with (a,b) Different input power levels and fixed load resistance value of 1.5kohm (c,d) Different load resistance values and fixed input power of -5dBm

Moreover, the frequency range between the two bands has S_{11} about -6 dB when the input power is equal to -5 dBm, and this could result in a wide-band rectifier which is very useful to harvest more power from space. The rectifier has good matching at -5 dBm where this value is close to the power available from typical sources such as WiFi, cellular, digital TV broadcasting, etc. In Figure 3.12 b, the input power is fixed at -5 dBm, and the load resistance varies from 1 kohm to 4.5 kohm. Load resistance of 1.5kohm provides the best results of matching at frequencies of 1.8 GHz and 2.4 GHz because the circuit is optimized at this value. As the input power increases the matching is improved, but the response begins to deteriorate after -5 dBm. This occurs

because the diode utilized in the proposed design is dedicated to operating at the low power levels.

The conversion efficiency and the output voltage can be calculated using the formulas given below as

$$Effeciency = \frac{P_{DC}}{P_{in}} * 100 \tag{3.25}$$

and output voltage

$$V_{out} = \sqrt[2]{P_{DC} X R_L} \tag{3.26}$$

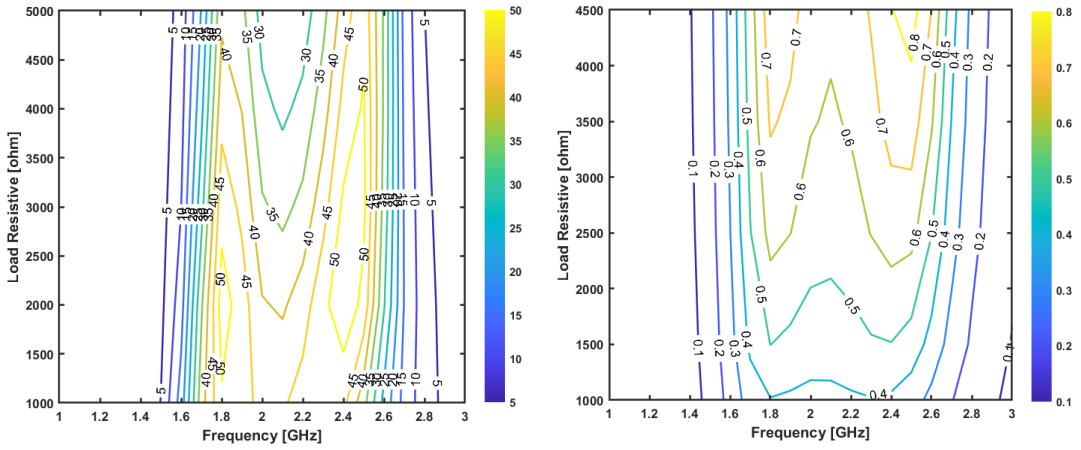

(a) **(b)**

Figure 3.13: (a) Conversion efficiency vs. frequency for different loads and fixed input power of -5dBm (b) Output DC voltage vs. frequency for different loads and fixed input power of -5dBm

Here, V_{out} and P_{DC} represent the DC output voltage and DC output power, respectively. P_{in} denotes the input power from the RF source. They are depicted in Figures 3.13 and 3.14. When R_L is equal to 1.5kohm, it gives rise to the highest efficiency, approximately about 53% for both bands, due to the benefit of CRLH dual-band matching network. As the matching increases, the more power will be transferred into the load. in other words, the efficiency increases, where the best matching occurs at a load value of 1.5 kohm. Apart from the optimum load value, especially when it increases,

the efficiency is noticeably decreased. This is reasonable as we stated before. On the contrary, the DC output voltage increases, as the load resistance increases. Even if the output voltage increases, the output DC power decreases, leading to the decrement in-

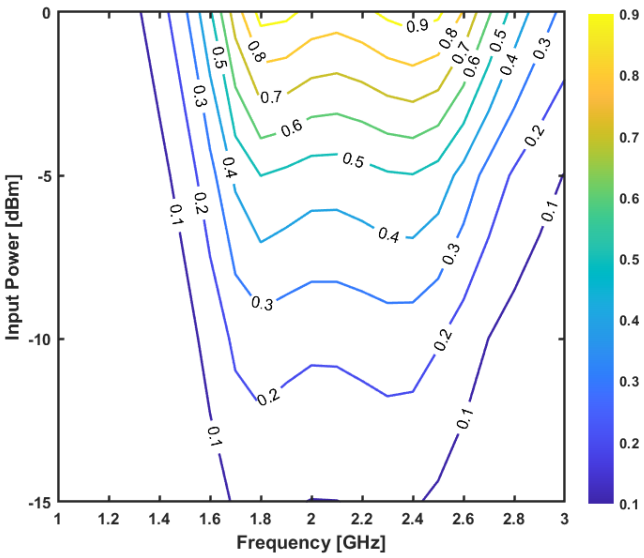

Figure 3.14: Output DC voltage vs. frequency for different input power and a fixed load of 1.5kohm

efficiency, see Figure 3.13 for more details. Figure 3.14 shows the output DC voltage versus frequency for different input power. Also, it increases when increasing the input power, and the output voltage reaches about 0.95 V at frequencies of 1.8GHz and 2.4 GHz. This voltage decreases to almost half when the input power becomes -5dBm. The dip between the two bands tends to diminish with decreasing in the input power and the two bands are emerged to be as a single wideband.

The S_{11} versus the input power is depicted in Figure 3.15 for 1.8 GHz and 2.4 GHz frequencies. The proposed circuit is well matched at about -5 dBm for both bands with large bandwidths. The simulated S_{11} is less than -20 dB which means that 99% of the input power is transferred into the load if we ignore the losses in lumped elements and transmission lines. Practically, some power will be absorbed and converted into heat.

Furthermore, the conversion efficiency at both bands versus the input power is il-

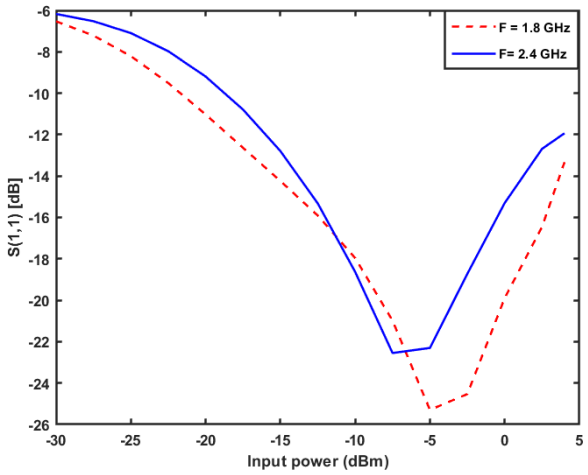

Figure 3.15: Simulation of S11 concerning input power at the two frequency band 1.8 and 2.4 GHz and a resistive load of 1.5Khom

lustrated in Figure 3.16. As can be seen, the efficiencies are almost equal at 0 dBm. After that, the diode fails to convert the power since the input voltage is larger than the diode's breakdown voltage. The efficiencies are almost 50%. At very low input power, the rectifier still operates and can supply DC voltages into the load. However, it becomes impossible when the input power is less than -25 dBm.

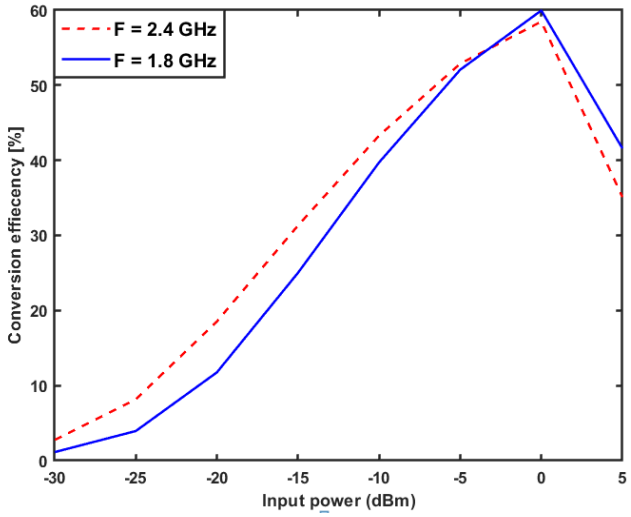

Figure 3.16: Simulation of conversion efficiency concerning input power at two frequency 1.8 and 2.4 GHz

Also, the conversion efficiency is simulated versus the input power with varying the load value for the first band. The efficiency reaches its maximum value the load

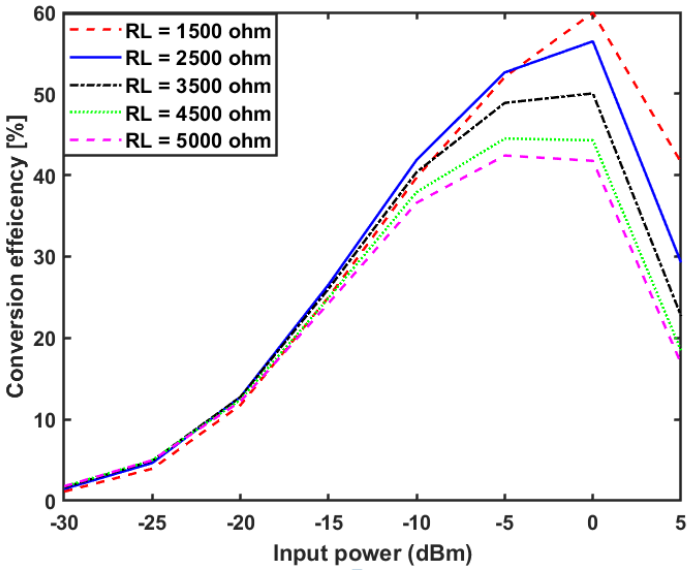

Figure 3.17: conversion efficiency concerning input power for different load resistive value

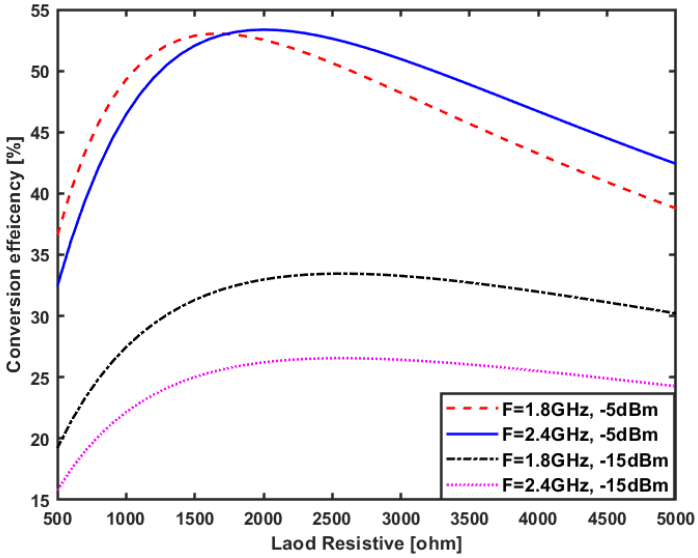

Figure 3.18: Conversion efficiency concerning resistive load at two frequency 1.8, 2.4 GHz and different input power

of 1.5 kohm and the power is almost 0 dBm, see Figure 3.17. Finally, the conversion efficiency and the S_{11} are simulated versus the load value for both bands and at the input powers -5 dBm and -15dBm as can be seen in Figures 3.18 and 3.19, respectively. The aim here is to demonstrate that our proposed design can operate at a wide range of loads. Consequently, we can say that the proposed design can be a good candidate for various applications.

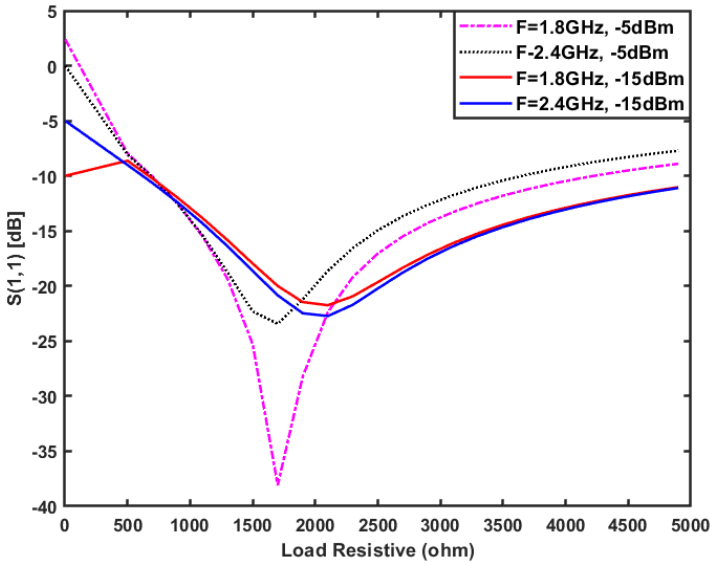

Figure 3.19: Reflection coefficient concerning resistance load at two frequencies 1.8, 2.4 GHz and different input power

3.4 Single Element Patch Antenna

The antenna type choice should be suitable for an energy harvesting system, a rectangular patch antenna is utilized due to its high gain to capture a sufficient amount of RF power from the ambient.

3.4.1 First Design with Microstrip Feed

A patch antenna with microstrip feed is designed using a High-Frequency Structure Simulator (HFSS) program, see Figure 3.20. First, the patch was designed at a low frequency of 1.8 GHz and the substrate used is Roger RT/ duroid 5880 with ϵ_r =2.2 and tangent losses of 0.0009 with a thickness of 1.575 mm^2. The dimension of the antenna can be calculated using the following equations [70].

$$W = \frac{c}{2\pi f}\sqrt{\frac{2}{\epsilon_r + 1}} \tag{3.27}$$

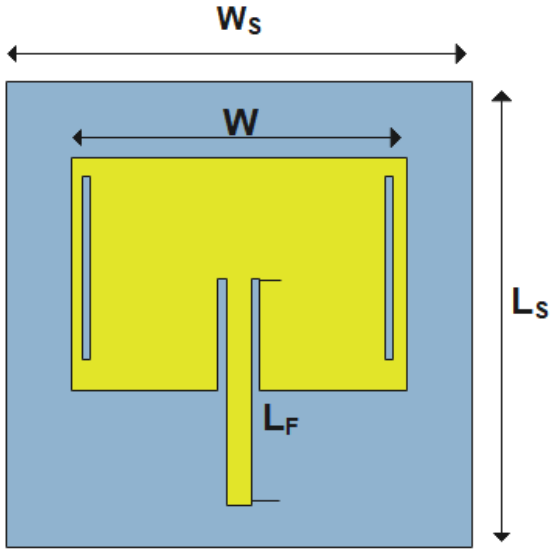

Figure 3.20: Schematic of dual-band rectangular patch antenna with two rectangular slots and microstrip feeding technology

$$\epsilon_{ref} = \frac{\epsilon_r + 1}{2} + \frac{\epsilon_r - 1}{2}\left(1 + 12\frac{h}{W}\right)^{-\frac{1}{2}} \tag{3.28}$$

$$L = \frac{c}{2f\sqrt{\epsilon_{ref}}} - 2\triangle L \tag{3.29}$$

$$\triangle L = 0.412h\frac{(\epsilon_{ref} + 0.3)(\frac{W}{h} + 0.264)}{(\epsilon_{ref} + 0.258)(\frac{W}{h} + 0.8)} \tag{3.30}$$

$$L_S = L + h \tag{3.31}$$

$$W_S = W + h \tag{3.32}$$

Where W is the width of the patch,

ϵ_r and ϵ_{ref} is the relative and effective dielectric constant of the patch,

h is the height of substrate,

L is the effective length of patch,

The $\triangle_L$ is the fringing effect,

L_S is the length of the substrate,

W_S is the width of the substrate.

A microstrip feed technology is used because it is easy to match. The feed is an

insect inside the radiated element to achieve 50-ohm impedance matching. Then the second band 2.4 GHz can produce by two rectangular slots of a half wavelength of the high frequency it placed near the edge of the radiated element because the current is zero at the edge when a notch create the current will circular around the slots thus it will radiate with a second resonant frequency. Parametric study for all antenna parameters is applied to achieve the best response and size for the antenna. Table 3.3 illustrate the value of antenna dimension after parametric study.

Table 3.3: Antenna parameter for first design

Parameter	Value	Parameter	Value
L_S	90 mm	L_{slot}	41.35 mm
W_S	90 mm	W_{slot}	1 mm
L	54.2 mm	L_F	40 mm
W	65.8 mm	W_F	4.8 mm

3.4.2 Antenna Result

The reflection coefficient of the antenna shown in Figure 3.21 where it is (-35 dB) at 1.8 GHz and (-11.8 dB) at 2.4 GHz and the bandwidth is narrow for two bands which is 180 MHz and 90 MHz for 1.8 an 2.4 GHz respectively.

The directivity of the two resonant frequency is depicted in Figure 3.22 the lower frequency of 1.8 GHz has a directivity of 6.92 dB, its radiation angle is (0) degree while the higher frequency of 2.4 GHz has a directivity of 5.8 dB, its radiate as an omnidirectional pattern and the maximum radiation angle is (44,-38) degree.

The gain of the antenna is the directivity multiplying by the efficiency. However, the efficiency of the antenna is 95% and 68% for the two frequencies respectively. It can observe the radiation efficiency of the radiating slot is low and this is one of the slot disadvantages. Thus the gain is 6.7 dB for 1.8 GHz and 4.1 dB for 2.4 GHz.

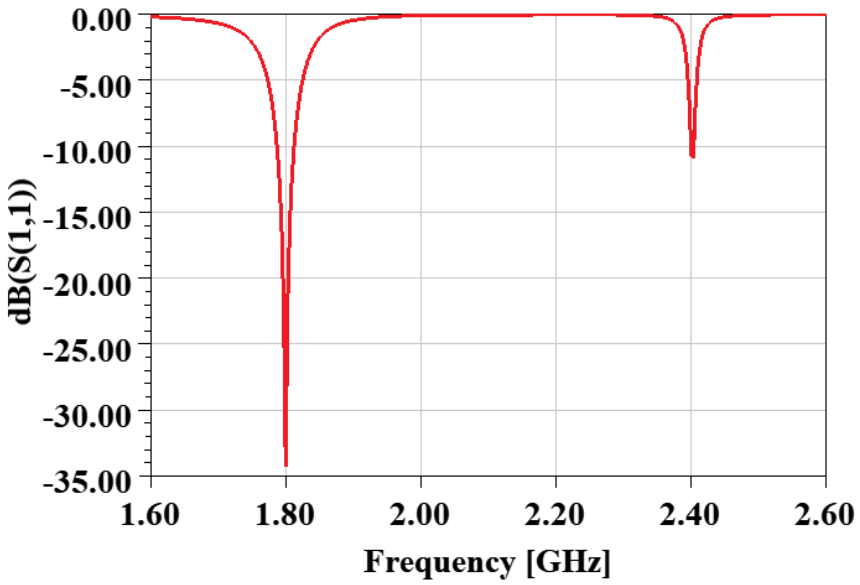

Figure 3.21: The reflection coefficient of the dual-band patch antenna

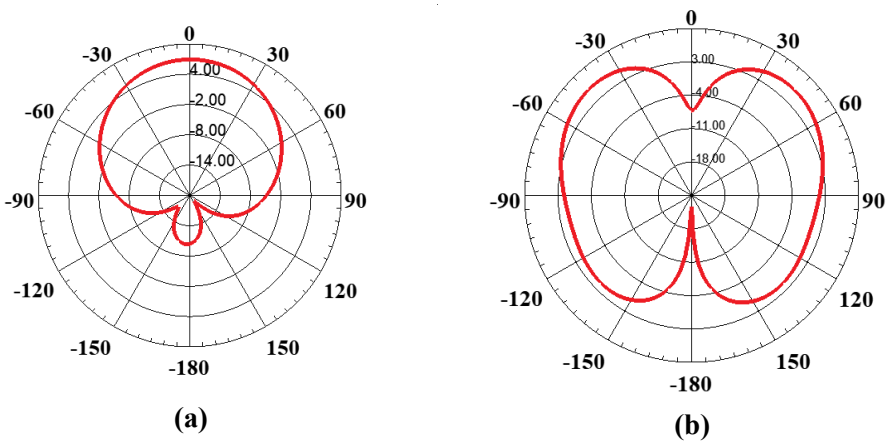

Figure 3.22: The directivity of antenna at (a) 1.8 GHz (b) 2.4 GHz

3.4.3 Second Design with Coaxial Cable

Another type of feeding technique will be utilized. A coaxial cable is used due to its ease of fabrication and has low spurious radiation. Furthermore, it can be placed anywhere in the patch to match well with 50-ohm input impedance.

The coaxial feed can be designed from three cylindrical (coaxial, shield, and probe(pin)) as shown in Figure 3.23. The coaxial cylindrical is the outside and it connect to the ground plane while probe cylindrical connects to the radiating element, the two cylinders are made of (pec) metal with very small thickness while shielding cylindrical made

of (Teflon or Polyester) to isolate the two metal cylindrical. The length of coaxial used is (5) mm, while the cylindrical diameter is (1.6, 1, 0.46) mm, respectively, that can calculate using the equation

$$Z_o = \frac{138 * \log_{10}(\frac{D}{d})}{\sqrt{\epsilon_r}} \tag{3.33}$$

Z_o is characteristic impedance in ohm.

ϵ_r is the relative permeability of dielectric.

D is the inner diameter of the outer conductor.

d is the diameter of the inner conductor.

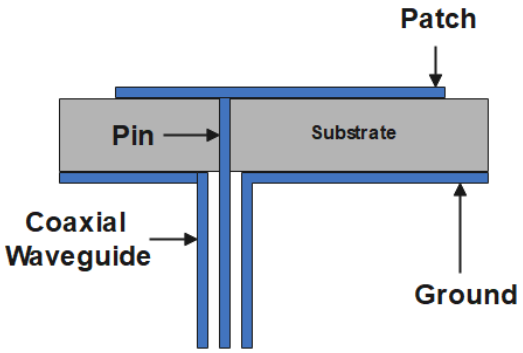

Figure 3.23: The structure of coaxial feed for patch antenna

The feed position is very critical due to its effect on the impedance matching of the antenna so, a parametric study in HFSS program is used to determine the perfect position for the feed. Eventually, the feed position shifted slightly from the center toward the edge of the patch because the input impedance is low at the center as mentioned before in chapter 2. The feed shifted in (y) axial and it still fixed at (x) axial.

A patch antenna with dual-band can achieve by adding a slot on the radiating element in different shapes her a U-shape with a length of (half wavelength of 2.4 GHz) is etched to produce resonant frequency at 2.4GHz as shown in Figure 3.24.

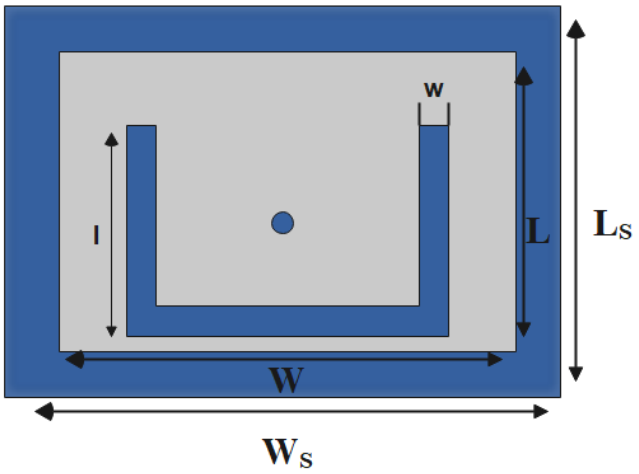

Figure 3.24: schematic of U slot dual-band patch antenna

Parametric study is applied for all dimensions and feed position will be applied to produce matching at 1.8 and 2.4 GHz, the final value of the dual-band patch antenna is illustrated in Table 3.4. A simulation for dual-band rectangular patch antenna parameters will be applied to demonstrate antenna performance.

Table 3.4: Antenna parameter for first design

Parameter	Value	Parameter	Value
L_S	65 mm	l	46.2 mm
W_S	65 mm	w	3.7 mm
L	52.8 mm	(x,y)	(0,4)
W	60 mm	horizontal slot	42 mm

3.4.4 Reflection coefficient

A reflection coefficient S_{11} of the antenna is shown in Figure 3.25. The antenna works well at the two bands 1.8 and 2.4 GHz where S_{11} is (-13 and -16) dB respectively. The reflection value less than (-10) dBm means that 99% of power will transfer from the source to the load. Figure 3.26 show that the Standing Wave Ratio (SWR) is 1.6 and 1.7 for the two bands respectively, the value is less than 2 that represent an acceptable

result. Furthermore, the bandwidth of 1.8 GHz is 150 MHz and 126 MHz for 2.4 GHz. The patch antenna at most has a narrow bandwidth, but it has a higher directivity and gain.

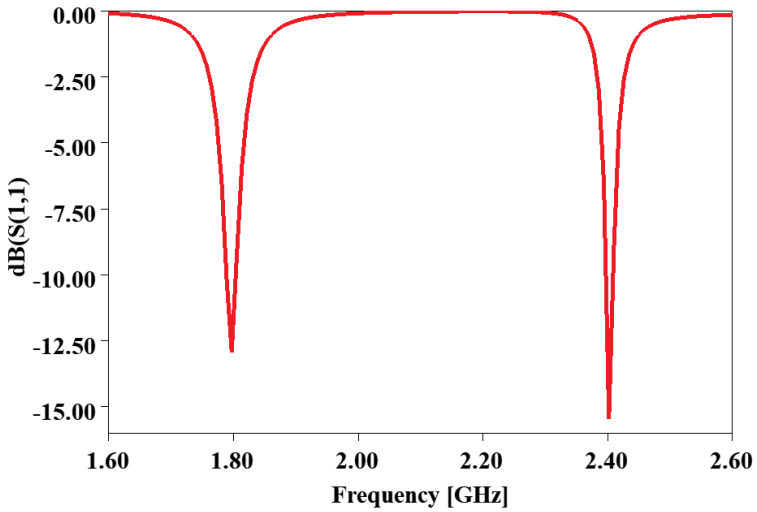

Figure 3.25: Reflection coefficient of the dual-band patch antenna

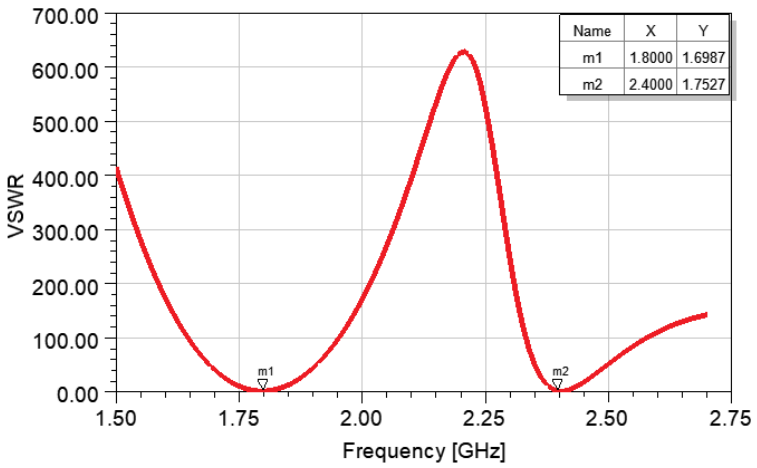

Figure 3.26: Voltage Standing Wave Ratio of the dual band patch antenna

The reflection coefficient of the higher frequency 2.4 GHz will be shifted toward low frequencies when the length of the slot increase and vice versa as shown in Figure 3.27. At the length of 41 mm the resonant is shifted to be at 2.55 GHz while at the length of 51 mm the resonant is shifted to be 2.25 GHz. Hence, the lower frequency 1.8 GHz has a very low sensitivity to the slot length because its resonance depends on the patch dimension.

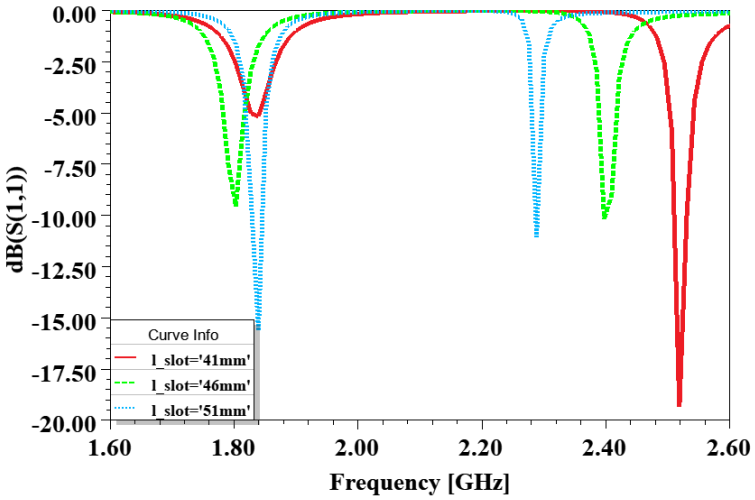

Figure 3.27: Reflection coefficient versus frequency for different slot length.

3.4.5 Directivity, Radiation Pattern, and Gain

The directivity of the antenna is shown in Figure 3.28. The directivity of 1.8 GHz is 6.9 dB and for 2.4 GHz it's equal to 7.08 dB. It can observe that the antenna has high directivity (all power transmit in one direction) and it has a good front-to-back ratio where all radiation power in front and no radiation toward the back. The front-to-back ratio value depends on the size of the ground plane of the antenna. The antenna has vertical polarization, where directivity degradation from the broadside moving toward evolution.

The half-power beamwidth (HPBW) is the decrease of the maximum power by 50% (3dB), the HPBW of 1.8 GHz is 100 at E-plane and 98 at H-plane while at 2.4 GHz is equal to 92 at E-plane and 96 at H-plane.

The current distribution of the surface is illustrated in Figure **??** the current range used is from 0 A/m to 50 A/m. The maximum current focus around the feeding position and the edge of the slot. It can observe the current distribution is reduced at a higher frequency. Co-polarization means the polarization of both the transmitting (reference

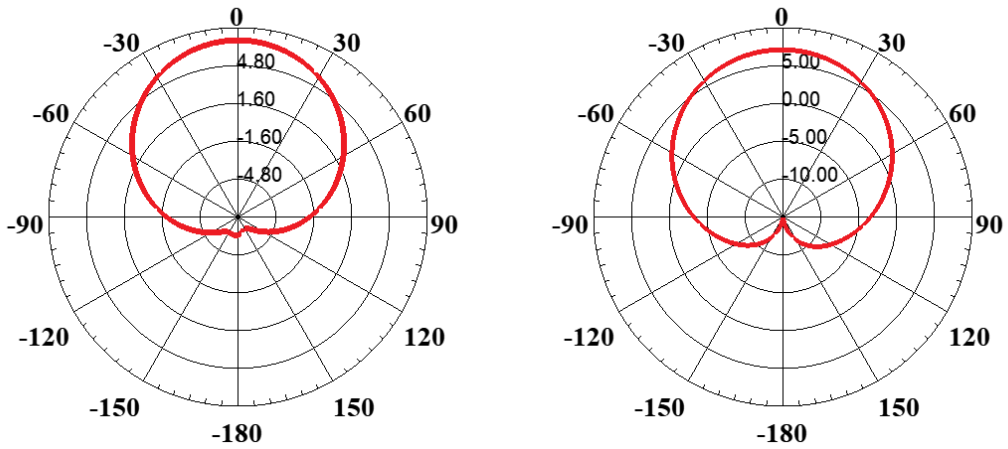

Figure 3.28: The directivity of the dual and patch antenna (a) 1.8 GHz (b) 2. 4 GHz

antenna) and receiving (test antenna) is the same while the cross-polarization means the polarization of both the antennas is perpendicular. Figures 3.30 and 3.31 show the co and cross-polarization at E-plain and H-plain for 1.8 and 2.4 GHz frequencies. It can observe at E-plain of both frequencies the cross-polarization is high which means the antenna receives power from vertical and horizontal polarization, it's not preferable for communication application because the power will be distributed and not focus on the target, but it's considered beneficial for energy harvesting system because it will allow harvesting power from versus direction.

The bandwidth of the patch antenna is narrow, it is about 150 MHz at 1.8 GHz and 126 MHz at 2.4 GHz. This result is shown in the reflection coaiffitiant of the antenna and can also observe in radiation pattern as show in Figures 3.32 and 3.33 where the radiation compote as a function of rotation angle and frequency. The radiation constrains around the two resonant frequency in the radiation angle. The cross polarization shows the power harvest from the orthogonal polarization.

Because the antenna gains depends on the efficiency and directivity of the antenna. The radiation efficiency should be calculated, it represents the ratio of the Radiated

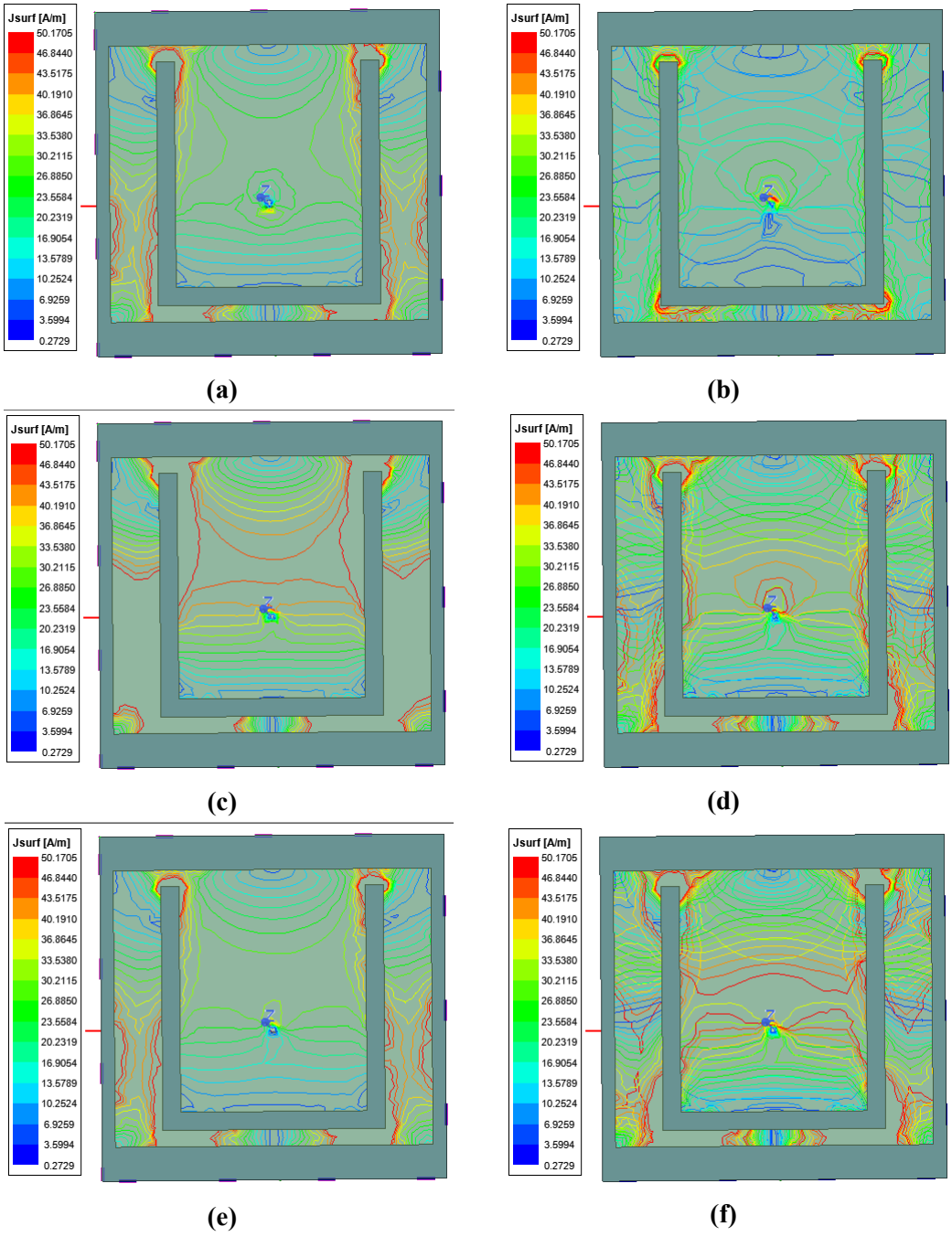

Figure 3.29: Current distribution of the patch antenna in three figures

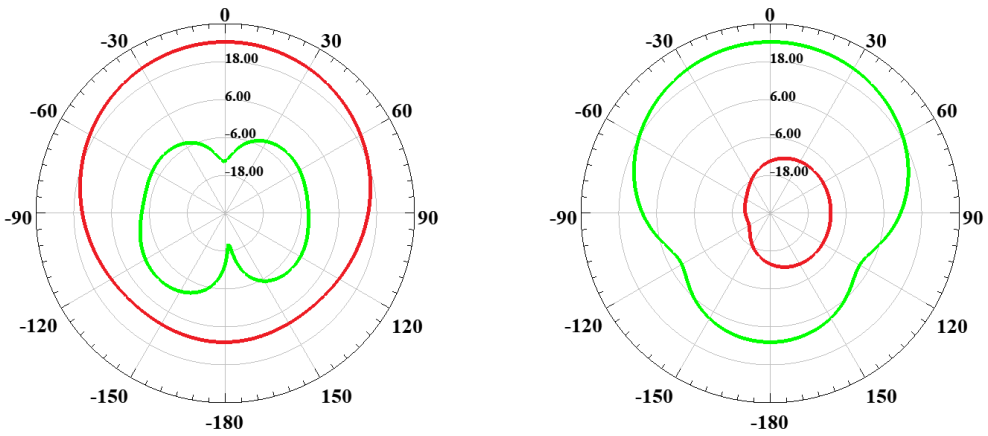

Figure 3.30: Co and cross-polarization at 2.4 GHz (a) E plane (b) H plane

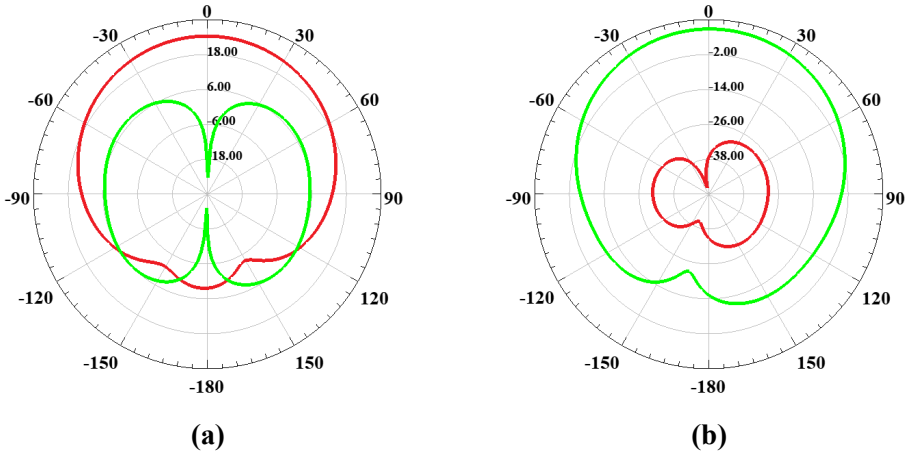

Figure 3.31: Co and cross-polarization at 1.8 GHz (a)E plane (b)H plane

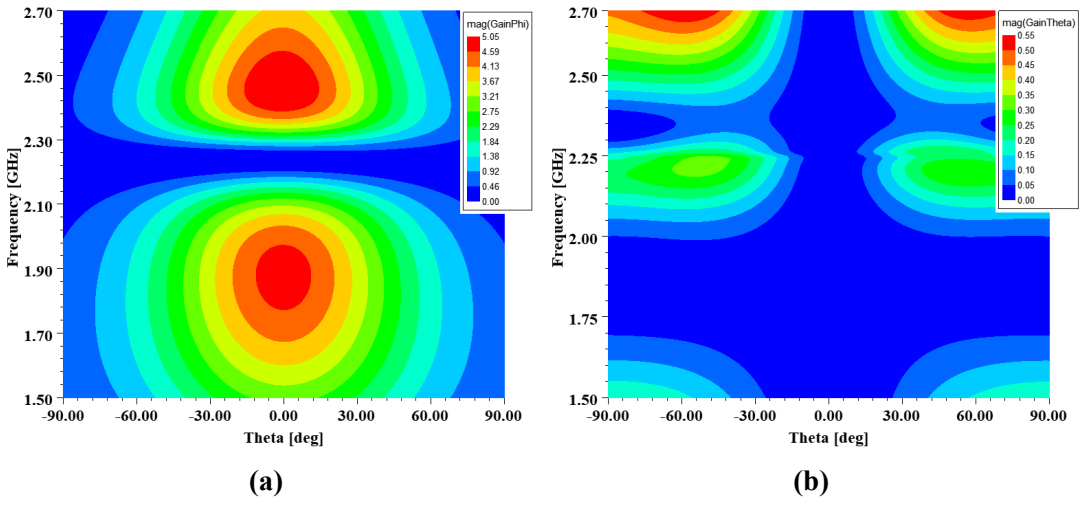

Figure 3.32: 3D radiation pattern of the antenna at 1.8 GHz (a) Sephercal corrdinate (b) Polar cordinat

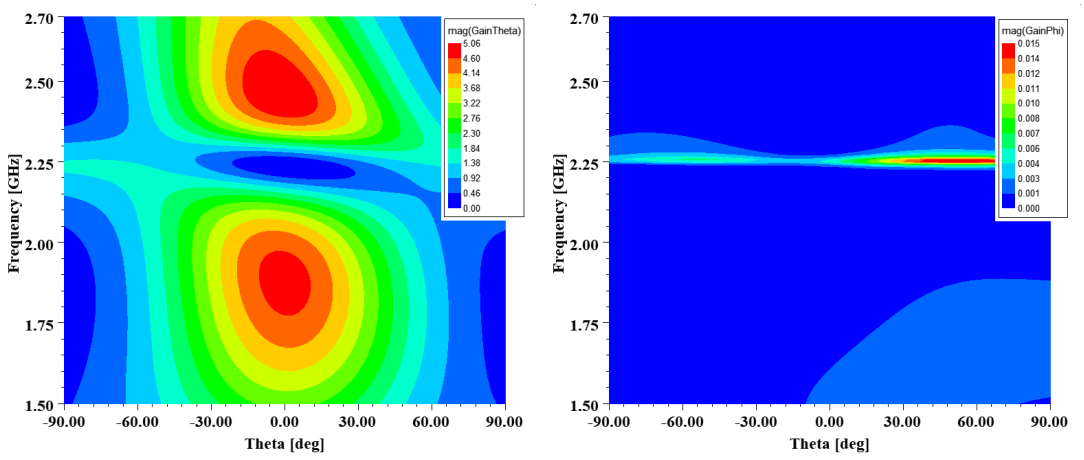

(a) **(b)**

Figure 3.33: 3D radiation pattern at 2.4 GHz (a) Sephirecal cordinat (b) Ploar cordinat

Power (Pr) to the Input Power (Pi), thus it's always lower than 100% and the antenna gain is often lower than antenna directivity this loss is due to the surface wave power, conductor, and dielectric losses. The radiative efficiency is 93.8% and 92.6% at 1.8 and 2.4 GHz respectively so the gain is 6.7 dBi at 1.8 GHz and 6.8 dBi at 2.4 GHz.

3.5 Rectenna Measurement

Rectenna consists of three components as mentioned in Chapter 2 antenna, matching network, and rectifier. In this thesis, the patch antenna was designed to capture power from dual-band 1.8 and 2.4 GHz at a low input power range of -5 dBm. Its design using Roger RT/ duroid 5880 substrates with a gain of 6.7 and 6.8 dB. The rectifying circuit of single series diode topology using HSMS 2850 Schottky diode and a dual-band CRLH impedance matching network is placed on the same substrate of Roger Duroid 3010 and placed in the backside of the antenna substrate to minimize the size and decrease losses that generate from using the SMA connector as shown in Figure 3.34.

The input impedance of the patch antenna in HFSS software is transfered to ADS software to connect with the rectifier and matching circuit. A Harmonic Balance (HB)

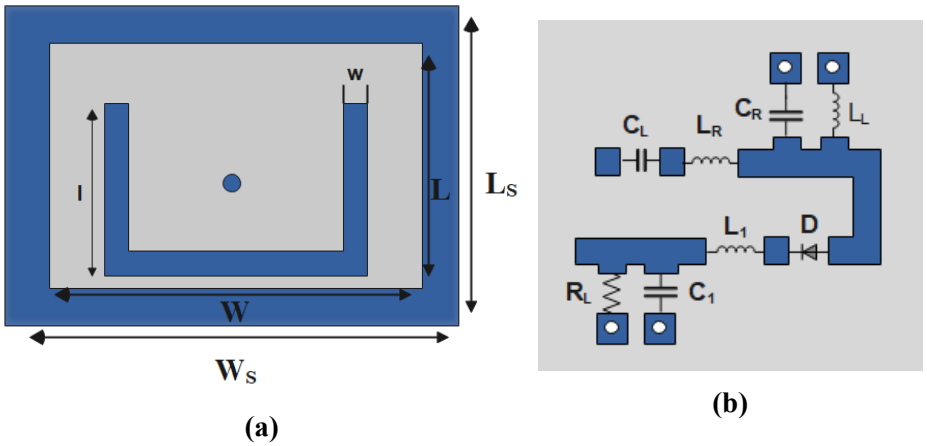

Figure 3.34: Single rectenna (a) The front side of the rectenna (b) The backside of the rectenna

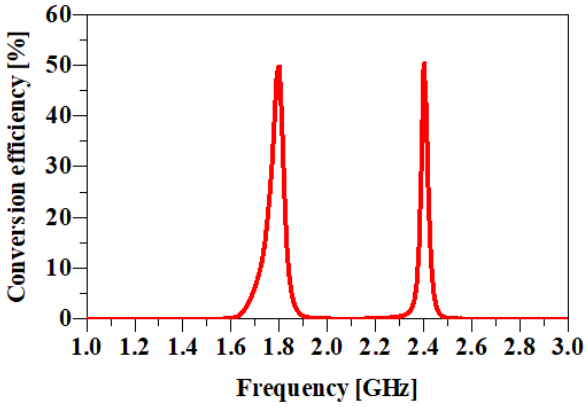

Figure 3.35: Reflection coefficient versus frequency for two bands 1.8 and 2.4 GHz

in ADS was utilized to calculate output DC voltage and conversion efficiency of antenna and rectifier (rectenna) after connecting. As shown in Figure 3.35 the conversion efficiency versus frequency at fixed input power -5 dBm is about 50.6% for the two bands 1.8 and 2.4 GHz. It can observe that the conversion efficiency of the rectifier with antenna is less than the conversion efficiency of the rectifier before connecting (52%) this owing to the impedance matching losses. The efficiency of the rectenna change with the angle of incident power and the maximum power received at zero angles (the receive angle of the antenna) as shown in Figure 3.36.

The output DC voltage of the rectenna as a function of frequency is depicted in Figure 3.37 a. where the voltage is 0.5 V of the two bands 1.8 and 2.4 GHz. In Figure

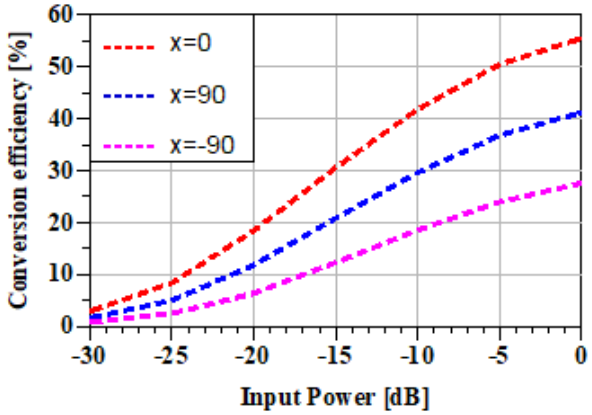

Figure 3.36: Conversion efficiency versus input power at three diffrent angle 0, 90, and -90

3.37 b. it can observe that output voltage dependent on the input power and increases when the power range increases. The voltage increases from 0.5 to 0.9 V at the input power increase from -5 to 0 dBm.

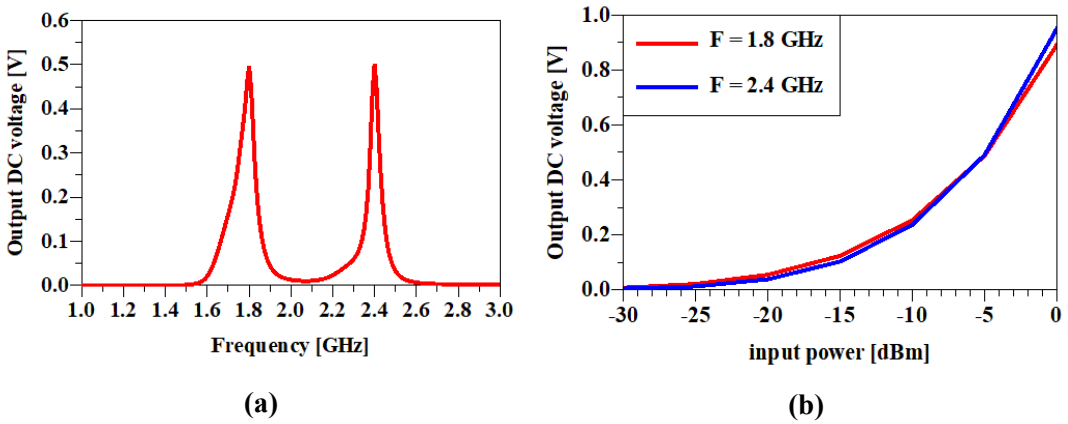

Figure 3.37: The output DC voltage of single rectenna (a) as a function of frequency (b) as a function of input power

The output voltage also changes with the angle of receiving power as shown in Figure 3.38 a sweep of input power is used and the maximum voltage achieve at 0 dB. At the input power of -5 dBm, the maximum voltage can achieve at zero angles and it decreases toward 90 and -90 degrees to reach the minimum value at these two angles. The single element rectenna was designed with a size of (65 X 65) mm2 and high directivity of 7 dB in vertical polarization. In Figure 3.39 a the power is measured as a

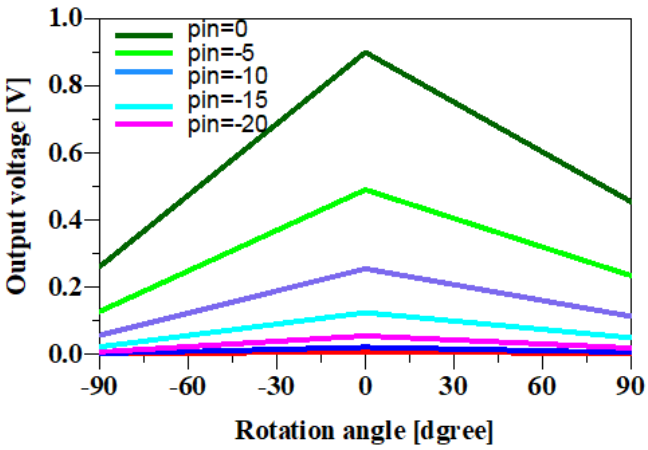

Figure 3.38: Output voltage versus rotation angle with a sweep for input power

function of frequency with a sweep in the angle, the harvested power is 1.6 mW at 1.8 and 2.4 GHz, and when the angle of the incident power is 0 degrees. While in Figure 3.39 b the power is measured versus the input power with a sweep in frequency it can observe the harvested power is equal for the two frequencies. The power harvested is small owing to the low power range in space thus to increase the capturing power to be sufficient for wireless and IoT applications an antenna array will be designed as will be discussed in the next chapter

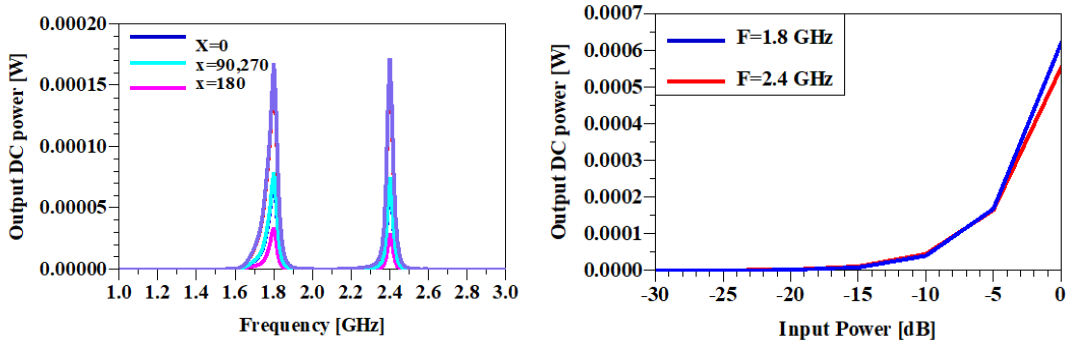

Figure 3.39: Output harvest power (a) as a function of frequency with different value of receive power angle (b) as a function of input power at the two frequencies 1.8 and 2.4 GHz

CHAPTER FOUR

Multi Rectenna

4.1 Introduction

In this chapter, the spatial and frequency diversities are exploited to design multi-band multi-direction rectenna design. The Multi rectenna can capture signals from different directions. This is as a single antenna with high directivity, but it has an omnidirectional radiation pattern. This feature makes the proposed design can receive signals from all directions in space. Thus, the multi rectenna is arranged in a 3D form, taking a shape of the symmetrical cube. Five antennas operating at dual bands are placed on five external faces of the cube, while the sixth face remains for wall mounting. Furthermore, there is also another sixth face for the cube but they are internal since our cube is empty from the inside. Each antenna has its counterpart rectenna placed inside the cube from the opposite direction. The RF energy harvested from single rectennas can be either connected in series or parallel. As will be demonstrated, each connection type has its advantages over the other one. In the end, the result of this work will be compared with other related works introduced by other researchers.

4.2 Multi Rectenna with Exploiting the Spatial Diversity Technique in the Realistic Environment

Various studies have shown that the rectenna can carry out high conversion efficiency and output DC power at a low input power range. However, in real-time situations, the RF signal between its source and the scavenger does not propagate in the Line-of-Sight (LoS), so this makes the received energy quite low. Thus, the DC power and the conversion efficiency will be low as well. To circumvent this deficit, spatial diversity is the best option to go through with to designing a rectenna array being able

to receive signals from several directions simultaneously. Also, it can receive several signals at the same time. This mitigates the received power fading due to the multipath propagation, unknown orientation, and unknown polarization of the incident signals. Multi ports approach is used to avoid the complexity and losses of the feeding network, especially at the low power range. Most antenna arrays in the literature are arranged in planer forms but, in our proposed arrangement, the multi rectennas are 3D. In the former configuration, the signals can be received from one direction, whereas our proposed design can capture the signals from almost all directions. In [46],the authors have used two antennas to harvest the power from only two directions. However, in [47], authors have increased the number of antennas utilized to capture from space, but the design operates at only a single frequency band.

In this chapter, implementation of the multidirectional spatial diversity rectenna array in a cube form is proposed. Furthermore, the design operates at dual frequency bands as a step to raise the harvested power without using extra designs, leading to low cost structures. The two frequency bands are GSM at 1.8GHz for outdoor applications and WiFi at 2.4GHz for indoor applications. However, the powers of these two RF sources are relatively low, so looking for a solution that aids to increase the amount of the received power is, as in our situation, mandatory. Because of the unknown direction of arrival of the received signals, an omnidirectional antenna should be used to capture power from all directions but this type of antenna always has a low gain. In the other hand, an array with high gain can have high gains but at the cost of the width of the radiation pattern. To combine both advantages of the omnidirectional antenna and the antenna array, a new antenna array with five antennas operating at dual-band is proposed, designed, simulated, and investigated. Multi antennas structure are able to capture RF signals from almost all directions exploiting the spatial diversity. As a result, the proposed design has both omnidirectional-like pattern and high gain as in

directional antennas. As will be seen later on in this chapter, an amount of the harvested power is increased vividly. In this thesis, a high directional patch antenna is the candidate antenna type utilized in our harvester. Also, as we said earlier, the antenna is modified by cutting out a U-shaped slot from the main patch radiator, resonating at dual frequencies which are 1.8GHz and 2.4GHz frequencies.

4.3 Multi Antennas

First of all, due to the dependence of an output voltage of the rectenna on the antenna radiation pattern primarily, designing a new rectenna array capable of receiving the RF signals from almost all directions is the main aim of this thesis. As known, a radiation pattern of the antenna plays a vital role in determining the overall radiation pattern of the whole proposed design [71]. The proposed rectenna geometry. Four antennas are placed on the four sides, while the fifth antenna is placed on the top face. The bottom face has no antenna, which has been left empty for mounting purposes. All patch antennas are united to form the whole cube shape.

This will affect the resonance frequency of the main patch radiator, so a parametric study is required to remove the shifting in frequency. Furthermore, all antenna dimensions are change to enhance its performance. For instance, when one dimension parameter is change, all other dimensions are fixed. This procedure aids to select the initial dimensions. Afterward, all parameters are slightly returned in a second round as a step to go with the best results, see Table 4.1 for numerical dimensions which are given in mm. As can be noticed, variations in the antenna dimensions compared to a single stand-alone element occur owing to the mutual coupling among elements resulting from the coupling of the space waves spreading from one antenna to another.

The reflection coefficients of the antenna elements are shown in Figure 4.1, only

Table 4.1: Multi antennas parameter after optimization

Parameter	Value	Parameter	Value
L_S	65 mm	l	46.2 mm
W_S	65 mm	w	3.7 mm
L	53.5 mm	(x,y)	(0,3.6)
W	60 mm	horizontal slot	42 mm

the results of one antenna element S_{11} are illustrated here, but when operating within multi antennas assembly. In this Figure 4.1 can observe easily that the antenna elements resonate at two frequencies around 1.8GHz and 2.4GHz with a reflection ratio larger than -10dB owing to the discontinuity in the cube edge.

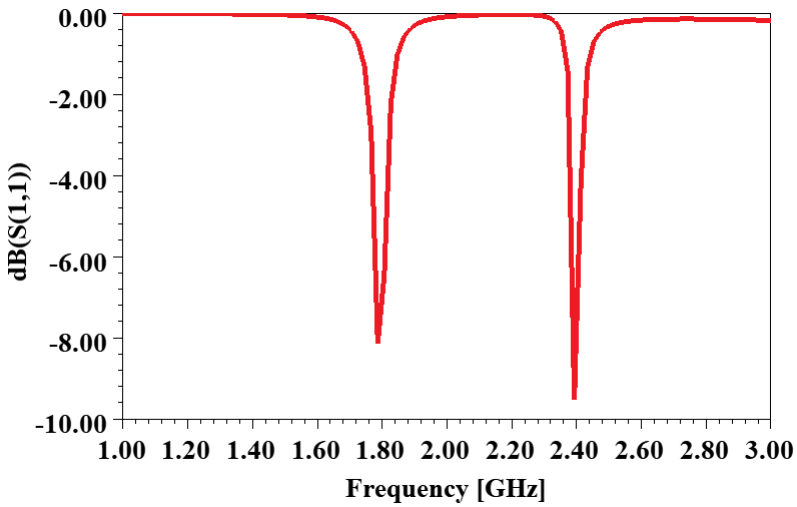

Figure 4.1: Reflection coefficient S of only the first antenna within the multi structure assembly before filling edges

Thus, to overcome this problem, the sharp edges of the cube will be filled with the same material of substrate RO Roger 5880, making the edges curvy to reduce the diffraction as shown in Figure 4.2.

As clear evidence, the results are highly improved after filling the edges as illustrated in Figure 4.3. Now, the reflection coefficient is about or smaller than -10 dB.

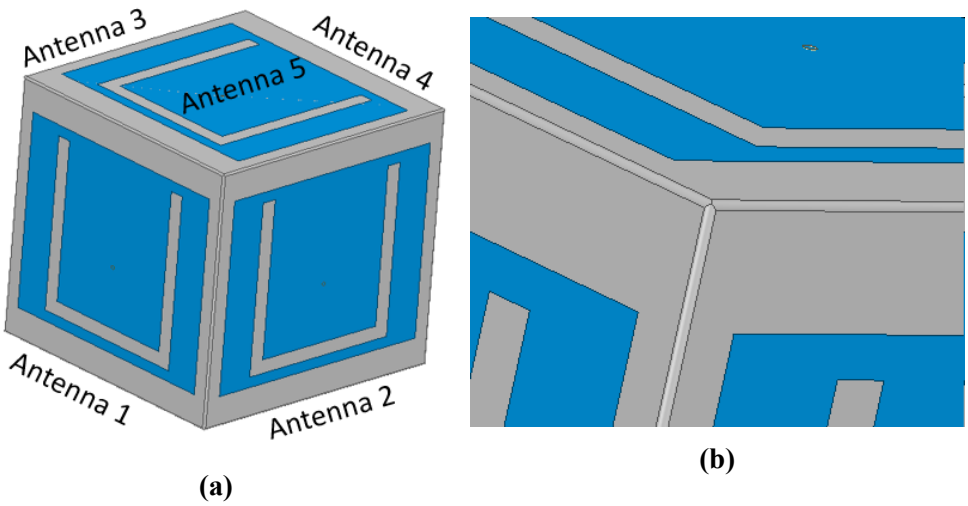

Figure 4.2: Cube multi antennas (a) The modified 3D cube array with filling edges (b) zoom in for one corner

There are slight discrepancies in the reflection coefficients of individual elements as shown in Figure 4.4 because of the locations of antennas.

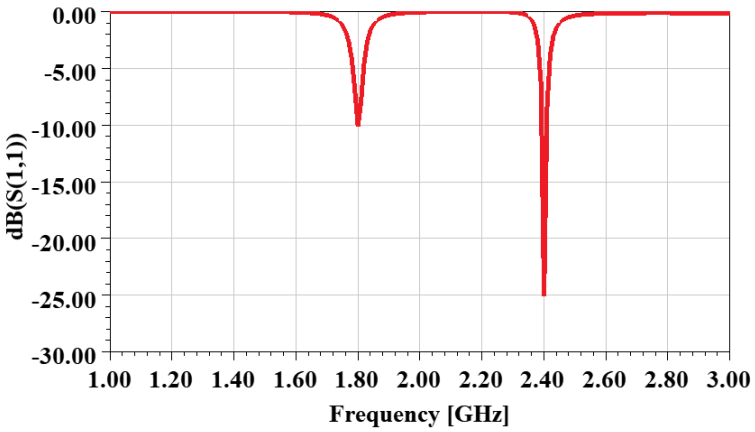

Figure 4.3: Reflection coefficient S of only the first antenna within the array assembly after filling edges

The main challenge for combining multi antennas in one array is how to decrease the effects of the mutual coupling. The mutual coupling can affect the radiation pattern and input impedance of each element. If the antennas are placed on one plane (i.e., E or H plane), the mutual effect is very high and the antenna should be separated by a sufficient distance (1/4 λ), making the array size very large. In this work, the antennas are packaged in the different directions of the cube, while the grounds of elements inside

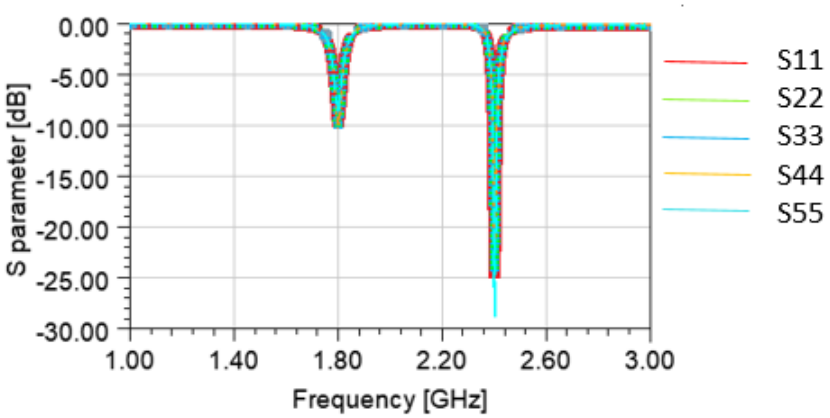

Figure 4.4: Reflection coefficients S of all antennas after filling edges (S(1,1), S(2,2), S(3,3), S(4,4), S(5,5))

the cube are united to obtain inside the metallic shield.This shield is useful for preventing coupling among antennas from the backside. It can be observed that the mutual couplings among antennas are lower at the resonant frequency of 2.4 GHz, whereas it is higher at the resonant frequency of 1.8 GHz. This is logical because the distance at the latter frequency becomes relatively smaller. The mutual coupling between the opposite antennas is lower than the adjacent ones. At the resonant frequency 1.8 GHz, the mutual coupling between Antenna 1 and 2 is equal to that of Antenna 1 and 3 (-14 dB) while between Antenna 1 and 4 is (-18dB) and between Antenna 1 and 5 is (-22 dB). All these results are relatively acceptable for this work. For more details, readers can refer to Figure 4.5.

The directivity of each antenna is the same but it differs in the direction. Figures 4.6 and 4.7 illustrate the directivity of each antenna separately for the two bands. Someone can see that the directivity at the resonant frequency of 1.8 GHz is 6.1 dB. If it is compared with the results introduced in the previous chapter, it can be seen that at this time the directivity is less now. When operating alone, the directivity is 7.3 dB, but with multi antenna, it becomes 6.1dB. The directivity loss is about 1.2 dB where this degradation belongs to the mutual coupling impacts. In contrast, at the resonant frequency

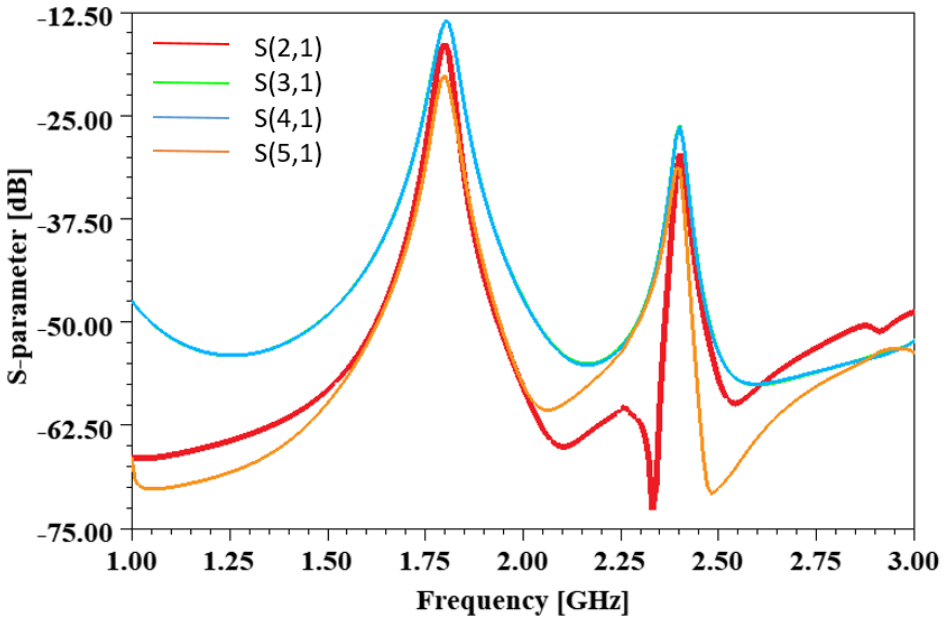

Figure 4.5: Mutual coupling between antennas

of 2.4 GHz, the directivity is the same as a single antenna because the antenna's mutual coupling is low. The antennas 1,2,3, and 4 radiate in ϕ =0 degree and θ of 0, 90, -90, and 180 degrees, respectively for the two bands. While Antenna 5 (the top one) radiate in ϕ =90 degree and θ = -90. Figure 4.8 shows all radiation patterns of the antennas overlaid in one plot. As can be seen, all the radiation patterns are identical except their main beam direction is different.

Each antenna has its own radiation pattern and this pattern is directed to a specific location. The gain of the antennas at 1.8GHz is 5.8 dB. Here, the gains are less than the directivities mentioned in the previous Figures 4.6. This is normal since efficiencies are less than 100% and the gain is equal to the directivity multiplied by the efficiency. Reduction in the efficiency from its ideal value which is 100% is because of losses associated with substrates, patches, coupling, etc. For the band 2.4GHz, the gain is 7.1 dB, the losses at this band are very low so its value is equal to the directivity (efficiency is high). To prove that the radiation pattern of the cube antenna is omnidirectional-like, the simulation setup is made. Firstly, the cube array rotates in a horizontal way around

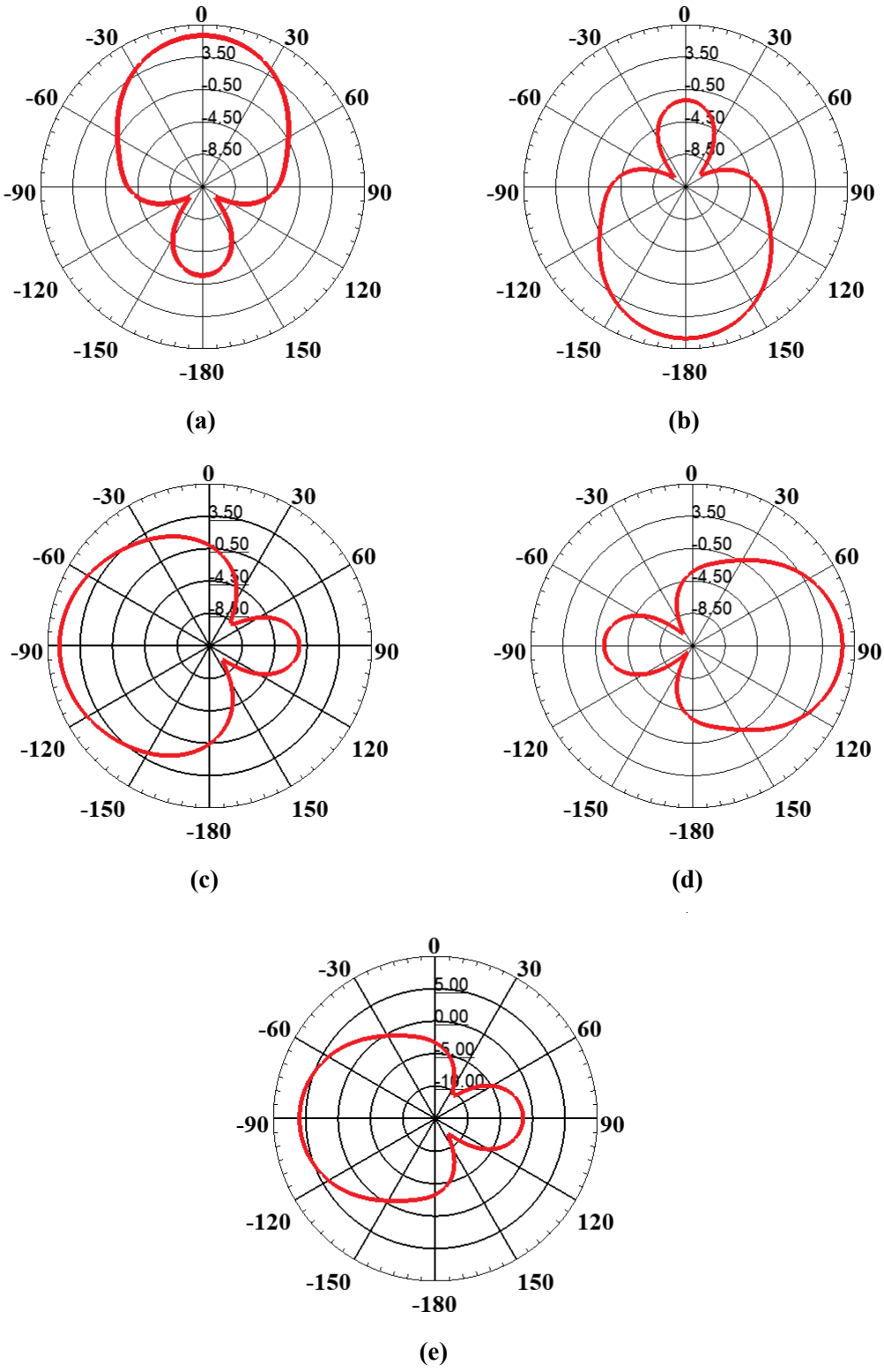

Figure 4.6: The directivity of all antenna in 1.8 GHz with different value of θ at (a) $\theta = 0°$ (b) $\theta = 180°$ (c) $\theta = -90°$ (d) $\theta = 90°$ and (e) $\theta = -90°$

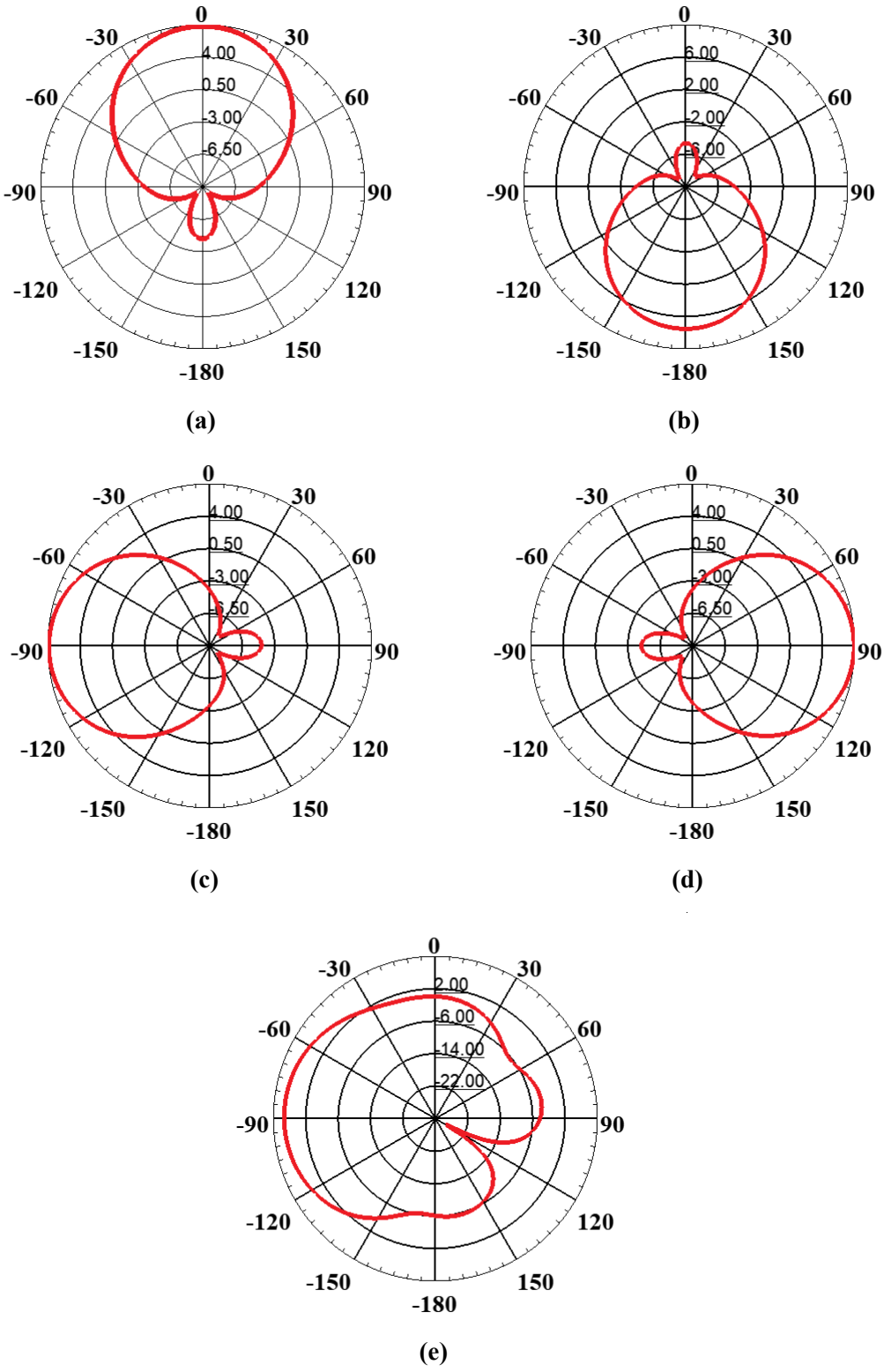

Figure 4.7: The directivity of all antenna in 2.4 GHz with different value of θ at (a) $\theta = 0°$ (b) $\theta = 180°$ (c) $\theta = -90°$ (d) $\theta = 90°$ and (e) $\theta = -90°$

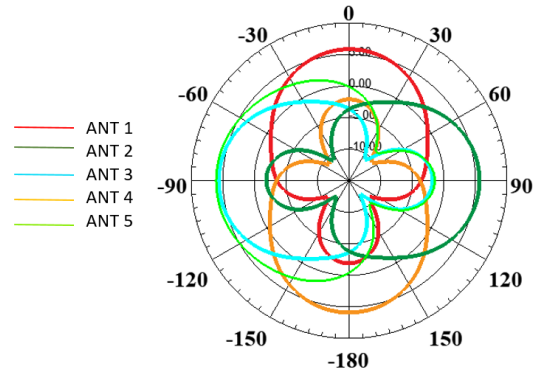

(a)

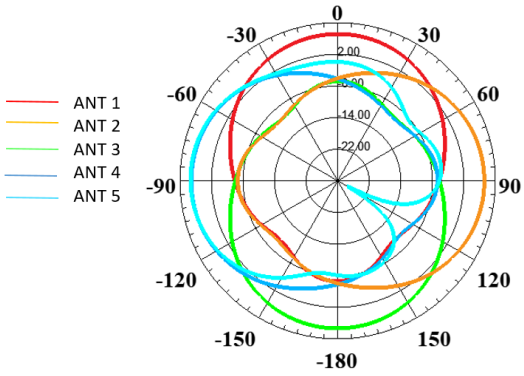

(b)

Figure 4.8: The directivity of all antennas together in one form at (a) 1.8 GHz (b) 2.4 GHz

its axis from 0 to 360 degrees according to the source of power as shown in Figure 4.9 a.

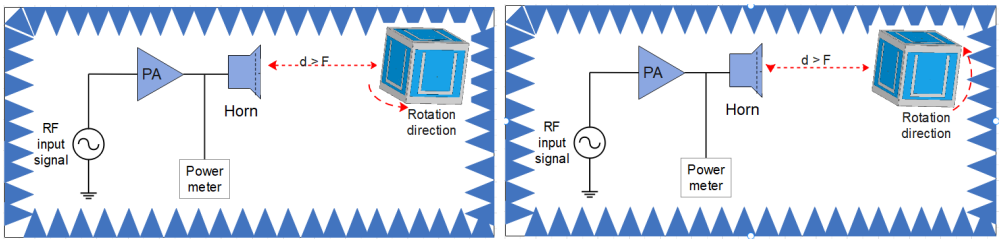

(a) (b)

Figure 4.9: The simulation setup for determining the received power when the receiving antenna rotating in 360-degree relative to the Horn antenna

Assuming the source antenna is ANT6 and the five antennas arranged in the cube form are ANT1, ANT2, ANT3, ANT4, and ANT5. Then, a magnitude of the received power is calculated for every single antenna with respect to the rotation angle. The reference angle starts from the ANT1 which denotes the 1st antenna on the cube. The

received power are named as following S16, S26, S36, S46, and S56 for ANT1, ANT2, ANT3, ANT4, and ANT5, respectively, see Figure 4.10. As can be seen, ANT1 receives the maximum power at the reference point 0-degree. ANT2 receives the maximum power at the 90-degree angle. To know all directions of the received powers for all antennas, Figure 4.10 has all information.

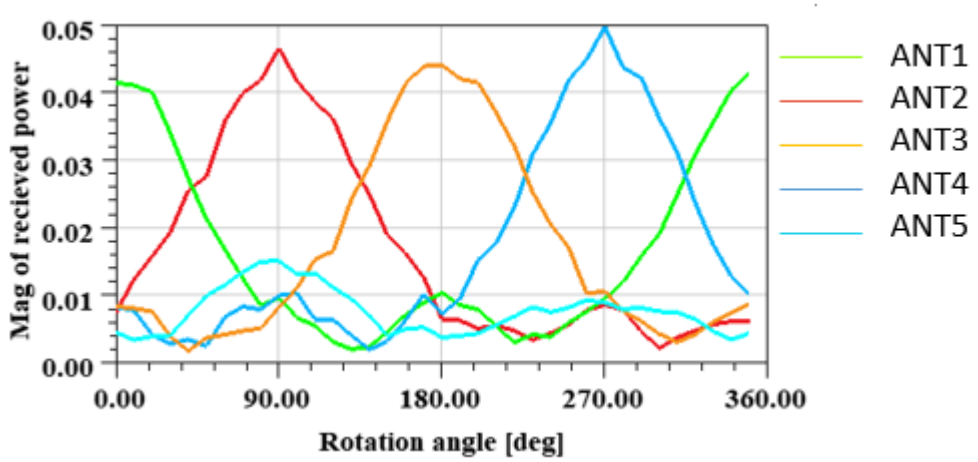

Figure 4.10: Magnitudes of the received power as a function of the rotation angle (rotating the cube in the horizontal direction)

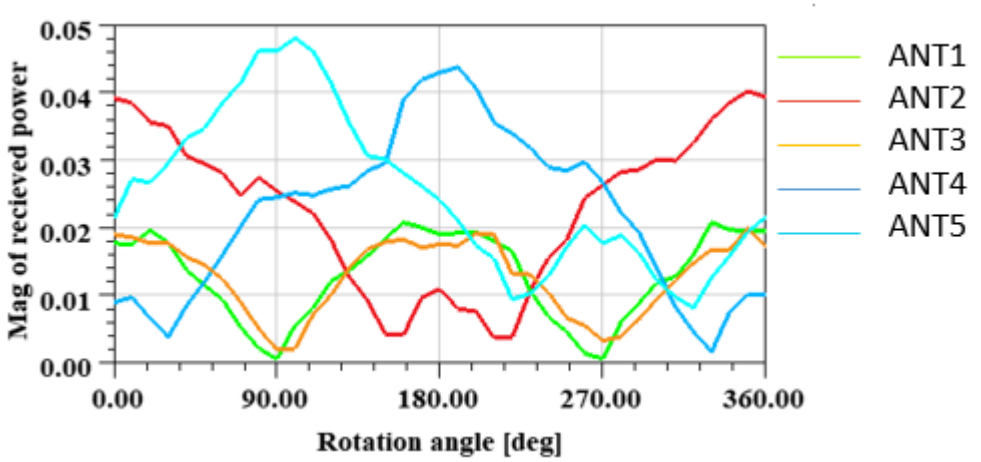

Figure 4.11: Magnitudes of the received power as a function of the rotation angle (rotating the cube in the vertical direction)

After that, the cube rotates in the vertical direction from 0 to 360 degrees. The magnitude value of the received power is recorded as shown in Figure 4.11, so ANT2,

ANT4, and ANT5 can operate. Other antennas can receive power, but the power is relatively quite low. Amounts of the received power are exploited to show the main theme of this thesis which is the energy harvesting from almost all directions and the ability to capturing power from space.

4.4 Multi Rectenna

The proposed cube multi rectenna has dimensions of 65X65X65mm3 designed by using the Ro/Roger 5880 substrate with ϵ_r=2.2 and tangent loss of 0.0027. It consists of five rectangular patch antennas where each antenna is connected to its rectifier circuit via the probe connection. The rectifier is placed in the backside of the antenna using the Roger 3010 substrate with ϵ_r=10.2 and tangent losses of 0.0009, where both substrates have a common ground to electrically isolate between them. Figure 4.12 shows the whole structure. This arrangement aids to produce compact size rectennas compared to ones where their antennas and rectifiers have no common ground.

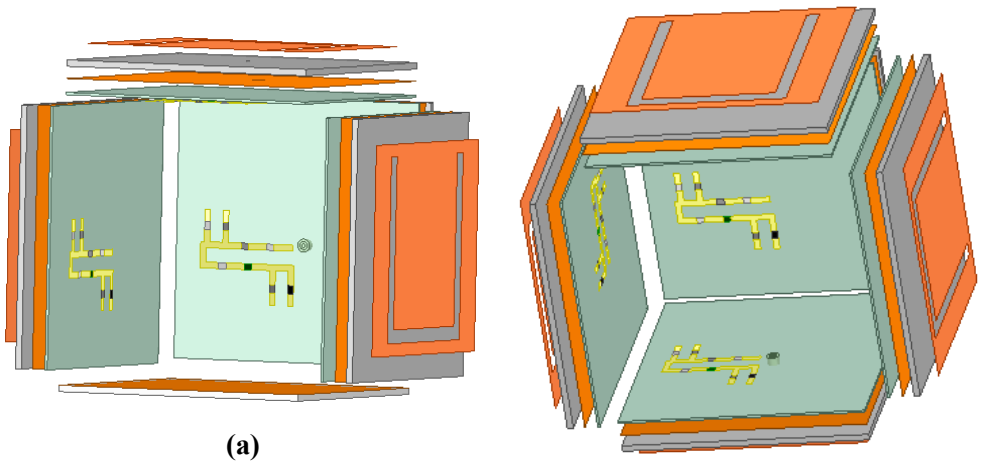

(a) (b)

Figure 4.12: Exploded view of multi Rectenna structure

To do so, the rectifier has been designed and simulated using the ADS software, while the antenna is designed using the HFSS software. To integrate these two soft-

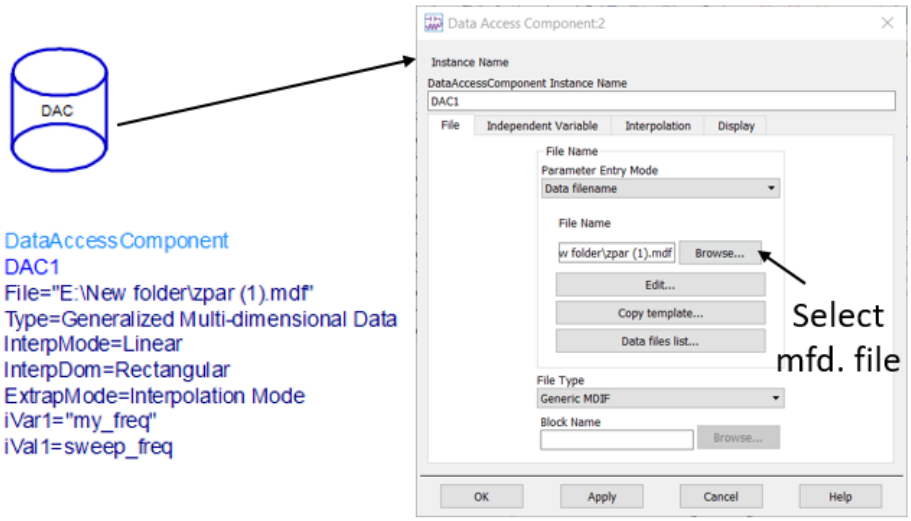

Figure 4.13: Data Access Component (DAC) Wizard

ware, some important parameters for the antenna like the input impedances, radiation patterns, and received powers are exported from the HFSS into ADS. The antenna input impedance Z parameter obtained from the HFSS is saved as a mfd file type, and then in ADS, Data Access Component (DAC) should be added into the schematic window that is shown in Figure 4.13. From the browse button, we can choose the mfd Z-file. After that, the input impedance of the source power of the rectifier circuit will be changed from the typical value of Zo=50 ohm to the file (DAC) file as shown in Figure 4.14. This procedure is repeated for all antennas when operating simultaneously to take into account the mutual coupling effects on the overall performance. Also, this makes use of real input impedances instead of using static conventional 50 ohm.

In addition, to determine the output DC voltage according to an angle of the incidence of the RF signals and see how this power is converted from AC to DC, the received power versus the angle of each antenna is imported from the HFSS to the ADS software to the MATLAB as a CSV file. Each antenna has its own the received power curve directed into a specific point in space. All curves of received power of antennas are able to cover the most points in space. These two interface environments

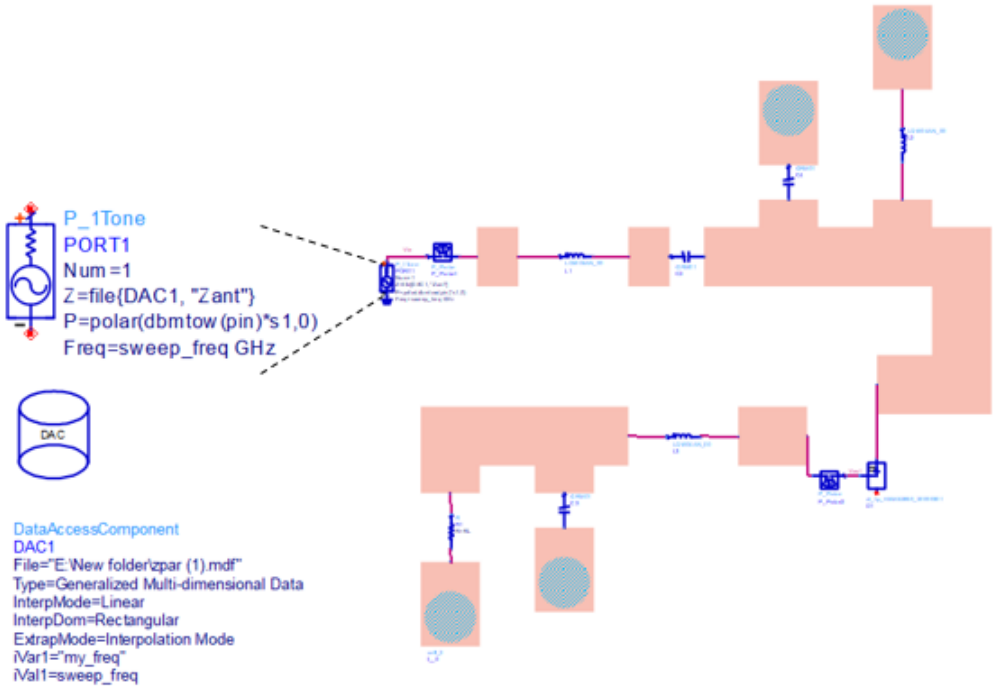

Figure 4.14: Power source of the rectifier circuit when using the real-time input impedance of the antenna imported from the HFSS software

ADS-HFSS and HFSS-MATLAB-ADS really accelerate the procedure to obtain results close to the real-time applications. Each CSV data is normalized and then fitted in MATLAB, and the fitting-equation obtained in MATLAB is utilized in the ADS software in the (VAR) tool. This option gives a function for each normalized curve as shown in Figure 4.15 that indicates a fitting curve and a function of it for one antenna, following the same procedure for all other antennas. At that time, each equation is multiplied by the input power of the rectifier, see Figure 4.14.

This procedure aims to make the rectifier input power reaching its maximum value which is determined by the designers and the diode properties. It occurs only when the angle of the incident power is equal to the operating angle of the antenna; else the input power is less. All curves of the received power fitted in MATLAB are employed as a theme power in the ADS RF power sources. Now, it can be said that each RF power source operates in a specific direction and then gradually power decreases. When the

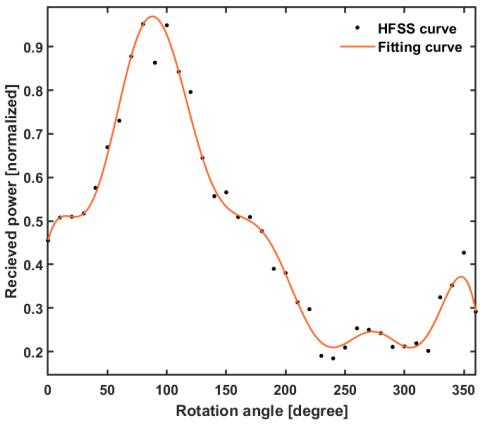

(a)

General model Fourier5:
f(x) = a0 + a1*cos(x*w) + b1*sin(x*w) +
a2*cos(2*x*w) + b2*sin(2*x*w) + a3*cos(3*x*w) + b3*sin(3*x*w) +
a4*cos(4*x*w) + b4*sin(4*x*w) + a5*cos(5*x*w) + b5*sin(5*x*w)
Coefficients (with 95% confidence bounds):
a0 = -0.2283 (-2.791, 2.334)
a1 = -0.4807 (-2.305, 1.344)
b1 = 1.254 (-3.002, 5.51)
a2 = 0.3942 (-2.3, 3.088)
b2 = 0.984 (-1.814, 3.782)
a3 = 0.6595 (-1.686, 3.005)
b3 = 0.009841 (-0.98, 0.9997)
a4 = 0.1825 (0.02471, 0.3402)
b4 = -0.3764 (-1.726, 0.9735)
a5 = -0.07199 (-0.6339, 0.4899)
b5 = -0.1821 (-0.3086, -0.05562)
w = 0.01183 (0.00892, 0.01475)

(b)

Figure 4.15: Fitting process(a) Fitting and original curve of ANT2 (b) The function of the fitting curve

rectenna array is simulated, the DC output voltage at each rectenna separately can be seen in Figure 4.16. It is clearly shown that most directions in 360-degree are covered. Even if there is a noticeable ripple, but when all powers coming from single rectifiers are combined, it will be highly diminished as will be seen later in the subsequent discussion Because the rectennas are assembled relying on the concept of MIMO tech-

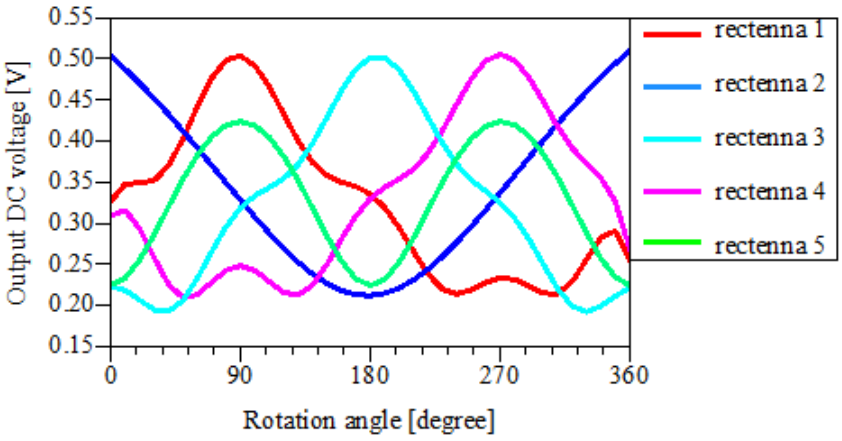

Figure 4.16: The DC voltage of each rectenna when working separately

nique, so the output DC power of individual rectifiers are added together using the DC combiner. There are two methods for DC power combining, connecting them either in parallel or series. It totally depends on the application. In other words, the current or voltage should be larger.

4.5 Parallel Connection

Theoretically, for the case of parallel-connection rectennas, the optimal value of the resistive load is divided by the number of the rectennas (N) [72] used in the multi rectenna, and then the output DC voltage is the same as a single rectenna. This is known that the parallel connection does not increase an amount of the voltage. However, the harvested DC power is increased. The best value for the power can be realized when all rectennas have the same efficiency.

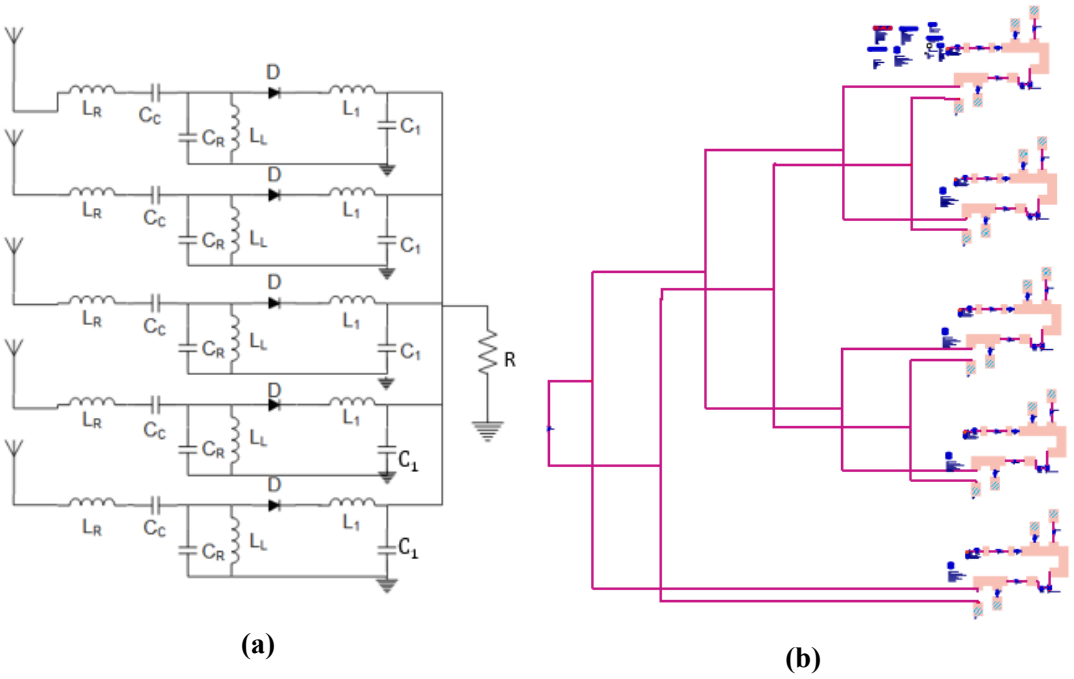

Figure 4.17: The schematic of parallel connection of five rectennas (a) simple form (b) from ADS

It means that all rectifiers have the same input power. This is not always the case, so the best value cannot be obtained at all [72]. However, the resulting degradation will be tolerated in acceptable to some extent as will be elaborated in the next parts. The proposed parallel connection of the multi rectenna is illustrated in Figure 4.17, where the positive terminal of the capacitor is connected to the positive terminal of the resistance and the ground to the negative terminal of the resistance. The optimal resistive

load used for a single rectenna is (1500 ohm), whereas it becomes about only 300ohm for a multi rectenna with five-element (N=5). Assuming all rectennas operate with the same input power of -5 dBm (regardless of the incident power angle). Hence, the output voltage remains the same as a single rectenna as can be displayed in Figure 4.18. Where the output DC voltage is about 0.496V at -5dBm input power for both the single

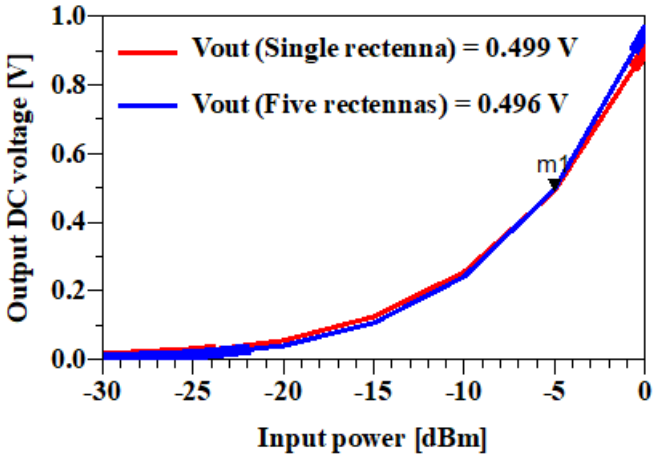

Figure 4.18: The output DC voltage of the single rectenna and multi rectenna as a function of input power. The value takes at -5 dBm input power

rectenna and multi rectenna.

A current of the array is a sum of currents of the individual rectennas as can see in Figure 4.19 where the current is 333 µW for the single rectenna and 1.6 mA for the multi rectenna.

Figure 4.20 shows the output DC powers for the single and the rectenna array as well as a function of the input power. The power of the rectenna array is about 816 µW that represents five-fold of the power of the single rectenna where the power of the single rectenna is 160 µW. The conversion efficiency of the rectenna array is 52.7% larger than the efficiency of the individual rectenna due to the increment in the amount of the harvested power as shown in Figure 4.21. All mentioned results compute for one frequency because the results are relatively equals for the two bands 1.8 and 2.4 GHz.

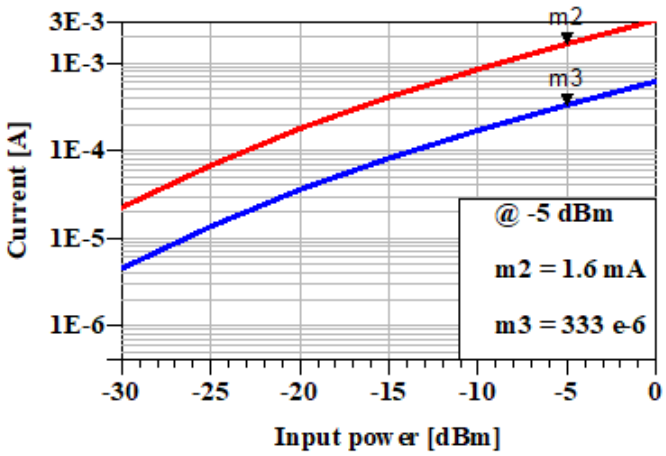

Figure 4.19: The current of balanced parallel DC combine for single and multi rectenna

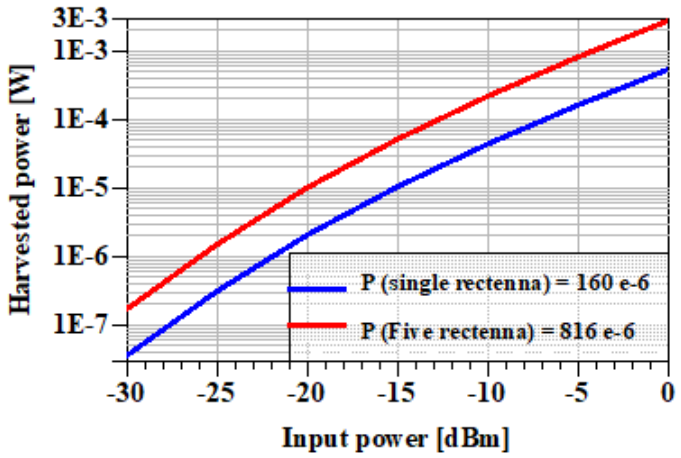

Figure 4.20: The output DC power of balanced for single rectenna and multi rectenna versus input power. at -5 dBm.

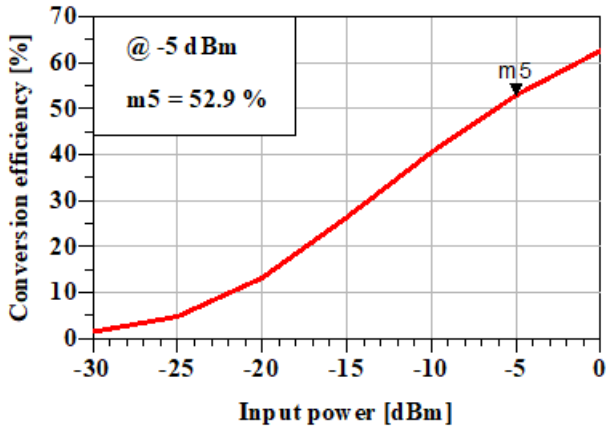

Figure 4.21: The conversion efficiency of the balanced parallel DC combine versus input power with a resistance of 300ohm

Here for the diversity rectenna array, every single rectenna receives power at a specific angle, and due to the geometry of the cube array; they cannot receive the same input power simultaneously. The unbalanced input power for the rectennas produces a degradation in the performance of rectennas [73].

As mentioned before, the cube rectenna is rotated in the horizontal and vertical directions to determining which rectenna operates at a specific angle. Firstly, the horizontal rotation (ie. phi=0 and theta sweep from 0 to 360 degrees) where the antenna from ANT1 to ANT4 will receive power with its maximum value, whereas the ANT5 receives the lowest power than other rectennas as can be seen in Figure 4.10. Consequently, each rectenna operates at a different input power level that makes it unbalanced and so the value of voltage and conversion efficiency will be degraded but they are tolerable. A bunch of tuning and modification stages is made to return both the DC output voltage and the DC output power values as in the balanced method. The output voltage as a function of the resistance value is calculated as in Figure 4.22 a. It can be observed that the DC output voltage increases when the load value increases. However, at the same time, when the load increases, the conversion efficiency of the rectenna decreases as shown in Figure 4.22 b. This represents a big challenge. Thus, to compromise looking for a load resistor that provides moderate values for both the DC output power and voltage is made. The chosen load value gives higher conversion efficiency of 48.9% and a suitable voltage of 0.507 V.

Figures 4.23 and 4.24 show the conversion efficiency and the output DC voltage of the array versus the input power with a sweep of the rotation angle, respectively. At -5 dBm input power the DC voltage is 0.507 V and conversion efficiency is 48.9% at 1.8 and 2.4 GHz, these values can increase by increasing the input power so at 0dBm the voltage is 0.9 V and conversion efficiency is 59%. Consequently, when calculating the DC voltage according to the frequency and incident angle shown in Figure 4.25, it can

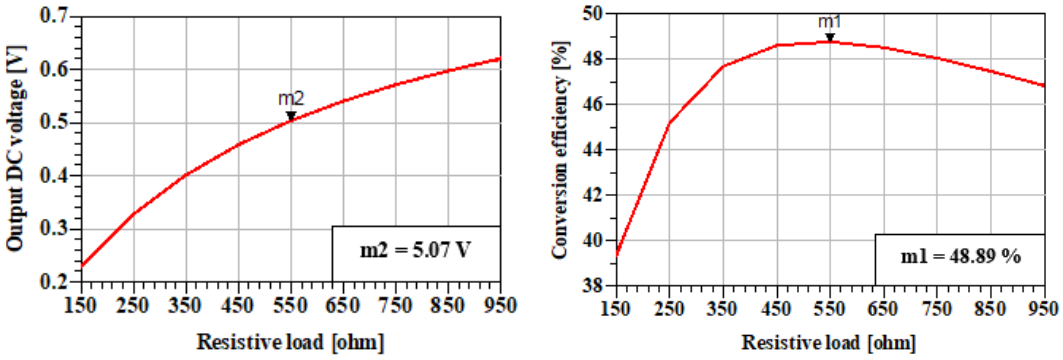

(a) (b)

Figure 4.22: (a) Output voltage (b) Conversion efficiency. as a function of resistance load of parallel DC combine

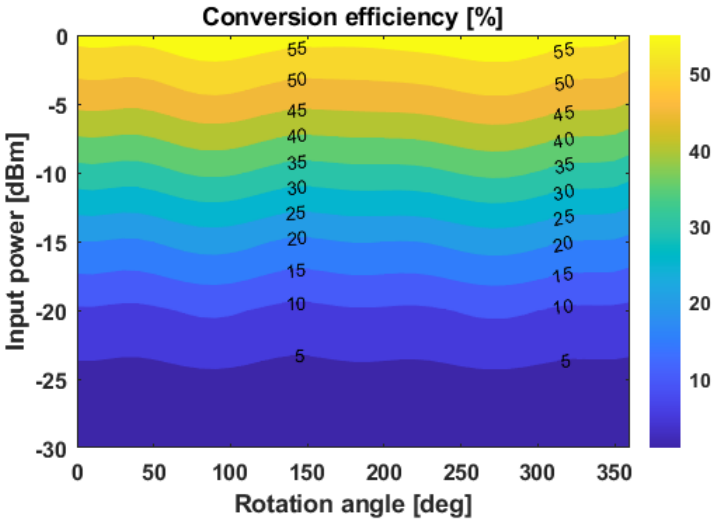

Figure 4.23: Conversion efficiency versus rotation angle with a sweep for input power

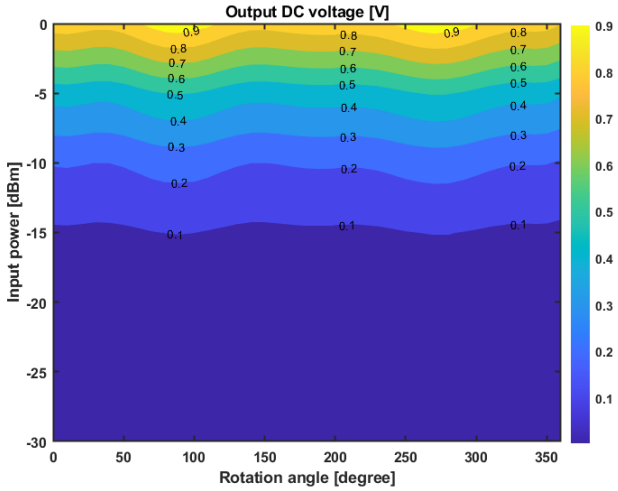

Figure 4.24: The output DC voltage of the multi Rectenna as a function of incident angle and input power.

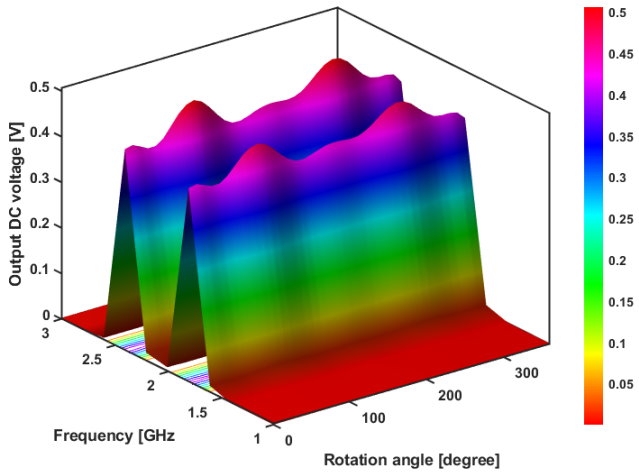

Figure 4.25: The output DC voltage of the multi Rectenna as a function of frequency and incident angle

be observed that the DC voltage curve takes the shape of received power that increases at a specific angle and decreases at others depending on the received amount of power at that angle.

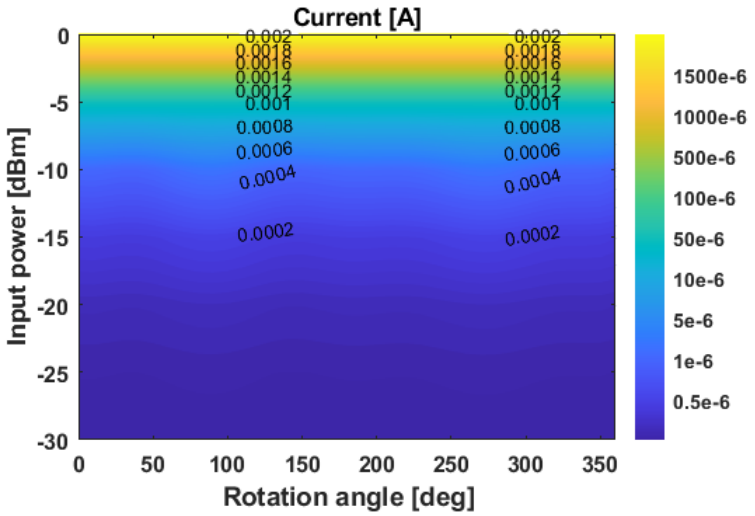

Figure 4.26: Output current versus input power

In the parallel connection, the current increases linearly with a number of the rectennas used in the proposed design. Figure 4.26 shows that the current is about 1mA at -5dBm input power. As known, the DC power can be calculated as $P_{dc} = V_{dc} \times I$, and because the voltage remains the same as the single rectenna does, the DC current and DC power will be increased. However, the accumulated value cannot reach the ideal

value which is the value of the output of the single element multiplied by a number of the rectenna elements in the proposed design due to the unbalanced characteristic of the parallel connection. Figure 4.27 a, b shows the unbalanced DC power in two pats to illustrate the amount of harvested power at very low (-30 to -20)dB and low (-15 to 0) input power.

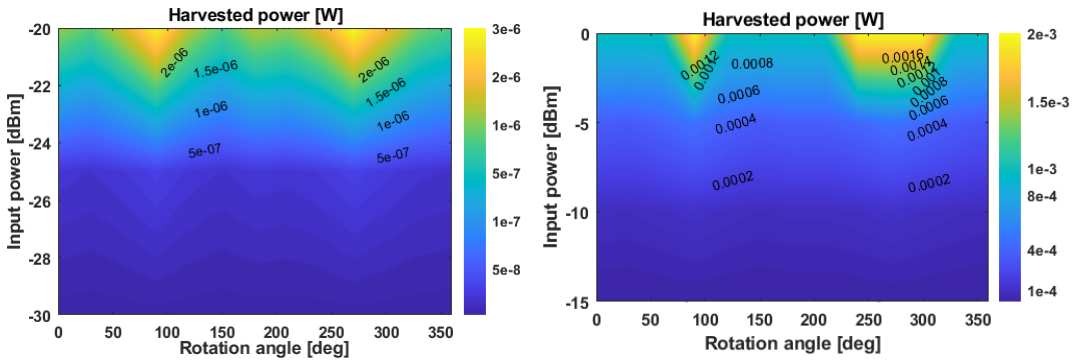

(a) Very low input power

(b) Low input power

Figure 4.27: The harvested DC power as a function of input power and a sweep of rotation angle

To illustrate the difference between the balanced and unbalanced characteristics as well as the single rectenna, these entire situations are depicted in Figure 4.28. The DC power of the single rectenna is 160µW, DC power of the balanced rectenna array is 500µW, and DC power of the balanced array is 816µW.

Secondly, when the rectenna array rotates in the vertical direction (i.e., Phi=90 and theta from 0 to 360) ANT2, ANT4, and ANT5 receive the maximum amount of power as seen in Figure 4.11 b at angles of phi=90 and theta=0, 90, and 180. The output DC voltage of each rectenna as a function of rotation angle and the input power is presented in Figure 4.29 in which indicates that ANT1 and ANT3 have the smallest received amounts of power of 2.2 V. The conversion efficiency is 42% at -5 dBm as can be illustrated in Figure 4.30 that is lower than the conversion efficiency of horizontal rotation that mentioned in Figure 4.23 because two of the antennas receive small

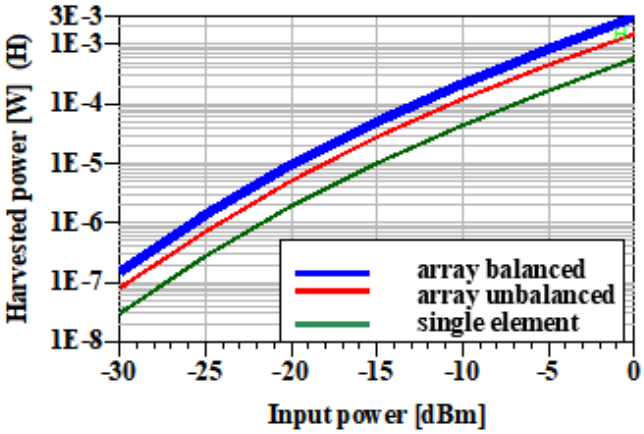

Figure 4.28: Comparision of the output DC power of a single rectenna and multi rectennas in a balanced and imbalanced characteristic

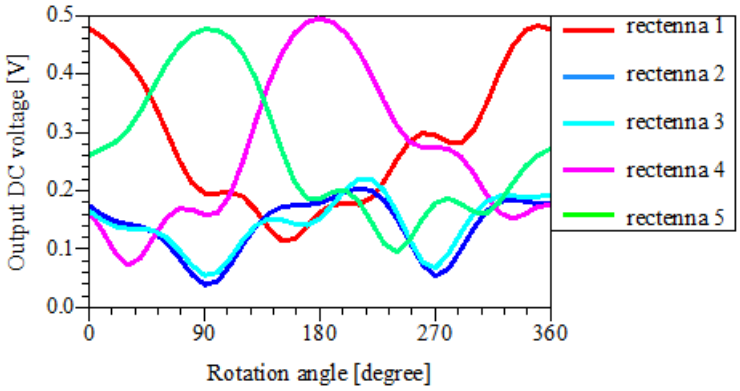

Figure 4.29: Output voltage of the vertical rotation versus angle of incidence power

amount of power . The voltage has also been reduced to be 0.367 V, see Figure 4.31 where the voltage is computed as a function of the rotation angle and sweep of input power. Figure 4.32 shows the output voltage as a function of frequency and a sweep of the rotation angle.

The maximum current is 1.2 mA at 0dBm but at the input power of -5dBm, the current is 640µA as shown in Figure 4.33. The design is well matched for both frequency bands 1.8GHz and 2.4GHz. However, the harvested power from this rotation is 238 µW as shown in Figure 4.34 that separate into two parts to illustrate all details. The results obtained in both situations (i.e., vertical and horizontal rotations) have confirmed that the proposed design can capture signals from almost all directions in space although

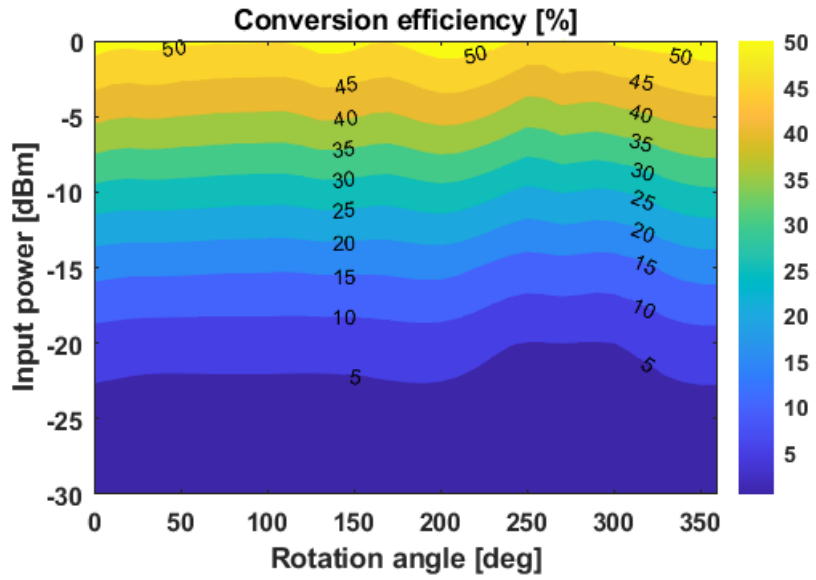

Figure 4.30: The conversion efficiency of multi Rectenna as a function of input power in vertical rotation.

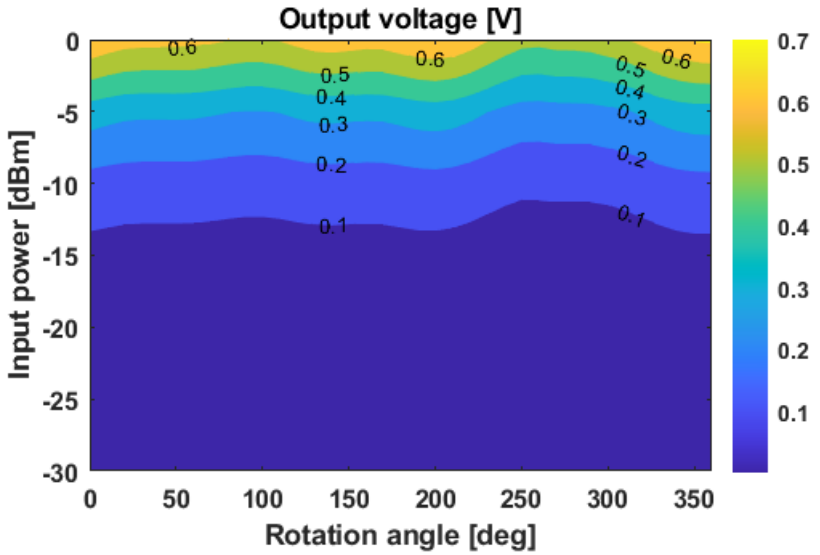

Figure 4.31: The output voltage as a function of rotation angle and sweep of input power

the DC output power and voltage for the vertical one are not good as the horizontal one does. This harvester is able to reduce or remove the use of batteries, especially in low-power sensors.

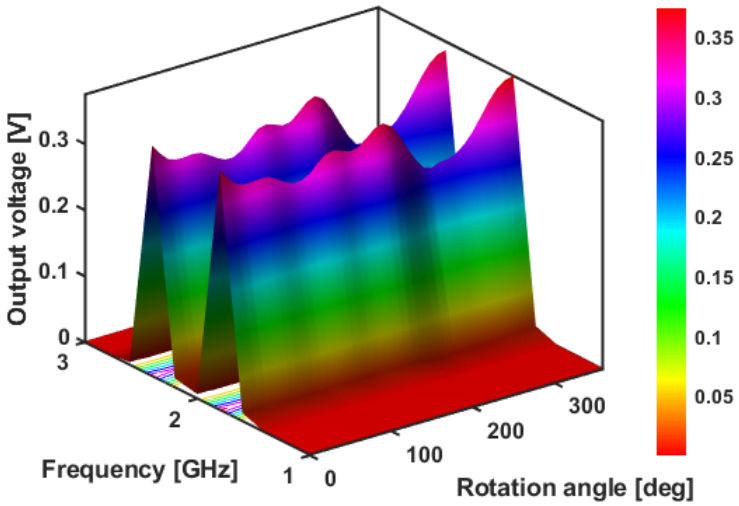

Figure 4.32: The output voltage as a function of rotation angle and sweep of frequency

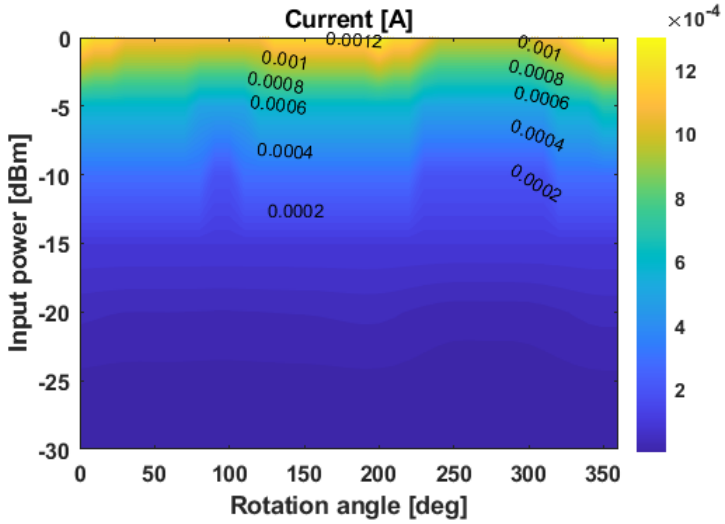

Figure 4.33: Output current versus input power

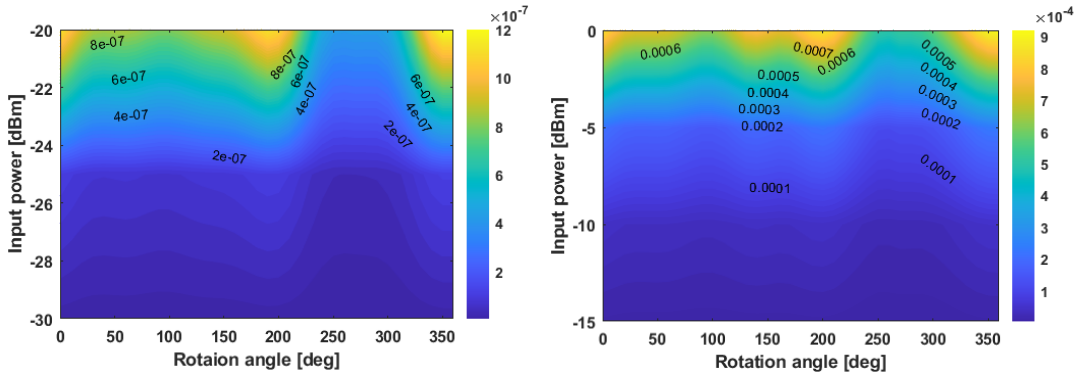

(a) **(b)**

Figure 4.34: The harvested power as a function of Rotation angle and sweep of input power for horizontal rotation

4.6 Series combination

The other way to combine the DC power resulting from rectennas elements is the series DC combining technique, see Figure 4.35. The negative terminal of the first rectifier connects to the positive terminal of the others and then all series rectennas connect to the load. Theoretically, the value of the load is multiplied by the number of the rectennas (N) used in the whole design, so the load value will be 7500 ohms [72] . For this connection, a higher voltage can be obtained at the output which is about 2.5V that represents the sum of voltages of all rectennas as shown in Figure 4.36. The output power also represents the power of the single element (167 µW) multiplied by (N=5) to be about (816 µW) as shown in Figure 4.37.

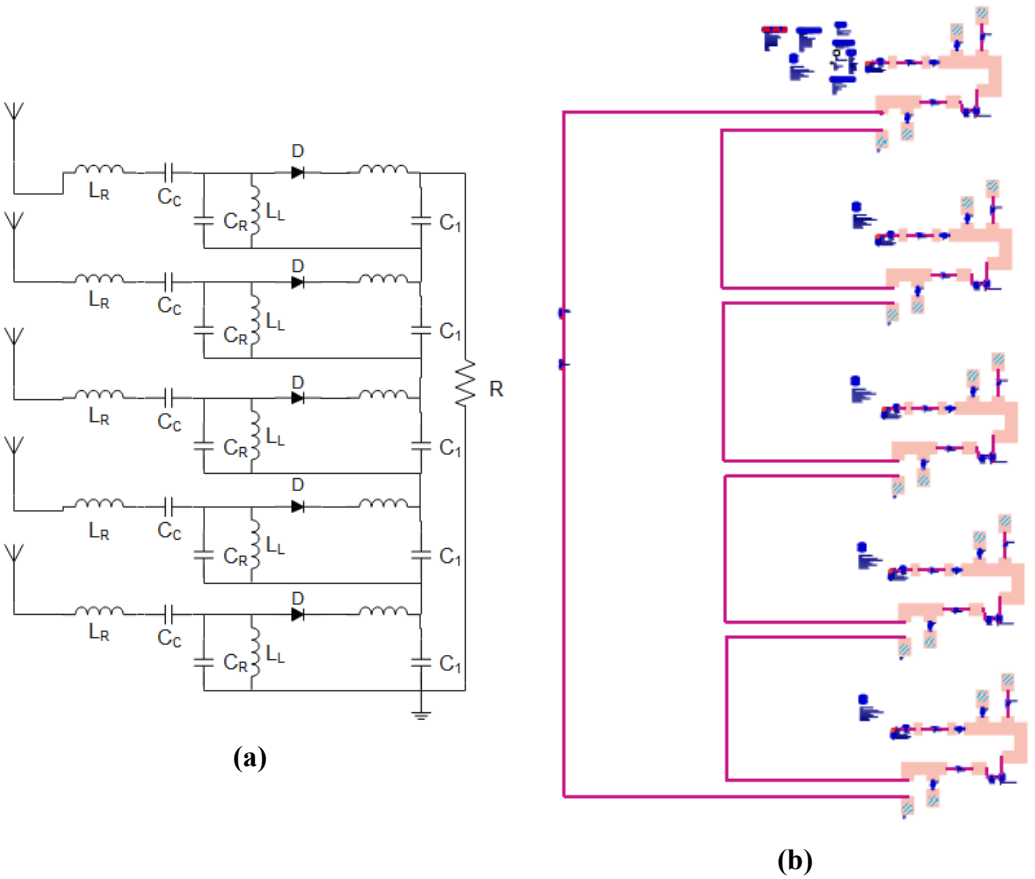

Figure 4.35: Schematic of series DC combine

The DC current of the rectenna array remains the same as for the single rectenna (335 µW) as shown in Figure 4.38. These numerical values are calculated at an input

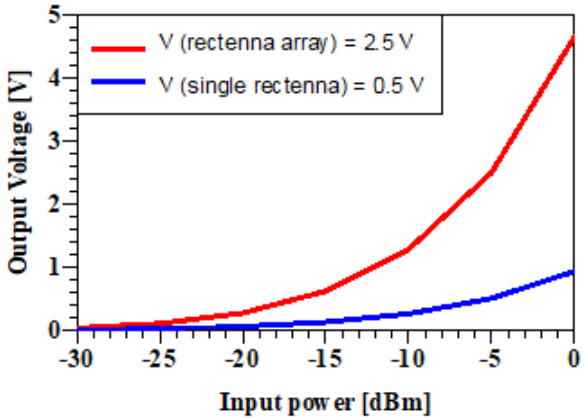

Figure 4.36: Output voltage of balance series DC combination. At (-5 dBm)

power of -5dBm, assumed for all rectennas at the same time. This process, which is not always the case, is called the balanced series DC combining technique. Hence, all results are for the two operating bands 1.8 and 2.4 GHz.

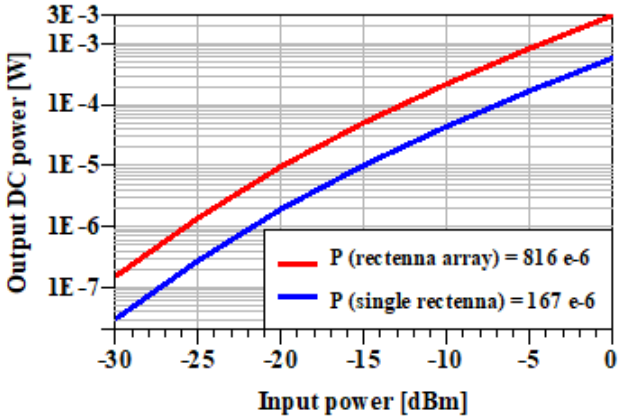

Figure 4.37: Output DC power of balanced series DC combine. At (-5dBm)

It is worth noting that, in both cases, the output DC powers of the two combining techniques are equal to their theoretical values; see Figures 4.20 and 4.37. However, the conversion efficiencies of the two combining DC techniques are also equal when each of them operates at its optimum load value, as illustrated in Figures 4.39 and 4.21.

As mentioned before, the cubical rectenna array can receive the power from almost all directions, so when the power source radiates in a direction of phi=0, for example, so when the array rotates horizontally, the antenna that will directly face the power source will receive the maximum power at that moment, except the ANT5. Thus, at any mo-

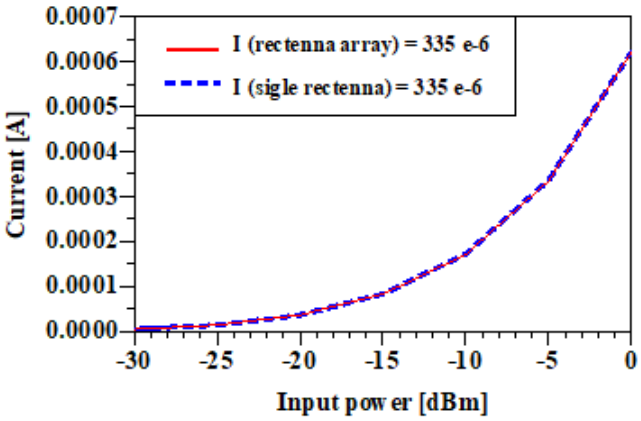

Figure 4.38: Output current of series DC combine at (-5 dBm)

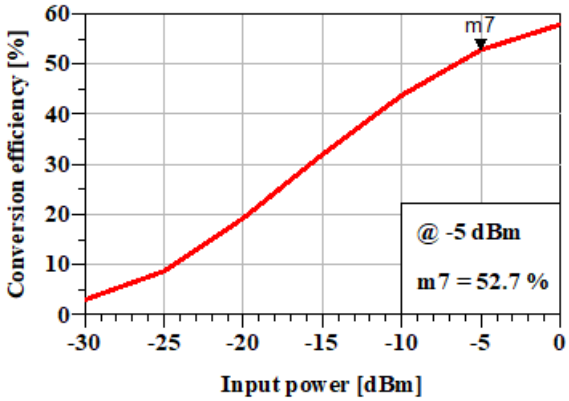

Figure 4.39: The conversion efficiency of balanced series DC combine versus input power at 7500ohm (resistance load)

ment, the input power differs for each antenna, leading to the unbalanced case. This situation deteriorates the amount of the received power. To compensate for this power shortage, the load resistance is tuning. The resistive value will be 10kohm instead of 7500ohm to increase the output DC voltage which is the important parameter in most applications. The new voltage value is 2.077 V as shown in Figure 4.40 a. To this end, the conversion efficiency is decreased to become as 46.3% due to the increase in losses in the circuit but its value is acceptable to some extent as shown in Figure 4.40 b.

The conversion efficiency as a function of Rotation angle and a sweep of input power is shown in Figure 4.41. The maximum efficiency at -5dBm is 46.3%. The figure shows that the efficiency varies in a wide range with a sweep of the incident angles

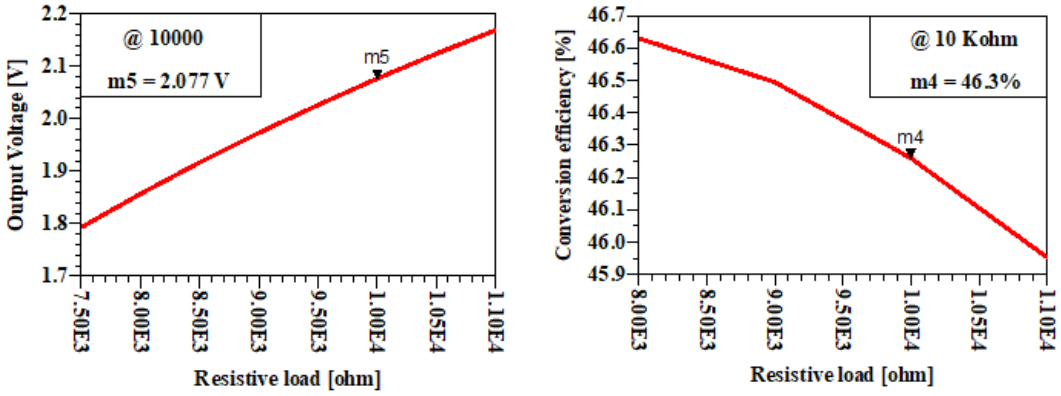

(a) (b)

Figure 4.40: the output voltage and conversion efficiency versus resistance load

of the RF signals. Because the input resistance of each rectifier branch depends on the value of the input power, so the maximum power point of each branch is different.

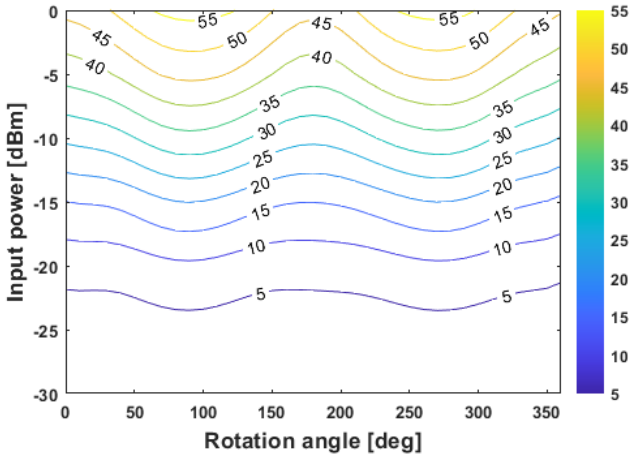

Figure 4.41: Conversion efficiency of unbalanced series DC combine as a function of input power and sweep of rotation angle

The output DC voltage as a function of the rotation angle and sweep of the input power is shown in Figure 4.42. The maximum voltage obtained by the proposed harvester is 3.5V achieved at the input power of 0dBm while the voltage is 2.077 V obtained at -5dBm. Figure 4.43 depicts the output DC voltage as a function of the rotation angle and a sweep of the frequency. There are two maxima in the plot at the frequencies of 1.8GHz and 2.4GHz and two rotation angles of 90 and 270 degrees since the design is matched at these frequencies. Thus, the maximum power transfer between the antenna (i.e., the power source and the rectifier) occurs.

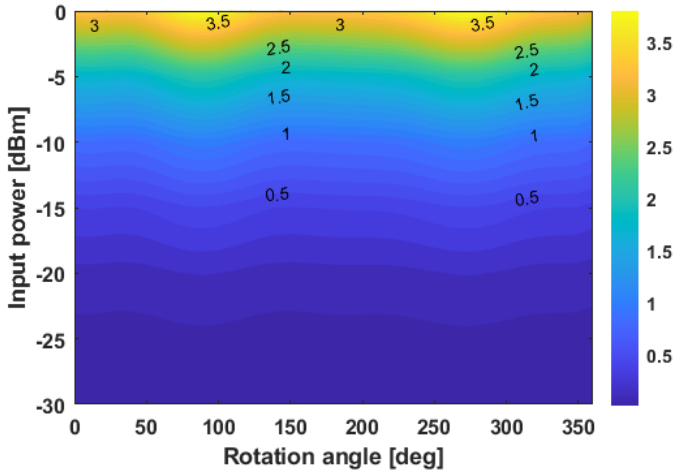

Figure 4.42: Output voltage of series combine as a function of rotation angle and sweep of input power

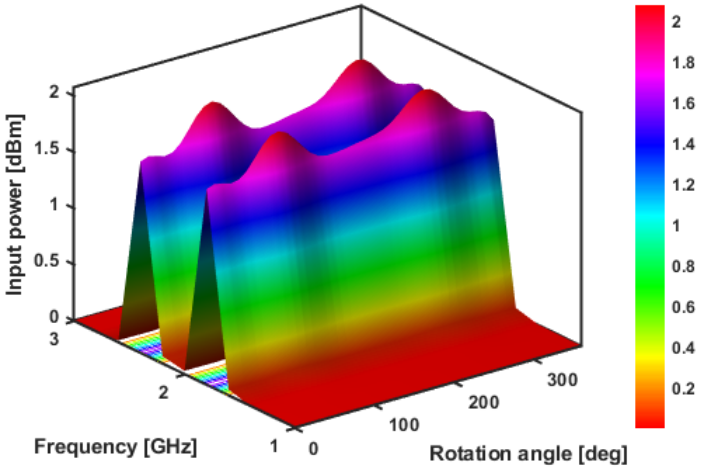

Figure 4.43: Output voltage vs. rotation angle with a sweep of the frequency

The current at this combine is low which equal to 302 µA as can show in Figure 4.44. The maximum harvested power from the series DC combining is 460 µW at -5dBm that illustrate in Figure 4.45, less than the harvested power obtained from the parallel DC combining show in Figure 4.27 due to the interference losses between rectennas. When the source of the power directs into phi =90 degrees, ANT2, ANT4, and ANT5 are receive the maximum power as demonstrated before in the parallel combining technique, so the output DC voltage will be 1.5V at -5dBm as shown in Figure 4.46. The resulting harvested power is 240µW as shown in Figure 4.47, with a conversion efficiency of

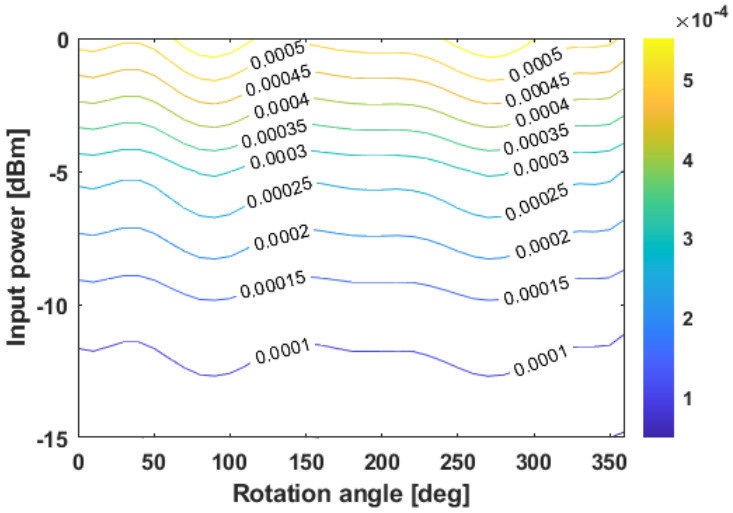

Figure 4.44: The current of series combine versus rotation angle and sweep of input power

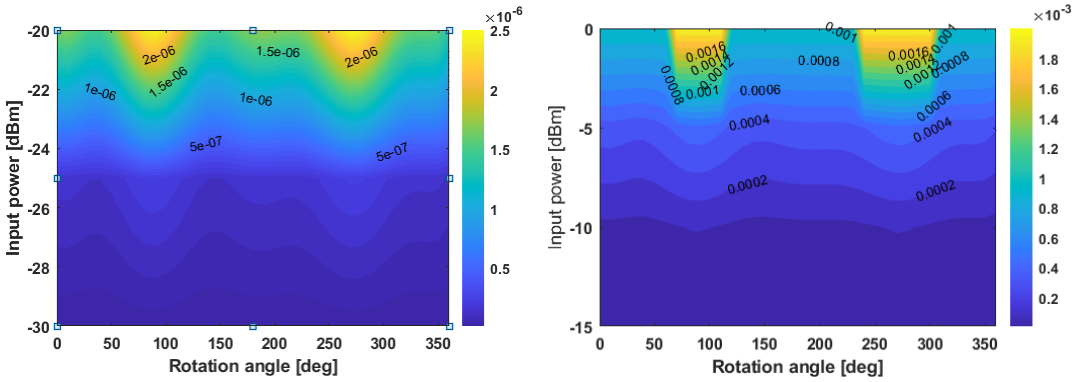

(a) **(b)**

Figure 4.45: Harvested power of series combine as a function of rotation angle and a sweep of input power

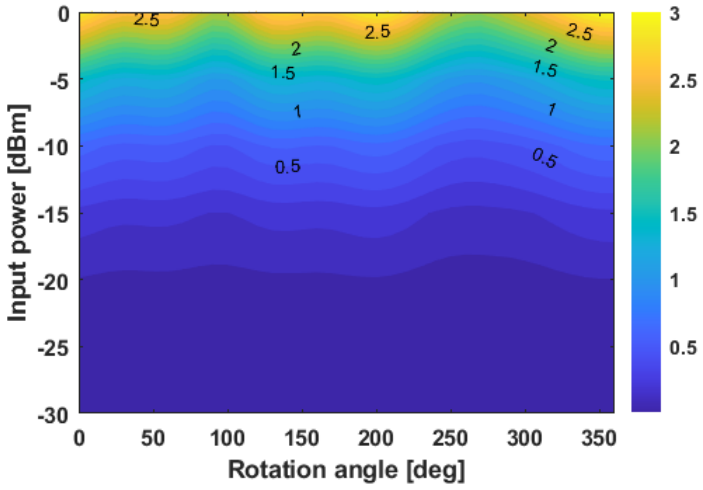

Figure 4.46: Output voltage versus input power with a sweep of rotation angle

40.4%, see Figure 4.48. The aim of compote the harvested power from the two directions is to show that the rectenna array can receive power from viruses direction and that will increase the harvested power.

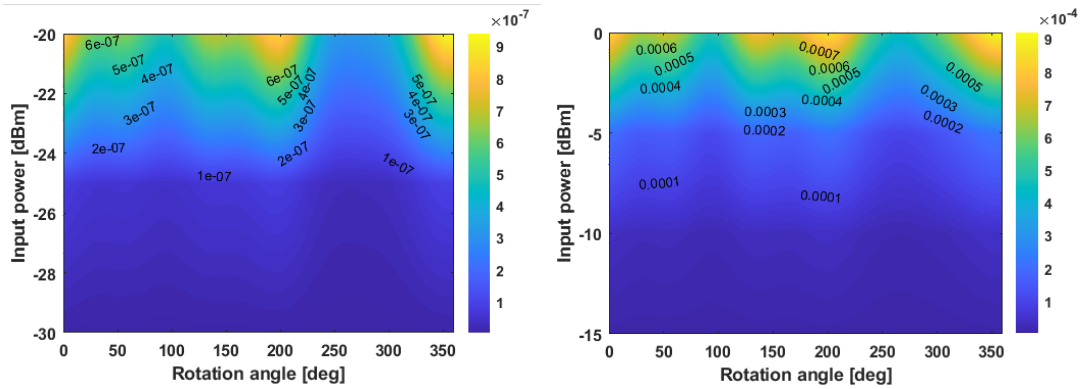

Figure 4.47: Harvested power of series combine as a function of rotation angle and a sweep of input power

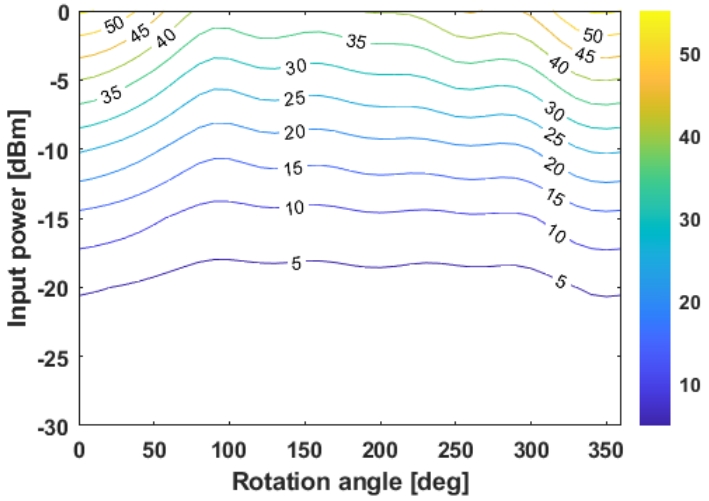

Figure 4.48: Conversion efficiency as a function of input power

4.7 Summary

It can be deduced that the most important things that can differentiate between the two DC combining techniques. Table 4.2 introduces numerical details that can give a good impression about these two methods. As can been noticed, the balance parallel DC combining has the highest results because all rectifiers have the same input power.

This assumption cannot be realized in the real-life. Thus, we have gone through the unbalanced techniques where rectifiers have no equal the input powers. The reason behind that is that each rectenna has its own antenna which is directed into a specific point in space exploiting the spatial diversity. This means signals that will be captured by antennas are not the same at the antennas inputs. Thus, the resulting captured powers provided to the rectifiers will be different. As a result, the unbalanced way will be the fact. The most difficult challenging had faced the research author is the performance degradation. To diminish this problem or at least reduce it, the optimization was run to compensate through varying the load resistance. At the two ways, the antenna can receive power when it rotates either in the horizontal or in the vertical direction.

The rotation has been carried out to mimic the only one fact which is to show that our proposed energy capturer can receive the power from almost all directions. Here, we have achieved one of the project goals which is called the omnidirectional-like energy harvester. Both combining DC techniques enable our proposed rectenna array to increase the harvested power, but the difference is how to increase the power. In the parallel DC combining, the current will be accumulated and increased, whereas the voltage will be the same as the single rectenna does. This situation will be reversed in the series connection. Thus, to choose which connection type is appropriate, it totally depends on the application needs. In other words, we need high either voltage or current. The parallel DC connection can produce current up to 1mA, while the series DC connection can produce voltage up to 2.1V at low input power of -5dBm. The output DC power from the parallel DC connection is 500 μW higher than the power resulted from the series DC connection which is about 460 μW owing to the higher resistance used in the series way.

Table 4.3. shows advantages of the proposed rectenna array in this thesis when

Table 4.2: Compression between DC combining types

connection type	rotation direction	Resistance	Voltage [V]	Current [mA]	efficiency (%)	Power [μW]
Parallel	horizontal balanced	300	0.49	1.6	52.7	816
Parallel	horizontal un-blanced	550	0.5	1	48.9	500
Parallel	vertical un-blanced	550	0.36	0.64	42	240
series	horizontal balanced	7500	2.5	0.33	52.9	816
series	horizontal unbal-anced	10000	2.07	0.3	46.3	460
series	vertical unbal-anced	10000	1.5	0.3	40.4	240

Table 4.3: Literature Review Summery Of Different Types Rectenna Design

Ref.	Freq. (GHz)	gain (dBi)	Size (mm^3)	Rectenna connec-tion	harvested power at input power	efficiency %	output voltage (V)
[48]	2.2	7.46	71X71 X20	parallel, series (bal-anced)	1.66 mW @31 dBm	50%	0.516, 1.087
[41]	1.8, 2.4	2.2, 4.9	100X130 X1.6	RF com-bine	145μW @ -8 dBm		0.54, 0.42
[74]	0.9, 1.8	5	240X240 X1.6	series	25μW @ -3 dBm	30	1.55
[77]	1.8	3.3	138 X 138 X 38	DC com-bining	10 μW @ -5 dBm	40%	/
[47]	2.45	5.23	60 X 60 X 60	parallel com-bining	2.5 μW @ -20 dBm	6.7%	/
this work	1.8, 2.4	5.8, 7.1	65X65 X65	series, parallel (unbal-anced)	460, 500μW @ -5 dBm	46.3, 48.9	2.1, 0.5

compared to other rectennas published in the literature. Most works have large sizes despite the frequency used in those works higher than our design frequency. In other words, the low resonant frequency has a large wavelength that makes the antenna size large. Also, we introduce an assembly configuration that makes our design is relatively small compared to all arrays used in the literature for wireless energy harvesting. The cube shape is advantageous. Some of authors use a single band with high input power to increase the harvested power as in [48] but this power cannot be available due to the low power density of the RF signals in the ambient. Furthermore, most works operate at a single frequency band. This is not preferred, so making our design operating at two bands is salient. The power harvested from space will be increased and we will cover almost all directions in space, thanks to the cube configuration. In [41] and [74] , authors use dual-band rectifiers to increase the captured power but the antenna arrays utilized in these designs receive the power from one direction. At the same input power, our proposed work has higher output DC power about 196μW at -8 dBm and 738μW at -3dBm due to capturing power from multi-direction, resulting in the increase in an amount of the harvested power. In [77] and [47], the authors design Rectenna harvest power from different direction but the Rectenna operate with one band making the harvesting power less.

CHAPTER FIVE

Conclusions

Dual-band rectifier was designed utilizing only lumped elements to have small size. Furthermore, values of the lumped elements were chosen depending on formulas derived also in Chapter 3. The derived formulas have enabled us to deal with any dual band matching network easily at any frequencies. The composite right/left-handed transmission lines technique was exploited to build the matching network. Schottky diode HSMS 2850 was adopted due to its low power junction. The rectifier topology utilized in the research was series single diode rectifier to avoid more losses. The proposed design receives more power compared to others reported in the literature since it operates at dual-frequency at 1.8 GHz and 2.4 GHz to harvest as much power as can. The operating power where the proposed design was supposed to work was -5 dBm.

This study was implemented by using the ADS simulation. A DC pass filter was applied after the diode to reduce the third harmonic, to smooth the output, and to enhance the circuit performance. The electrical and electronic elements were placed on the Roger-3010 substrate; the rectifier had good performance at both bands where S_{11} is -21 and -25 dB at 1.8 GHz and 2.4 GHz, respectively. The output voltage was 0.5 V for the two bands and the conversion efficiency was about 52%. The overall size of the proposed CRLH rectifier was about 5×5.5 mm2, knowing that our proposed rectifier is new design and considers as one of the main contribution in this research work.

Next, the last part in the single rectennas is the antenna. To make this antenna compatible with the proposed rectifier, a dual-band U-slot patch antenna operating at 1.8 GHz and 2.4 GHz was designed using a Ro/Roger-5880 substrate. The size of the

proposed single rectenna was 65×65 mm2. The patch antenna has a high gain of 6.7 dBi and 6.8 dBi for 1.8 GHz and 2.4 GHz, respectively. Thus, it was able to capture more power. The output voltage of single rectenna was 0.5V and the harvested power was 167μW. This power was very small. Also, the single rectenna is unidirectional and cannot cover all angles from -90° to 90°. These two drawbacks were investigated and overcome by the last part of research.

Eventually, five rectennas arranged in a cubical form were proposed. This arrangement, which is called the spatial diversity, enabled the proposed design to scavenge the power from almost all directions (i.e., omnidirectional properties). For multi rectenna stricture the gain is 5.8 dBi and 7.1 dBi for 1.8 GHz and 2.4 GHz, respectively, were realized for each single rectenna. The reduction in the gains compared to the stand-alone single rectenna was due to the mutual coupling which degraded the matching. The overall size of the multi rectennas is 65×65×65 mm3. Later, the output DC power of each rectennas was collected in a parallel or series DC combining.

The proposed multi rectenna stricture can capture power at $\phi = 0^\circ$ and 90° with the different angles of θ. At ϕ=0. Furthermore, with the parallel DC combining, the output DC power was 500 μW which is slightly than the series DC power combining with value of 460 μW. The output current of the parallel DC power combining was 1 mW while the voltage was 0.5 V. However, in the series DC power combining, the current was small while the voltage is 2.1 V.

5.1 Future Works

1. The proposed design was operating with linear polarization, so this is considered a big issue, especially when the power source is unknown. Therefore, building a Rectenna with circular polarization will defeat this problem.

2. Fabricate the proposed design.

3. Use a hybrid technique Of DC power combining to have advantages of both ways.

4. The rectifier can be designed with a broad band to cover almost active bands used daily.

5. Each face in the cube has a single antenna, so this work can be extended to have an array on each face.

6. The mathematical model of the dual-band CRLH matching network can be extended to be multi-band CRLH technique.

Bibliography

[1] Sengupta, D. L., & Sarkar, T. K. (2003). Maxwell, Hertz, the Maxwellians, and the early history of electromagnetic waves. *IEEE Antennas and Propagation Magazine*, 45(2), 13-19.

[2] Carlson, W. B. (2015). Tesla: Inventor of the electrical age. *P*rinceton University Press.

[3] Brown, W. C. (1984). The history of power transmission by radio waves. *IEEE Transactions on microwave theory and techniques*, 32(9), 1230-1242.

[4] Cao, S., & Li, J. (2017). A survey on ambient energy sources and harvesting methods for structural health monitoring applications. *Advances in Mechanical Engineering*, 9(4), 1687814017696210.

[5] Khan, M. S. A., Hoq, M. T., Karim, A. Z., Alam, M. K., Howlader, M., & Rajkumar, R. K. (2019). Energy Harvesting—Technical Analysis of Evolution, Control Strategies, and Future Aspects. *Journal of Electronic Science and Technology*, 17(2), 116-125.

[6] Enescu, D. (2019). Thermoelectric energy harvesting: basic principles and applications. *Green energy advances*, 1.

[7] Abdal-Kadhim, A. M., & Leong, K. S. (2017, April). Application of thermal energy harvesting from low-level heat sources in powering up WSN node. In *2017 2nd International Conference on Frontiers of Sensors Technologies (ICFST)* (pp. 131-135). IEEE. Shenzhen, China

[8] Beeby, S. P., Tudor, M. J., & White, N. M. (2006). Energy harvesting vibration sources for microsystems applications. *Measurement science and technology*, 17(12), R175.

[9] Sharma, H., Haque, A., & Jaffery, Z. A. (2018, October). An efficient solar energy harvesting system for wireless sensor nodes. *In 2018 2nd IEEE International Conference on Power Electronics, Intelligent Control and Energy Systems (ICPE-ICES)* (pp. 461-464). IEEE.

[10] Minnaert, B., & Veelaert, P. (2010). WHICH TYPE of solar cell is best for low power indoor devices?. *In Innovation for Sustainable Production: i-SUP 2010* (pp. 8-12). Ghent University, Department of Electronics and information systems.

[11] Roundy, S., Wright, P. K., & Rabaey, J. M. (2004). Vibration Sources and Conversion Model. In Energy Scavenging for Wireless Sensor Networks (pp. 27-39). *Springer, Boston, MA*.

[12] Zelenika, S., Hadas, Z., Bader, S., Becker, T., Gljušćić, P., Hlinka, J., ... & Vrcan, Ž. (2020). Energy harvesting technologies for structural health monitoring of airplane components—a review. *Sensors*, 20(22), 6685.

[13] Bridgeless, L. P. (2016). Vibration based piezoelectric energy harvesting utilizing bridgeless rectifier circuit. *Jurnal Kejuruteraan*, 28, 87-94.

[14] Nechibvute, A., Chawanda, A., Taruvinga, N., & Luhanga, P. (2017). *Radio frequency energy harvesting sources.*

[15] Zeng, M., Li, Z., Andrenko, A. S., Zeng, Y., & Tan, H. Z. (2018). A compact dual-band rectenna for GSM900 and GSM1800 energy harvesting. *International Journal of Antennas and Propagation*, 2018.

[16] Shen, S., Zhang, Y., Chiu, C. Y., & Murch, R. (2020). Directional Multiport Ambient RF Energy-Harvesting System for the Internet of Things. *IEEE Internet of Things Journal*, 8(7), 5850-5865.

[17] Piñuela, M., Mitcheson, P. D., & Lucyszyn, S. (2013). Ambient RF energy harvesting in urban and semi-urban environments. *IEEE Transactions on microwave theory and techniques*, 61(7), 2715-2726.

[18] Gao, S. P., & Zhang, H. (2019, October). Topology Comparison of Single-diode Rectifiers: Shunt Diode vs. Series Diode. *In 2019 12th International Workshop on the Electromagnetic Compatibility of Integrated Circuits* (EMC Compo) (pp. 177-179). IEEE.

[19] Tissier, J., Koohestani, M., & Latrach, M. (2019, June). A Comparative Study of Conventional Rectifier Topologies for Low Power RF Energy Harvesting. *In 2019 IEEE Wireless Power Transfer Conference (WPTC)* (pp. 569-572). IEEE.

[20] Baddipadiga, B. P., & Ferdowsi, M. (2016). A high-voltage-gain dc-dc converter based on modified dickson charge pump voltage multiplier. *IEEE Transactions on Power Electronics*, 32(10), 7707-7715.

[21] Kumar, S. S., Ramkumar, M. S., Amudha, A., Balachander, K., & Emayavaramaban, G. (2019). Cascade Cockcroft-Walton voltage multiplier applied to transformerless high step-up dc-dc converter. *Mathematical & Computational Forestry & Natural Resource Sciences*, 11(1).

[22] Muhammad, S., Jiat Tiang, J., Kin Wong, S., Iqbal, A., Alibakhshikenari, M., & Limiti, E. (2020). Compact rectifier circuit design for harvesting GSM/900 ambient energy. *Electronics*, 9(10), 1614.

[23] Zeng, M., Li, Z., Andrenko, A. S., Liu, X., & Tan, H. Z. (2017). Differential voltage octuple rectifiers for wireless energy harvesting. *Microwave and Optical Technology Letters*, 59(7), 1574-1578.

[24] Sedeek, A., Tammam, E., & Hasaneen, E. S. (2018, December). High efficiency 2.45 GHz low power hybrid junction rectifier for RF energy harvesting.

In 2018 International Japan-Africa Conference on Electronics, Communications and Computations (JAC-ECC) (pp. 147-150). IEEE.

[25] Liu, C., Tan, F., Zhang, H., & He, Q. (2016). A novel single-diode microwave rectifier with a series band-stop structure. *IEEE transactions on microwave theory and techniques*, 65(2), 600-606.

[26] Hamano, K., Tanaka, R., Yoshida, S., Miyachi, A., Nishikawa, K., & Kawasaki, S. (2017, June). Design of concurrent dual-band rectifier with harmonic signal control. *In 2017 IEEE MTT-S International Microwave Symposium (IMS)* (pp. 1042-1045). IEEE.

[27] Aboualalaa, M., Mansour, I., Mansour, M., Bedair, A., Allam, A., Abo-Zahhad, M., ... & Pokharel, R. K. (2018, June). Dual-band rectenna using voltage doubler rectifier and four-section matching network. *In 2018 IEEE Wireless Power Transfer Conference (WPTC)* (pp. 1-4). IEEE.

[28] ur Rehman, M., Ahmad, W., & Khan, W. T. (2017, November). Highly efficient dual band 2.45/5.85 GHz rectifier for RF energy harvesting applications in ISM band. *In 2017 IEEE Asia Pacific Microwave Conference (APMC)* (pp. 150-153). IEEE.

[29] Chandravanshi, S., & Akhtar, M. J. (2017, November). A dual band differential rectifying circuit for RF energy harvester. *In 2017 IEEE Asia Pacific Microwave Conference (APMC)* (pp. 491-494). IEEE.

[30] Chandrasekaran, K. T., Agarwal, K., Alphones, A., Mittra, R., & Karim, M. F. (2020). Compact Dual-Band Metamaterial-Based High-Efficiency Rectenna: An Application for Ambient Electromagnetic Energy Harvesting. *IEEE Antennas and Propagation Magazine*, 62(3), 18-29.

[31] Contreras, A., Rodríguez, B., Steinfeld, L., Schandy, J., & Siniscalchi, M. (2020, February). Design of a Rectenna for Energy Harvesting on Wi-Fi at 2.45 GHz. *In 2020 Argentine Conference on Electronics (CAE)* (pp. 63-68). IEEE.

[32] Çelik, K., & Kurt, E. (2019). A novel meander line integrated E-shaped rectenna for energy harvesting applications. *International Journal of RF and Microwave Computer-Aided Engineering*, 29(1), e21627.

[33] Zheng, G., Dang, K., Sun, B., & Zhang, J. (2019). Design of perfect electrical conductor wall-loaded 2.45 GHz high-efficiency rectenna. *International Journal of RF and Microwave Computer-Aided Engineering*, 29(3), e21604.

[34] Mansour, M., & Kanaya, H. (2019, June). Implementation of a High-Efficient and Simple CPW Rectenna at the 2.45 GHz ISM Radio Band. *In 2019 IEEE Wireless Power Transfer Conference (WPTC)* (pp. 316-320). IEEE.

[35] Tissier, J., & Latrach, M. (2019). A 900/1800 MHz dual-band high-efficiency rectenna. *Microwave and Optical Technology Letters*, 61(5), 1278-1283.

[36] Niotaki, K., Kim, S., Jeong, S., Collado, A., Georgiadis, A., & Tentzeris, M. M. (2013). A compact dual-band rectenna using slot-loaded dual band folded dipole antenna. *IEEE Antennas and Wireless Propagation Letters*, 12, 1634-1637.

[37] Gajanan, P., Arora, B., Goel, T., & Patnaik, A. (2019, December). A Dual-band Microwave Energy Harvesting Rectenna System for WiFi Sources. *In 2019 IEEE Indian Conference on Antennas and Propogation (InCAP)* (pp. 1-4). IEEE.

[38] Lin, D. B., Yu, C. K., Lin, C. K., & Lee, Y. H. (2017, October). Dual band rectenna with one rectifier. In 2017 *International Symposium on Electronics and Smart Devices (ISESD)* (pp. 268-272). IEEE.

[39] Li, X., Yang, L., & Huang, L. (2019). Novel design of 2.45-GHz rectenna element and array for wireless power transmission. *IEEE Access*, 7, 28356-28362.

[40] Chandravanshi, S., & Akhtar, M. J. (2020). An efficient dual-band rectenna using symmetrical rectifying circuit and slotted monopole antenna array. *International Journal of RF and Microwave Computer-Aided Engineering*, 30(4), e22117.

[41] Mahfoudi, H., Takhedmit, H., & Tellache, M. (2018). Dual-band dual-polarized stacked rectenna for RF energy harvesting at 1.85 and 2.45 GHz.

[42] Reed, R., Pour, F. L., & Ha, D. S. (2020, August). An Efficient 2.4 GHz Differential Rectenna for Radio Frequency Energy Harvesting. *In 2020 IEEE 63rd International Midwest Symposium on Circuits and Systems (MWSCAS)* (pp. 208-212). IEEE.

[43] Assimonis, S. D., Fusco, V., Georgiadis, A., & Samaras, T. (2018). Efficient and sensitive electrically small rectenna for ultra-low power RF energy harvesting. *Scientific reports*, 8(1), 1-13.

[44] Wang, S., & Chang, H. Y. (2020, August). A 3D Rectenna with All-polarization and Omnidirectional Capacity for IoT Applications. *In 2020 IEEE/MTT-S International Microwave Symposium (IMS)* (pp. 1188-1190). IEEE.

[45] Fezai, F., Menudier, C., Thevenot, M., Monediere, T., & Chevalier, N. (2016). Multidirectional Receiving System for RF to dc Conversion Signal: Application to home automation devices. *IEEE Antennas and Propagation Magazine*, 58(3), 22-30.

[46] Kimionis, J., Isakov, M., Koh, B. S., Georgiadis, A., & Tentzeris, M. M. (2015). 3D-printed origami packaging with inkjet-printed antennas for RF harvesting sensors. *IEEE Transactions on Microwave Theory and Techniques*, 63(12), 4521-4532.

[47] Vuong, T. P., Verdier, J., Allard, B., & Benech, P. (2019). Design and measurement of 3D flexible antenna diversity for ambient RF energy scavenging in indoor scenarios. *IEEE Access*, 7, 17033-17044.

[48] Almoneef, T. S. (2020). Design of a rectenna array without a matching network. *IEEE Access*, 8, 109071-109079.

[49] Huang, Y. (2021). *Antennas: from theory to practice*. John Wiley & Sons.

[50] Lo, Y. T., & Lee, S. W. (2013). *Antenna Handbook: theory, applications, and design*. Springer Science & Business Media.

[51] Maas, S. A. (2003). *Nonlinear microwave and RF circuits*. Artech house.

[52] Ramesh, G. P., & Rajan, A. (2014, April). Microstrip antenna designs for RF energy harvesting. *In 2014 International Conference on Communication and Signal Processing* (pp. 1653-1657). IEEE.

[53] Agwil, R. O., Benchikh, S., Djillali, H., & Tatu, S. O. (2020). Antenna rectifier using quadrature hybrid coupler for power-harvesting applications. *International Journal of RF and Microwave Computer-Aided Engineering*, 30(9), e22279.

[54] Tanagardi, M. (2019). *Radiation Pattern Reconfigurable Horn Antenna Based on Parasitic Layer Concept* (Doctoral dissertation, Utah State University).

[55] Yiğitler, H. (2018). Narrowband radio frequency inference: Physical modeling and measurement processing.

[56] Epp, L. W., Khan, A. R., Smith, H. K., & Smith, R. P. (2000). A compact dual-polarized 8.51-GHz rectenna for high-voltage (50 V) actuator applications. *IEEE Transactions on Microwave Theory and Techniques*, 48(1), 111-120.

[57] Visser, H. J. (2006). *Array and phased array antenna basics*. John Wiley & Sons.

[58] Balanis, C. A. (2015). *Antenna theory: analysis and design*. John wiley & sons.

[59] Song, C., Huang, Y., Carter, P., Zhou, J., Yuan, S., Xu, Q., & Kod, M. (2016). A novel six-band dual CP rectenna using improved impedance matching technique for ambient RF energy harvesting. *IEEE Transactions on Antennas and Propagation*, 64(7), 3160-3171.

[60] Zhang, Z. (2017). *Antenna design for mobile devices*. John Wiley & Sons.

[61] Wang, B., & Cao, Z. (2019). A review of impedance matching techniques in power line communications. *Electronics*, 8(9), 1022.

[62] Qin, X., He, G., Yang, X., & Gao, S. (2021). A Compact Rectifier Design Method Utilizing Harmonics.*Applied Sciences*, 11(5), 2295.

[63] Pozar, D. M. (2000). *Microwave and RF design of wireless systems*. John Wiley & Sons.

[64] Yoo, T. W., & Chang, K. (1992). Theoretical and experimental development of 10 and 35 GHz rectennas. *IEEE Transactions on Microwave Theory and Techniques*, 40(6), 1259-1266.

[65] McSpadden, J. O., Fan, L., & Chang, K. (1998). Design and experiments of a high-conversion-efficiency 5.8-GHz rectenna. *IEEE transactions on microwave theory and techniques*, 46(12), 2053-2060.

[66] Mohammed, A. S., Kamal, S., Ain, M. F., Ahmad, Z. A., Ullah, U., Othman, M., ... & Ab Rahman, M. F. (2019). Microstrip patch antenna: A review and the current state of the art. *Journal of Advanced Research in Dynamical and Control Systems*, 11(Sp. 7), 510-524.

[67] Pozar, D. M. (2011). *Microwave engineering*. John wiley & sons.

[68] Medley, M. W. (1993). *Microwave and RF circuits: analysis, synthesis, and design*. Artech House.

[69] Moon, B. T., & Myung, N. H. (2013). A dual-band impedance transforming technique with lumped elements for frequency-dependent complex loads. *Progress In Electromagnetics Research*, 136, 123-139.

[70] Alsaleh, A. A., Islam, M. R., Nordin, M. A. W., & Al-Askari, S. (2016, July). Design and Optimization of Dual Band Microstip Patch Antenna Using Slots Pair. *In 2016 International Conference on Computer and Communication Engineering (ICCCE)* (pp. 439-442). IEEE.

[71] Van Hoang, T. Q., Séguenot, E., Ferrero, F., Dubard, J. L., Brachat, P., & Desvilles, J. L. (2013). 3D voltage pattern measurement of a 2.45 GHz rectenna.*IEEE transactions on antennas and propagation*, 61(6), 3354-3356.

[72] Takhedmit, H., Cirio, L., Merabet, B., Allard, B., Costa, F., Vollaire, C., & Picon, O. (2011). A 2.45-GHz dual-diode rectenna and rectenna arrays for wireless remote supply applications. *International journal of microwave and wireless technologies*, 3(3), 251-258.

[73] Shinohara, N., & Matsumoto, H. (1998). Dependence of dc output of a rectenna array on the method of interconnection of its array elements. *Electrical Engineering in Japan*, 125(1), 9-17.

[74] Shen, S., Zhang, Y., Chiu, C. Y., & Murch, R. (2019). An ambient RF energy harvesting system where the number of antenna ports is dependent on frequency. *IEEE Transactions on Microwave Theory and Techniques*, 67(9), 3821-3832.

[75] Zhang, T. T., Law, M. K., Mak, P. I., Vai, M. I., & Martins, R. P. (2018). Nanowatt class energy-efficient capacitive sensor interface with on-chip temperature drift compensation. *IEEE Sensors Journal*, 18(7), 2870-2882.

[76] Oshima, S., Matsunaga, K., Kondo, T., & Morimura, H. (2015). Ultralow power Sensor Node with Nanowatt Wireless Circuit Technology. *NTT Technical Review*, 13(1).

[77] Shen, S., Zhang, Y., Chiu, C. Y., & Murch, R. D. (2018). Compact quad-port dual-polarized dipole rectenna for ambient RF energy harvesting *IET*.

[78] Caliò, R., Rongala, U. B., Camboni, D., Milazzo, M., Stefanini, C., De Petris, G., & Oddo, C. M. (2014). *Piezoelectric energy harvesting solutions. Sensors*, 14(3), .4755-4790

List of Publications

1. Marwa Jasim Alhily, Dr. Nasr Al-Khafaji, and Dr. Salim Wadi. ”Compact Dual-Band RF Rectifier for Wireless Energy Harvesting Using CRLH Technique.” Indonesian Journal of Electrical Engineering and Computer Science. http://doi.org/10.11591/ijeecs.v24.i1.pp338-346

2. ”CRLH technique based dual band ambient RF energy harvesting for compact rectifier.” Has been accepted in the 7^{th} International Conference on Renewable Energy and Materials Technology (ICOREMT). The accepted manuscripts will be published in IOP Conference Series in Scopus Journal Earth and Environmental Science.

3. . “Dual Band Rectenna Array with Omni-directional Properties”. In AL-Furat Journal of Innovation in Electronic and Computer Engineering. In Review

الخلاصة

حصاد الطاقة هي تقنية واعدة في مجال انترنيت الاشياء التي تعتمد بصورة رئيسية على الحساسات، وا لتي بدورها تحتاج الى مصدر مستمر للطاقة. هذا بحد ذاته يعتبر تحدي كبير لان البطارات تحتاج الى التغيير بين وقت واخر مما يسبب عبئ ثقيل على البيئة. على اي حال، البحث عن حلول اصبح ضرورة ملحة. حيث ان الحل يكمن باعادة استخدام الطاقة الضائعة في الموجات الراديوية لتوفير الطالقة اللازمة لعمل الاجهزة.

معظم التصاميم السابقة لل Rectenna تعمل بقدرات ادخال عالية وهذه القدرات لايمكن ايجادها لان كثافة القدره للموجات الراديويه في المحيط لا تتعدى بضع مايكروواط. لهذا الباحثين قاموا باستخدام عدد من Rectenna لحل هذه المشكلة. تصميم مجموعة من Rectenna يحتاج الى حجم كبير لان الهوائيات يجب ان تنفصل بمسافة كافية لتفادي cappling matual والذي يكون سببا في تقليل الاداء. بصورة عامة، تلتقط الهوائيات الاشاره من زوايا محدده وهذا يعتبر مشكلة بحد ذاته.

لان Schottky diode HSMS2850 يمتلك جهد عتبه قليل، يعتبر جيد للاستخدام في دوائر المحول وبذلك يكون مناسب للقدرات القليلة. المحول المقترح يعمل ضمن الترددات الخلويه 1.8 كيكا هيرتز وكذلك ترددات الواي فاي 2.4 كيكا هيرتز بقدرة ادخال من -30 الى -5 ديسيبيل. تصميم شبكة الربط CRLH باستخدام العناصر المنفصلة فقط للحصول على حجم صغير للمحول 5 X 5.5 ملم. المعادلة الخاصة بشبكة الربط تم اشتقاقها للمساعدة في تحديد قيم العناصر المستخدمة..

للحصول على هوائي يعمل بترددين دون اضافه اجزاء خارجية، تم قطع شكل U من الجزء الباعث للهوائي لكي يعمل ضمن الترددين 1.8 و 2.4 كيكا هيرتز وبكسب 6.7و 6.8 ديبسيبيل بالتتابع. يوضع المحول في الجهة الخلفية للهوائي لتصغير الحجم الكلي، وهذا يجعل التصميم معقدا بعض الشيء. فرق الجهد الخارجي للمحول هو 0.5 فولت وقدرة الاخراج 167 مايكرواط. Rectenna المذكور سابقا سوف يستخدم في بناء مجموعة من Rectennas على شكل مكعب. يحتوي هذا المكعب على خمس هوائيات ويكون قادر على استلام القدرة من خمس اتجاهات بكسب 5.8 دييسيبيل عند 1.8 كيكاهيرتز 1.7 ديسيبيل عند 2.4 كيكا هيرتز.

مجموعه REctennas مصممة بحيث كل هوائي يرتبط بالمحول بصورة مباشرة. بعد ذلك، تجمع اخراجات المحولات للحصول على القدرة الكلية. ويكون الربط بطريقتين عند ربط التوازي، يكون فرق

الجهد مشابه لRectenna المفرد 5.0 فولط، يبنما يزداد التيار ليصبح 1 ملي امبير والقدرة 500 مايكروواط عند قدرة الادخال -5 ديسيبيل ويكفاءه تحويل 48.9. اما عندر ربط التوالي، فان الفولتية تزداد لتصبح 1.2 فولت ولكن التيار يكون مشابه للRectenna المفرد وهو 333 مايكروواط بينما القدرة الكلية المستحصلة فهي 460 مايكروواط عند نفس قدرة الادخال.

مجموعة حصادات الطاقة للموجات الراديوية في نطاقات متعدده تعمل بخصائص البث متعدد الاتجاهات

الاطروحة

مقدمه الى قسم هندسة تقنيات الاتصالات كجزء من متطلبات نيل درجه

الماجستير

تقدم بها

مروه جاسم محمد

اشراف

د.سالم محسن وادي

2021